



Fys - 3931  
Master's Thesis in Space Physics

---

Characterization of a magnetized plasma in  
cylindrical geometry

Giulio Tribulato

June, 2007

Faculty of Science  
Department of Physics and Technology  
University of Tromsø



*I didn't think it was physically possible,  
but this both sucks and blows.*

Bart Simpson



# Acknowledgements

Despite this entire thesis is wrote in English, I would like to write the acknowledgments in Italian, just because it seems more real to me. I am sorry for the non Italian speaker.

Grazie a mia madre e mia sorella, le uniche persone che non hanno mai smesso di credere in me, anche quando tutti (me compreso) avevano già smesso da un bel pezzo.

Grazie ad Åshild che ha accettato di lavorare con me senza conoscermi e mi ha consigliato e seguito in questi mesi. Grazie a Claudia che mi ha dato la possibilità di fare la tesi qui a Tromsø e per essere arrivata in mio aiuto quando le cose non funzionavano tanto bene. Grazie a Christopher per il suo aiuto con la double probe, i consigli e l'incoraggiamento, ho imparato molto nei pochi giorni che hai passato qui. Grazie a Kjell Arne, Torfinn e Inge che mi hanno aiutato a mandare avanti il laboratorio.

Grazie ai miei amici dell'università, che mi hanno accompagnato ed aiutato (ma anche distratto parecchio) in questi anni, in ordine sparso: Laura e Silvia (vi devo ancora una cena), Michele e P.B. (i miei teorici preferiti), BIFFI!!!, Giorgia, Eleuname (quest'estate, ti prometto, monto lo Zalman), Giò, Gippetto, Marco, Tia, SteFreddi (viva Brescia), er Mazza, Stampella, Sara ed Au (per i passaggi in macchina, l'incoraggiamento costante e tutti i fumetti). Un ringraziamento particolare alle due persone con cui ho maggiormente: studiato (il giusto), cazzeggiato (un pò più del giusto) e fatto integrali (troppi) in questi anni. Grazie a Roberto e le edizioni Decarli, senza le quali laurearsi avrebbe richiesto ere geologiche (qualcuno tiri giù la lavagna che l'ometto c'è rimasto appeso per favore). Grazie a Luca per il nostro semaforo e per il viaggio in Erasmus (quando iniziamo a scrivere le Salvuzziadi? ho già il titolo: "Salvuzzo: l'uomo che si credeva un cucchiaino").

Grazie agli amici che ho conosciuto in Erasmus e con cui ho vissuto in questi mesi: Eva, Sonja, Karen, Miriam, Virginia e grazie soprattutto a los Cichitgnos, senza di loro sarebbe stata molto più dura.

Grazie a tutti gli amici che hanno lavorato con me al cinema, vendere Poc corn per otto ore al giorno non sarebbe stato così divertente senza di

voi, ne dimenticherò qualcuno ma ci provo: Tanya (uè Mongè), Samy, Anna, Don Pucho (è sempre un piacere), Mascherina (e Babi), Luchino e Marchino (spizzi?), Giovvy, Angela, Pimpere, Borghesia, Ramona, Monica ed il capo indiscusso: Ilaria (no, non te lo cambio il fusto delle coca).

Grazie agli Abramos, ai nonni Grassadonia a Daniela Albano e Marco Masoni.

Grazie alla Prof.essa Antonella Campaner, la miglior insegnante di fisica e matematica che il peggior studente di fisica e matematica possa incontrare. Prof. se non L'avessi incontrata, oggi, probabilmente, non sarei arrivato qui.

Grazie a Duilio e famiglia (allargata) che sono praticamente la mia seconda casa (Duilio questa estate non abbiamo più scuse...ci tocca fondere le schede di rete).

Grazie ai miei amisci (la s non è un errore) Colo, Cubo, Gred e Vetro, è passato un pò di tempo da quando abbiamo finito il liceo, ma per fortuna siete ancora qui, spero ci sarete sempre e che restiate i soliti pivez.

# Contents

<b>1</b>	<b>Introduction</b>	<b>1</b>
1.1	Space plasma . . . . .	2
1.1.1	Atmosphere . . . . .	2
1.1.2	Ionosphere . . . . .	3
1.1.3	Magnetosphere . . . . .	4
1.1.4	Ionosphere-Magnetosphere coupling . . . . .	5
1.2	Laboratory Plasma . . . . .	6
1.2.1	Hot-filament discharge . . . . .	7
1.2.2	Helicon source . . . . .	7
1.2.3	Q-machine . . . . .	8
1.3	Plasma scaling . . . . .	8
1.3.1	Buckingham Theorem . . . . .	8
1.3.2	Plasma dimensionless parameter . . . . .	10
1.4	Phenomena in the machine . . . . .	12
1.4.1	Ion Cyclotron Waves . . . . .	16
1.4.2	Double Layer . . . . .	18
<b>2</b>	<b>Machine</b>	<b>23</b>
2.1	Main Chamber . . . . .	23
2.2	Vacuum and pressure control . . . . .	25
2.2.1	Rotary pump . . . . .	26
2.2.2	Turbomolecular pump . . . . .	28
2.2.3	Pressure measurement and flow control . . . . .	29
2.3	Antenna section and RF source . . . . .	30
2.3.1	Helicon waves . . . . .	30
2.3.2	Njord antenna . . . . .	34
2.3.3	Power and tuning system . . . . .	36
2.3.4	Dc source and biasing . . . . .	40
2.4	Magnetic field . . . . .	41

<b>3</b>	<b>Diagnostic</b>	<b>49</b>
3.1	Sheath theory . . . . .	49
3.1.1	Collisionless sheath . . . . .	50
3.1.2	The Bohm sheath criterion and the presheath . . . . .	51
3.1.3	Child-Langmuir law . . . . .	55
3.2	Probe Theory . . . . .	56
3.2.1	Langmuir Probe . . . . .	56
3.2.2	Compensated probe . . . . .	58
3.2.3	Double probe . . . . .	63
3.3	Construction and testing . . . . .	64
3.3.1	Compensated probe . . . . .	64
3.3.2	Double probe . . . . .	69
3.4	Diagnostic external hardware . . . . .	70
3.4.1	Probes support and motor system . . . . .	70
3.4.2	Compensated probe acquisition system . . . . .	71
3.4.3	Double probe acquisition system . . . . .	72
<b>4</b>	<b>Data analysis</b>	<b>75</b>
4.1	Compensated probe analysis software . . . . .	75
4.2	Axial scan . . . . .	78
4.2.1	Pressure scan . . . . .	79
4.2.2	Magnetic scan . . . . .	86
4.3	Radial scan . . . . .	93
4.3.1	Pressure scan . . . . .	96
4.3.2	Magnetic scan . . . . .	99
<b>5</b>	<b>Conclusion and further improvements</b>	<b>103</b>
5.1	Diagnostics and further measurements . . . . .	103
5.2	Suggestion for technical improvements . . . . .	104
<b>A</b>	<b>Programs code</b>	<b>107</b>
A.1	Langmuir_multi . . . . .	107
A.2	Langmuir_core . . . . .	109
A.3	Error_analysis . . . . .	116
A.4	Error_analysis_core . . . . .	118



# List of Figures

1.1	Temperature in the atmosphere layers varying height. Credit: [2] . . . . .	3
1.2	Aurora with typical filament shape on Saturn. Credit: J. Trauger (JPL), NASA . . . . .	6
1.3	Potential (solid), Electric field (dashed) and charge density (dotted) in a double layer. Credit: A.Meige, Ph.D Thesis, ANU, 2006. . . . .	18
1.4	On the right: potential distribution of a double layer, on the left: phase space plot in which the different families, hatched and clear areas, are recognizable . Credit: A.Meige, Ph.D Thesis, ANU, 2006. . . . .	19
2.1	Lateral section of Njord . . . . .	24
2.2	Model of Njord with main elements visible . . . . .	25
2.3	Rotative pump section . . . . .	27
2.4	Turbomolecular pump section . . . . .	28
2.5	Njord antenna lodging lateral section . . . . .	35
2.6	Double saddle antenna . . . . .	36
2.7	Equivalent circuit of the $\pi$ -network, the two capacitance are mounted into the tuning box . . . . .	37
2.8	Magnetic field generated by source coils supplied by 6A. . . . .	42
2.9	Magnetic field generated by source coils (6A) and by chamber coil (20A). . . . .	43
2.10	Magnetic field generated by source coils (6A) and by chamber coil (-20A). . . . .	43
2.11	Magnetic field along $\hat{\mathbf{z}}$ generated by source coils supplied by 2,4 and 6A . . . . .	44
2.12	Magnetic field along $\hat{\mathbf{z}}$ generated by source coils (6A) and chamber coil: 20,40A (solid line) -20,-40A (dotted) . . . . .	45
2.13	Source coils temperature for current equal to 2 (solid),4 (dotted),6 (dashed) and 8(dot-dashed) . . . . .	46

3.1	Density and potential profile of plasma in presence of a wall. . . . .	51
3.2	Electron density (solid), ion density with $u_{i0} \geq u_B$ (dotted), ion density with $u_{i0} < u_B$ (dashed) . . . . .	53
3.3	An example of Langmuir characteristic (solid) and it's first derivative (dashed) . . . . .	56
3.4	Logarithmic plot of Langmuir characteristic (solid), $V_f$ posi- tion (left dashed), $V_p$ position (right dashed) . . . . .	57
3.5	Equivalent circuit of a Langmuir probe . . . . .	59
3.6	Equivalent circuit of compensated Langmuir probe . . . . .	61
3.7	Double probe electric scheme (Up), typical I-V characteristic (Down), Credit: [12] page 182. . . . .	63
3.8	Frequency response of the band-pass filter . . . . .	66
3.9	Sketch of the compensated probe circuit and housing used in Njord . . . . .	67
3.10	Compensated probe sketch used in Njord . . . . .	68
3.11	Double probe sketch used in Njord . . . . .	69
3.12	Typical double probe acquisition system circuit. Credit: C.Watts, UNM. . . . .	72
4.1	Frontal section of the antenna and the dome. . . . .	78
4.2	Plasma potential as a function of position for different pressure values and source coils current of 6A. Compensated Langmuir probe. . . . .	79
4.3	Plasma density as a function of position for different pressure values, source coils current 6A, power 600W. Compensated Langmuir probe. . . . .	80
4.4	Plasma and floating potential as a function of pressure, with source coils current of 2 and 6A and axial position $Z = 210$ and 390mm. Compensated Langmuir probe. . . . .	81
4.5	Electron temperature as a function of pressure, with source coils current of 2 and 6A and axial position $Z = 210$ and 390mm. Compensated Langmuir probe. . . . .	82
4.6	Plasma density as a function of pressure, with source coils current of 2 and 6A, axial position $Z = 210$ and 390mm and power of 600W. Compensated Langmuir probe. . . . .	83
4.7	Plasma density as a function of pressure, with source coils current of 2 and 6A, axial position $Z = 210$ and 390mm and power of 900W. Double probe. . . . .	84
4.8	Plasma potential as a function of position for different source coils current and a pressure of $1 \times 10^{-3}$ mbar. Compensated Langmuir probe. . . . .	86

4.9	Plasma density as a function of position for different source coils current and a pressure of $1 \times 10^{-3}$ mbar. Compensated Langmuir probe. . . . .	87
4.10	Plasma and floating potential as a function of source coils current, pressure from $1 \times 10^{-3}$ mbar to $3 \times 10^{-4}$ mbar and axial position $Z = 210$ and $390$ mm. Compensated Langmuir probe. . . . .	88
4.11	Electron temperature as a function of source coils current, pressure of $1 \times 10^{-3}$ mbar and $3 \times 10^{-4}$ mbar and axial position $Z = 210$ and $390$ mm. Compensated Langmuir probe. . . . .	89
4.12	Plasma density as a function of source coils current, pressure of $1 \times 10^{-3}$ mbar and $3 \times 10^{-4}$ mbar, axial position $Z = 210$ and $390$ mm and power of $600$ W. Compensated Langmuir probe. . . . .	90
4.13	Plasma density as a function of source coils current, pressure of $1 \times 10^{-3}$ mbar and $3 \times 10^{-4}$ mbar, axial position $Z = 210$ and $390$ mm and power of $900$ W. Double probe. . . . .	91
4.14	Plasma density as a function of chamber coil current, source coils current $6$ A, pressure of $4 \times 10^{-4}$ mbar and $3 \times 10^{-4}$ mbar, axial position $Z = 210$ and $390$ mm and power of $900$ W. Double probe. . . . .	92
4.15	Plasma potential as a function of radial position for different values of pressure (right panel) and magnetic field (left panel). Double probe. . . . .	94
4.16	Plasma density as a function of radial position for different values of pressure (right panel) and magnetic field (left panel), power of $900$ W. Double probe. . . . .	95
4.17	Plasma and floating potential as a function of pressure, with source coils current of $3$ and $6$ A and radial position $R = 0$ and $120$ mm. Compensated Langmuir probe. . . . .	96
4.18	Electron temperature as a function of pressure, with source coils current of $3$ and $6$ A and radial position $R = 0$ and $120$ mm. Compensated Langmuir probe. . . . .	97
4.19	Plasma density as a function of pressure, with source coils current of $3$ and $6$ A, radial position $R = 0$ and $120$ mm and power of $600$ W. Compensated Langmuir probe. . . . .	98
4.20	Plasma and floating potential as a function of magnetic field, pressure of $1 \times 10^{-3}$ mbar and $3 \times 10^{-4}$ mbar and radial position $R = 0$ and $120$ mm. Compensated Langmuir probe. . . . .	99
4.21	Electron temperature as a function of magnetic field, pressure of $1 \times 10^{-3}$ mbar and $3 \times 10^{-4}$ mbar and radial position $R = 0$ and $120$ mm. Compensated Langmuir probe. . . . .	100

- 4.22 Plasma density as a function of magnetic field, pressure of  $1 \times 10^{-3}$  mbar and  $3 \times 10^{-4}$  mbar, radial position  $R = 0$  and 120mm and power of 600W. Compensated Langmuir probe. . 101
- 4.23 Plasma density as a function of chamber coil current, source coils current 6A, pressure of  $3 \times 10^{-4}$  mbar and  $1 \times 10^{-3}$  mbar, radial position  $R = 0$ mm and power of 900W. Double probe. . 102

# Chapter 1

## Introduction

Njord is a new plasma device built at the physics department of the University of Tromsø for investigating low-temperature plasmas. A rich variety of plasma phenomena exist in geospace environment and there is a long history of experimental investigations in neutral atmosphere, ionosphere and magnetosphere of Earth and other planets. Unfortunately those experiment are quite challenging since there are many difficulties on performing measurements in situ. Some examples: a satellite or a rocket for plasma measurements usually travels at approximately 1-5 km/sec, the data acquired are a snapshot of the medium extremely localized in space and time. Using a single satellite data it is impossible to discern between the spacecraft flying through a quasi-static structure or a moving one overtaking the spacecraft. The medium we want to investigate is out of our control and the number of probes a satellite can bring is limited. For having a realistic view of the environment we should have a statistical picture through many returns, but for a satellite about 90 minutes occurs for a successive passes through. Meanwhile, the environment could be deeply changed.

In virtue of these difficulties laboratory experiment have been regarded as a complementary approach to address the fundamental physics of plasma in space. The spatial dimension is, obviously, not possible to reproduce, but with careful consideration on boundary conditions and attention to scaling laws for our parameters, it is possible to make laboratory experimental observations that are relevant to space physics. Laboratory experiment are conducted in controlled and reproducible environments, they are repeatable with different diagnostic techniques, with high spatial and temporal resolution. We can therefore acquire a larger amount of data and obtain a better statistical description. But most important is the possibility to (often) isolate one problem at a time and study it under controlled conditions.

The main object of this work is to carry out an experimental character-

ization of the plasma inside Njord. In particular for further studying on: plasma expansion and acceleration from the source into the main chamber, spontaneous formation of current-free double layer and ion beams. It's necessary, for those studies, to find the degree to which this laboratory device can produce scaled conditions that are relevant to space plasma and the operating parameters (i.e. magnetic field configuration, pressure, source power) of the device.

## 1.1 Space plasma

The Earth, like other planets as Jupiter, Saturn, Uranus and Neptune has it's own magnetic field that near the surface can be approximated with a dipole; while at, increasing height, the multipole approximation becomes less accurate. The field in fact is distorted by the influence of electric currents in the ionosphere and magnetosphere and by the direct action of the solar wind. The boundary between the solar wind and the magnetosphere is called magnetopause and is defined as the location where the outward magnetic pressure of the Earth magnetic field balance the solar wind. Since the solar wind is a supersonic flow on the boundary a standing shock wave, the bow shock, develops in front of the magnetopause. On the night side of the Earth the magnetic field is stretched by the solar wind forming the magnetotail. In the magnetosphere exist various plasma regime, mainly dominated in the higher level by the solar wind plasma and by the ionospheric plasma in the lower ones.

### 1.1.1 Atmosphere

Travelling upward from the Earth surface we first encounter the Atmosphere that is subdivided in layers defined by extrema in the temperature profile [2]. The Troposphere from surface to about 10-16 km contains 75% of the atmospheric mass and has a negative temperature gradient of 6.5 K/km. The following layer, the Stratosphere, lasts up to 50 km and has a positive temperature gradient due to the UV absorption. Then the temperature gradient is again negative in the mesosphere up to 80 km. Above, in the thermosphere, the temperature increase again because the electromagnetic radiation is absorbed, leading to the formation of the ionospheric layers. In the higher part of the thermosphere the temperature remain constant between 1300 K (nightside) and 2000 K (dayside). The density in the atmosphere range between  $\sim 2.5 \times 10^{19} \text{ cm}^{-3}$  near the surface, to  $10^{16} \text{ cm}^{-3}$  at  $\sim 50 \text{ km}$  where some level of ionization can be detected

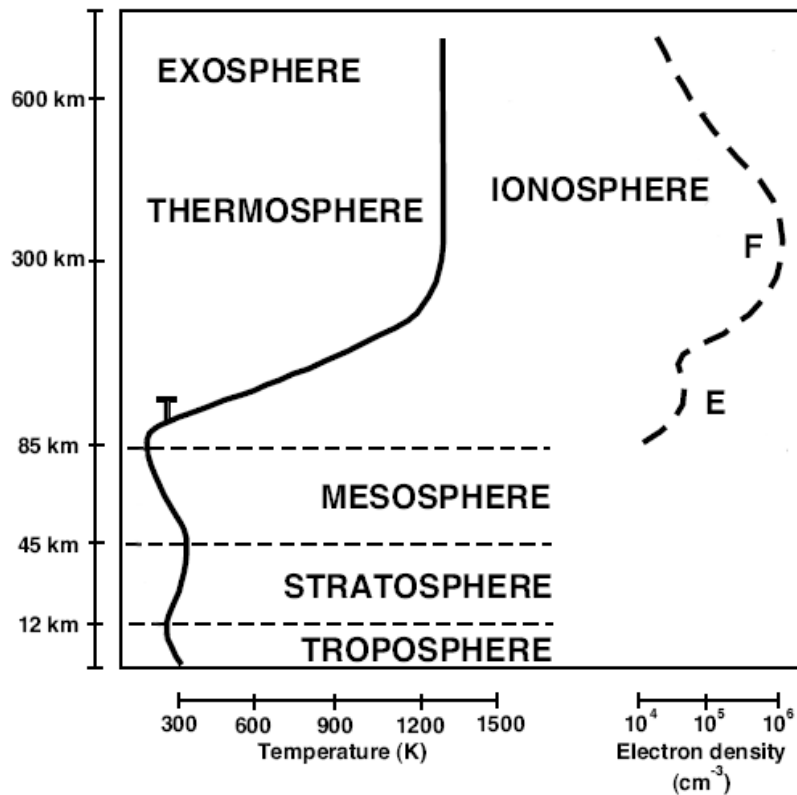


Figure 1.1: Temperature in the atmosphere layers varying height. Credit: [2]

### 1.1.2 Ionosphere

The ionosphere start at  $\sim 50$ -70 km and due to the high density of neutral component its behavior is dominated by gas dynamics and electromagnetic interactions. A further subdivision can be done in three layers [3].

The D layer is the innermost layer, 50 km to 90 km above the surface of the Earth. Ionization here is due to Lyman series-alpha H hydrogen radiation. During the night cosmic rays produce a residual amount of ionization that allow the D layer to exist, even if it's strongly reduced with respect of the daytime. Recombination is high in this layer, thus the net ionization effect is very low and as a result high-frequency (HF) radio waves are not reflected by the D layer. The collision frequency between electrons and other particles in this region during the day is about  $10^{-7} s^{-1}$ .

The E layer is the middle layer, 90 km to 120 km above the surface of the Earth. Ionization is due to soft X-ray (1-10 nm) and far ultraviolet (UV)

solar radiation ionization of molecular  $O_2$ . This layer can only reflect radio waves having frequencies less than about 10 MHz. The vertical structure of the E layer is primarily determined by the opposite effects of ionization and recombination. At night the E layer, as the D one, begins to disappear because the primary source of ionization is no longer present. This results in an increase in the height where the layer maximizes because recombination is faster in the lower layers. Diurnal changes in the high altitude neutral winds also plays a role. The increase in the height of the E layer maximum increases the range to which radio waves can travel by reflection from the layer.

The F layer or region, is 120 km to 500 km above the surface of the Earth. It is the top most layer of the ionosphere. Here extreme ultraviolet (UV) (10-100 nm) solar radiation ionizes atomic oxygen. The F region is the most important part of the ionosphere in terms of HF communications. The F layer combines into one layer at night, and during daytime, it divides into two layers, the F1 and F2. The F layers are responsible for most skywave propagation of radio waves, and are thickest and most reflective of radio on the side of the Earth facing the sun. The plasma density at 500 km can exceed  $10^6 \text{ cm}^{-3}$  while particle temperature ranges between 0.1 eV to 0.5 eV

### 1.1.3 Magnetosphere

The magnetosphere is defined as the zone in which the particle motion is completely determined by the Earth magnetic field [1]. In the ionosphere the neutral density is too high and therefore the two zones are divided. Here the density of ionized particles greatly exceeds that of the neutral, but the total density is so low that the plasma can be considered collisionless. On the outer boundary the magnetosphere is delimited by the sun position: at daytime above the equator the height is about  $10 R_E$  while at night can extent for hundred of  $R_E$  into the magnetotail. Here,  $R_E$  is the Earth radius. The great difference between these two values is, as we previously said, given by the bending effect of the solar wind.

The population in the magnetosphere is a mixture of ionospheric and solar wind plasma made of thermal and high-energy charged particles. The solar wind contribution is mainly  $H^+$  and few  $He^{++}$  with energies of  $\sim 1 \text{ KeV}$ , while the ionospheric source is  $H^+$ ,  $O^+$  and some  $He^+$  with energies between 0.1 to a few KeV. The two He species are, due to charge exchange and ionization process, not discernable. The  $O^+$  density is also modified by the Earth's gravitational force, so that only high-energy  $O^+$  can reach high altitudes [4]. While the plasma injection from the ionosphere could be explained by the current coupling, the presence of solar wind plasma into the higher



regions of the magnetosphere requires a different explanation. The magnetopause is not an impenetrable boundary; plasma transfer between the two regions is mainly due to magnetic reconnection that occurs when field lines of opposite polarity meet. This configuration is called the X-point and occurs between the Earth's magnetic field and the interplanetary magnetic field (IMF), generated by the sun. The most important evidence for magnetic reconnection, is the strong dependence of the solar wind plasma flow into the magnetosphere by the IMF position. This is most likely to occur at the dawn side. On the equatorial plane, the magnetic field lines coming from the sun get in contact with the magnetopause with an inclination of about  $45^\circ$ , so that on the dawn side the Earth magnetic field is parallel to the IMF while on the dusk side the two field lines are almost perpendicular. These two configurations are named the open and closed magnetosphere, respectively.

#### 1.1.4 Ionosphere-Magnetosphere coupling

The ionosphere and the magnetosphere are coupled together by currents and plasma flow [1, 2]. Since the ionosphere is dominated by ions-neutrals collision the conductivity is finite and the frozen law approximation is no longer valid. It is possible to define three different conductivities: the field-aligned conductivity (in plasma physics the reference field, unless specified, is always the  $\mathbf{B}$  field), the Pedersen conductivity that refers to currents parallel to  $\mathbf{E}$  and the Hall conductivity that belongs to currents perpendicular to both  $\mathbf{E}$  and  $\mathbf{B}$  fields. In all three cases it is clear that the conductivity is highly anisotropic. The largest of these conductivities is the field-aligned that corresponds to the ordinary conductivity given by:

$$\sigma_{\parallel} = ne^2 \left( \frac{1}{m_i \nu_i} + \frac{1}{m_e \nu_e} \right),$$

where  $m_e$ ,  $m_i$  are electron and ion masses and  $\nu_e$ ,  $\nu_i$  are collision frequencies,  $n$  is the neutral density and  $e$  the elementary charge. At high altitudes the magnetic field is mainly perpendicular to the ionospheric layers, this lets the so called Birkeland current couple the ionosphere to the magnetosphere and contributes to aurora phenomena in the polar regions.

The ionospheric current system is quite complicated and a complete description is beyond the scope of this introduction.



Figure 1.2: Aurora with typical filament shape on Saturn. Credit: J. Trauger (JPL), NASA

## 1.2 Laboratory Plasma

A high number of different machine have been used to create laboratory plasmas, usually with common characteristics but also with some unique device optimized for some space relevant operating regime. It is obviously impossible to reproduce all possible space regimes in a single machine, that is why it is necessary to create different devices, each one for a different region of space we want to study. The common components for a laboratory plasma device are: a vacuum chamber with gas supply, an ionization source, some kind of diagnostics and in most cases a magnetic field for confinement. It is often preferable to have a low base vacuum (a starting vacuum condition with gas supply closed and plasma switched off) to clean the inside chamber of impurities and to have extremely low atmospheric gas compared with the gas we want to use for plasma production. This second point is important

since most of the data analysis requires the knowledge of the mass particle used in plasma creation.

The ionization sources used in laboratory plasmas are numerous and different, here we will describe three of them: Q-machine, hot-filament-discharge and helicon source. The first one is historically important because it is been widely used for plasma wave and instabilities studies, the other two are the ones we use for plasma production in Njord.

### 1.2.1 Hot-filament discharge

Hot-filament discharge is one of the simpler and easier methods for creating plasma. It consists of a filament, usually wolfram, that is heated by letting a current flow through it. The thermionically emitted electrons are accelerated by a biased anode into a low density neutral gas; the impacts of those so called primary electrons on the neutral gas create the plasma. To vary the plasma density it is only necessary to vary the current through the filament. Thus it is possible to obtain a wide range of operating parameters. For example, the plasma density in this devices can range between  $10^4\text{cm}^{-3}$  to  $10^{12}\text{cm}^{-3}$  while the electron temperature ranges from  $\sim 0.1\text{eV}$  to  $\sim 3\text{-}4\text{eV}$ . Differently from the Q-machine the ion temperature is not equal to that of electrons, but it is instead near the neutral gas temperature used. The easy way we can produce plasma with this technique allow the production of a large plasma volume <sup>1</sup>.

### 1.2.2 Helicon source

Helicon source use helicon waves for creating high-density plasma. Those waves propagates in a magnetized plasma for frequencies between the ion and electron cyclotron frequency and belongs to the whistler-mode. The main difference between helicon and other RF discharge plasma is the capability of this wave to penetrate in the inner part of the plasma and heat electrons far away from the source boundary. This allow the creation of plasma with a density up to  $10^{14}\text{cm}^{-3}$  and with electron temperature of  $\sim 2\text{-}10\text{eV}$  <sup>2</sup>.

---

<sup>1</sup>The complete description of hot-filament apparatus we use in Njord will be presented in chapter 2.1, page 23

<sup>2</sup>A complete description of Helicon source theory and apparatus we use in Njord will be presented in chapter 2.3, pag. 30

### 1.2.3 Q-machine

The Q-machine (Quiescent-machine) gets its name from the capacity of the device to produce quiescent plasma or free of inherent particle drifts and thus free of low-frequency instabilities [5]. This kind of machine was first built in the 1960 at the University of Princeton, it consist of a hot plate (the source) which is heated using a filament behind the plate so that it thermionically emits electrons. For creating ions, and thus fulfilling the quasi-neutrality condition, an alkaline-metal vapor is directed on the plate. In this way it is possible to create a plasma with same temperature population for ions and electrons ( $\sim 0.2\text{eV}$ ) and with a plasma density between  $10^8\text{cm}^{-3}$  to  $10^{10}\text{cm}^{-3}$ [5]. On the other side of the vacuum chamber, opposite to the hot plate, there is a so called cold plate. Despite it is name this plate is usually heated to avoid deposition of ions that would change the plasma parameter. The heating is anyway insufficient to generate electron emission.

## 1.3 Plasma scaling

In the first part of the introduction we said that to realize relevant laboratory experiments for space plasma phenomena it is necessary to know the right scaling law for system parameters we want to simulate. The objective is to understand the manner in which the various physical quantities that describe a phenomena combine in determining the qualitative characteristic of the phenomena. The scaling laws are a set of relevant physical quantities that remain unchanged between two different systems; a classical example from aerodynamics are the Mach and Reynolds numbers. The scaling laws theory belongs to the math field of dimensional analysis and is based on the Buckingham Theorem<sup>3</sup>.

### 1.3.1 Buckingham Theorem

A formal proof of the theorem is far beyond the scope of this thesis<sup>4</sup>, we will try here to present a short explanation. Let's first identify a complete set of independent quantities  $Q_1, \dots, Q_n$  that defines the value of  $Q_0$  through

$$Q_0 = f(Q_1, \dots, Q_n), \quad (1.3.1)$$

---

<sup>3</sup>The Buckingham Theorem is also known as  $\pi$ -theorem

<sup>4</sup>An algebraical proof has been realize by E.Isaacson and M.Isaacson, *Dimensional Methods in Engineering and Physics*, Wiley, New York,1975.

where for a complete set, we mean that the value of  $Q_0$  should depend only on the  $Q_1, \dots, Q_n$  set, while for independent we mean that each element of the set doesn't depend on the others. This step is crucial since the dimensional analysis could work only if these assumption are fulfilled. Now we should choose a system of units so that we can univocally define the  $Q_i$  quantities, the usual MKS system is a common choice for simple mechanical problem. Once we select the unit system we should write down our quantity dimensions in the form

$$[Q_i] = L^{l_i} M^{m_i} t^{\tau_i} , \quad (1.3.2)$$

where  $l_i, m_i$  and  $\tau_i$  are powers of length, mass and time of the  $n$  quantities. Now we take from  $Q_1, \dots, Q_n$  a complete dimensionally independent subset  $Q_1, \dots, Q_k$  ( $k \leq n$ ) and express the  $Q_0, Q_{k+1}, \dots, Q_n$  elements as product of powers of  $Q_1, \dots, Q_k$ . Equation (1.3.2) tell us that it is possible to write all physical quantities dimension as the product of a system set dimensions, but it is also possible to express dimension as the product of another set. The two definitions complete and independent have the same meaning as before, but now they are applied referring to the dimension. While the  $k$  value is unique (is the dimension of the system set) the choice of the  $Q_1, \dots, Q_k$  is not and lead to different solutions (the effective utility of each solution must be further verified). Once the new set had been choose we can rewrite

$$[Q_i] = [Q_1^{N_{i1}}, \dots, Q_k^{N_{ik}}] , \quad (1.3.3)$$

for  $i = 0, i > k$  and  $j = 1 \dots n - k$ . In this more general notation the  $N_{ij}$  terms stand for  $l_i, m_i$  and  $t^{\tau_i}$  of equation (1.3.2). Now we can finally define the dimensionless  $n - k$  independent variables as

$$\Pi_i = \frac{Q_{k+i}}{Q_1^{N_{(k+i)1}}, \dots, Q_k^{N_{(k+i)k}}} , \quad (1.3.4)$$

and a dimensionless form of the dependent variable  $Q_0$

$$\Pi_0 = \frac{Q_0}{Q_1^{N_{01}}, \dots, Q_k^{N_{0k}}} . \quad (1.3.5)$$

Now we can rewrite equation (1.3.1) as

$$\Pi_0 = f(Q_1, \dots, Q_n; \Pi_1, \dots, \Pi_{n-k}) , \quad (1.3.6)$$

in which all quantities are dimensionless except for the  $Q_1, \dots, Q_k$ , those cannot be put into a dimensionless form since by definition they are dimensionally independent of each other. Moreover for every physically meaningful

equation the dimension must be homogeneous thus the terms  $Q_1, \dots, Q_k$  on equation (1.3.6) can be absent leading to

$$\Pi_0 = f(\Pi_1, \dots, \Pi_{n-k}) . \quad (1.3.7)$$

This equation is the end of our dimensional analysis and contains the Buckingham theorem:

**Theorem 1 (Buckingham Theorem)** *when a complete relationship between dimensional physical quantities is expressed in dimensionless form, the number of independent quantities that appear in it is reduced from the original  $n$  to  $n - k$ , where  $k$  is the maximum number of the original  $n$  quantities that are dimensionally independent.*

The Buckingham theorem tells us that, because all complete physical equations must be dimensionally homogeneous (i.e. we should have the same physical dimension on both hands of an equation), a restatement of any such equation in an appropriate dimensionless form will reduce the number of independent quantities in the problem by  $k$ . The  $\pi$ -theorem itself merely tells us the number of dimensionless quantities that affect the value of a particular dimensionless dependent variable. It does not tell us the forms of the dimensionless variables.

### 1.3.2 Plasma dimensionless parameter

For applying the Buckingham theorem to the plasma case we should first consider some fundamental plasma parameters to use them as a starting point. Let assume we have a two species plasma that fulfill the quasi-neutrality condition, we can thus say that the density of the two species are almost everywhere equal or using formula

$$n_i \simeq n_e . \quad (1.3.8)$$

Let also suppose that the two population are at thermal equilibrium with each other ( $T_i = T_e$ , where  $T$  is measured in eV and count in the Boltzmann constant), we can then define the thermal speed of particles as

$$v_{ts} = \sqrt{\frac{2T}{m_s}} , \quad (1.3.9)$$

where the subscript  $s$  stand for the different species. A fundamental time scale parameter is given by the plasma frequency

$$\omega_p^2 = \frac{ne^2}{\varepsilon_0 m}, \quad (1.3.10)$$

that is bigger for electrons than for ions and belongs to electrostatic oscillation due to small charge separation. Such oscillation will be observable only if the observation time will be longer than  $\tau_p = 1/\omega_p$ . Multiplying  $\tau_p$  by the thermal speed  $v_{ts}$  we obtain the Debye length that is a fundamental space parameter defined as

$$\lambda_D = \sqrt{\frac{\varepsilon_0 T}{ne^2}}. \quad (1.3.11)$$

Observation on length scales shorter than the Debye length will not be able to detect plasma phenomena due to the well known Debye shielding effect. Let introduce the average distance between particles, derived from plasma density, and the distance of closest approach<sup>5</sup> as

$$r_d = n^{-1/3}, \quad r_c = \frac{e^2}{4\pi\varepsilon_0 T}. \quad (1.3.12)$$

The ratio  $r_d/r_c$  give us information on the coupling of the plasma. For small values the dynamic of particles is mostly influenced by the electrostatic force (strong coupling) while for the opposite case the electrostatic force doesn't play a fundamental role on particles motion(weak coupling). A dimensionless quantity describing the coupling strength of a plasma is defined as

$$\Lambda \propto (r_d/r_c)^{3/2} \propto \frac{\lambda_D}{r_c}, \quad (1.3.13)$$

so that  $\Lambda$  is large for strong coupling and small for weak ones.  $\Lambda$  together with the Debye length and the plasma frequency are the most important parameters for plasma physics.

In presence of a magnetic field it is necessary to introduce new parameters that take into account the anisotropy due to the  $\mathbf{B}$  field. Particles moving in a magnetized plasma will suffer a gyro-motion around the field lines. The radius of the helical orbits is smaller for stronger magnetic field, since the particles become more tightly bound around the field line. Hence this is a quantity that indirectly describes the intensity of the field and it is defined as:

---

<sup>5</sup>The distance of closest approach is define as the distance at which the total energy of a charged particles in the electrostatic field of another equals zero



$$\rho = \frac{v_{\perp}}{\omega_c}, \quad (1.3.14)$$

where  $\omega_c = eB/m$  is the cyclotron frequency. Thus we can define a plasma of size  $L$  to be magnetized if the gyroradius is much lesser than  $L$ . Another way to discern between magnetized and non magnetized plasma is the  $\beta$  parameter defined as the ratio between the kinetic and the magnetic pressure:

$$\beta = \frac{p}{p_{mag}} = \frac{nk_B T}{B^2/2\mu_0}. \quad (1.3.15)$$

For larger  $\beta$  value we are in presence of a weakly magnetized plasma (the opposite of  $\rho$ ).

With the introduction of the magnetic field we are able to completely describe a plasma from the basic parameters:  $\mathbf{B}$ ,  $e$ ,  $m$ ,  $n$ ,  $T$ ,  $\varepsilon_0$  and  $\mu_0$ . To be sure that those seven parameters are enough to describe entirely a plasma system we can apply the Buckingham theorem. We know that for describing those quantities we need a system set composed of: length, mass, time and fundamental charge. Since  $k = 4$  and  $n = 7$  we must find  $n - k = 3$  dimensionless parameter to describe the system. Obviously the possible combination of dimensionless quantities is a number, and as we said the Buckingham theorem does not give any help in finding the most fiscally significant. In our previously analysis we found two parameters ( $\Gamma$  and  $\beta$ ) that are dimensionless and quite meaningful. It is possible to show that together with those two solutions a consistent third one is  $n\rho^3$  that could be seen as a measure of the density of a gyro-sphere. So that a complete dimensionless set is given by

$$\Pi_1 = \Lambda, \quad \Pi_2 = \beta, \quad \Pi_3 = n\rho^3. \quad (1.3.16)$$

If the plasma we are studying presents others more interesting quantities, is't possible to enlarge the basic parameter set and then find new dimensionless quantities. As we said the difficult part of this procedure is to find those combinations that are easy to read and physically significant.

## 1.4 Phenomena in the machine

The Njord configuration is built in order to understand plasma flows, beams and wave instabilities in such plasmas. It is possible to foresee that two are the main phenomena that will be first encounter: Ion Cyclotron Waves (ICW) and double layers. While the first belongs to the known plasma wave theory,



a double layer is a different structure. In this section we will expose the main theory about these phenomena and their space and laboratory relevance.

Waves are a common response to applied perturbations, and provide the propagation system through the medium. A portion of space plasma, with magnetic field, can support a great variety of electromagnetic and electrostatic wave; to exist, each wave mode should be a valid solution of the dispersion relation. This relation is a function that describe the properties of the plasma relating the angular frequency  $\omega$  (rad/s) and the wave vector  $\mathbf{k} = 2\pi/\lambda$  ( $\text{m}^{-1}$ ), that defines wavelength and direction of propagation [6]. The electric field of a sinusoidal wave can be written as:

$$\mathbf{E}(\mathbf{r}, t) = \mathbf{E}_0 \exp\{i(\mathbf{k} \cdot \mathbf{r} - \omega t)\} . \quad (1.4.17)$$

The measurable quantity is the real part of this complex expression. The exponent in (1.4.17) is the phase. A surface with constant phase, is displaced by the phase velocity defined as

$$\mathbf{v}_\phi = \frac{\omega}{k^2} \mathbf{k} . \quad (1.4.18)$$

For electromagnetic waves the refraction index is defined as  $n = c/v_\phi$ . The phase velocity does not carry information, in fact it can exceed the speed of light without contradicting the theory of relativity. The information can be carried by a modulated wave on which a variation of amplitude or frequency is superimposed. The speed at which information moves in this modulated signal is defined as the group velocity

$$v_g = \frac{\partial \omega}{\partial \mathbf{k}} , \quad (1.4.19)$$

that is the speed of the wave packet, thus it cannot exceed the speed of light. Defining the dispersion relation as  $\omega = \omega(k)$  we can see that for horizontal asymptote the group velocity becomes zero and the wave cannot propagate thence all the energy carried by the wave is feed into stationary oscillations.

We defined a wave as a perturbation of our system, it is possible then to define each plasma parameter as the superposition of the average state and the perturbation

$$\mathbf{B} = \mathbf{B}_0 + \mathbf{B}_1 , \quad \mathbf{E} = \mathbf{E}_0 + \mathbf{E}_1 , \quad \mathbf{u} = \mathbf{u}_0 + \mathbf{u}_1 , \quad (1.4.20)$$

where  $\mathbf{B}$  is the magnetic field,  $\mathbf{E}$  the electric field and  $\mathbf{u}$  the bulk speed; the average state is indicated with index '0' and the perturbation with index

'1'. We can moreover define  $\mathbf{j}$  as the current,  $\varrho$  as the density and  $p$  as the pressure, and write them using the same syntax as before

$$\mathbf{j} = \mathbf{j}_0 + \mathbf{j}_1, \quad \varrho = \varrho_0 + \varrho_1, \quad p = p_0 + p_1. \quad (1.4.21)$$

Since the perturbation are stochastic their average must be zero

$$\langle \mathbf{B}_1 \rangle = \langle \mathbf{E}_1 \rangle = \langle \mathbf{u}_1 \rangle = \langle \mathbf{j}_1 \rangle = \langle \varrho_1 \rangle = \langle p_1 \rangle = 0.$$

Now we can start our analysis with the basic equation of magnetohydrodynamics, starting from Maxwell equations

$$\nabla \cdot \mathbf{E} = \frac{\varrho_c}{\varepsilon_0}, \quad (1.4.22a)$$

$$\nabla \cdot \mathbf{B} = 0, \quad (1.4.22b)$$

$$\nabla \times \mathbf{E} = -\frac{\partial \mathbf{B}}{\partial t}, \quad (1.4.22c)$$

$$\nabla \times \mathbf{B} = \mu_0 \mathbf{j}, \quad (1.4.22d)$$

Ohm's law

$$\mathbf{j} = \sigma(\mathbf{E} + \mathbf{u} \times \mathbf{B}), \quad (1.4.23)$$

equation of continuity

$$\frac{\partial \varrho_c}{\partial t} + \nabla \cdot (\mathbf{u} \varrho_c) = 0, \quad (1.4.24)$$

equation of motion

$$\varrho \frac{\partial \mathbf{u}}{\partial t} + \varrho(\mathbf{u} \cdot \nabla) \mathbf{u} = -\nabla p + \mathbf{j} \times \mathbf{B} + \varrho \mathbf{g} + \varrho \nu \nabla^2 \mathbf{u}, \quad (1.4.25)$$

and equation of state

$$\frac{d}{dt} \left( \frac{p}{\varrho^\gamma} \right) = 0. \quad (1.4.26)$$

The new quantities introduced are:  $\varrho_c$  the charge density,  $\varepsilon_0$  the permittivity on free space,  $\mu_0$  the permeability on free space,  $\mathbf{g}$  the acceleration of gravity,  $\nu$  the kinematic viscosity and  $\gamma$  the specific heat ratio. Considering that the perturbation are small with respect to the average values we can substitute (1.4.20) and (1.4.21) into (1.4.22)–(1.4.26) obtaining two sets of equations, one for the average and one for the fluctuating quantities. In the former set we should only use average quantities, while in the latter both

fluctuating and average quantities. The fluctuating times fluctuating quantities are of a higher order of approximation and they can be ignored because they are smaller. Solving for the set of equation of average values we obtain

$$\nabla \times \mathbf{B}_0 = \mu_0 \mathbf{j}_0 , \quad (1.4.27a)$$

$$\nabla \times \mathbf{E}_0 = 0 , \quad (1.4.27b)$$

$$\nabla \cdot \mathbf{B}_0 = 0 , \quad (1.4.27c)$$

$$\frac{\mathbf{j}_0}{\sigma} = \mathbf{E}_0 + \mathbf{u}_0 \times \mathbf{B}_0 , \quad (1.4.27d)$$

$$\varrho_0 \cdot (\mathbf{u}_0 \cdot \nabla) \mathbf{u}_0 = -\nabla p_0 + \mathbf{j}_0 \times \mathbf{B}_0 , \quad (1.4.27e)$$

$$\nabla \cdot (\varrho_0 \mathbf{u}_0) = 0 , \quad (1.4.27f)$$

$$p_0 = C \varrho_0^\gamma . \quad (1.4.27g)$$

Note that in the equation of motion we choose to simplify by eliminating friction and gravity. The average medium is assumed to be homogeneous in pressure, density and magnetic field, moreover we assumed that the bulk of plasma is at rest ( $\mathbf{u}_0 = 0$ ) so that  $\mathbf{j}_0 = 0$  (1.4.27a) and also  $\mathbf{E}_0 = 0$  (1.4.27d). This could be seen as a description for a plasma of high conductivity ( $\sigma \rightarrow \infty$ ). After these consideration we can write down the homogeneous linear system for the fluctuating quantities

$$\nabla \times \mathbf{B}_1 = \mu_0 \mathbf{j}_1 , \quad (1.4.28a)$$

$$\nabla \times \mathbf{E}_1 = -\frac{\partial \mathbf{B}_1}{\partial t} , \quad (1.4.28b)$$

$$\nabla \cdot \mathbf{B}_1 = 0 , \quad (1.4.28c)$$

$$\mathbf{E}_1 = -\mathbf{u}_1 \times \mathbf{B}_0 , \quad (1.4.28d)$$

$$\varrho_0 \frac{\partial \mathbf{u}_1}{\partial t} = -\nabla p_1 + \mathbf{j}_1 \times \mathbf{B}_0 , \quad (1.4.28e)$$

$$\frac{\partial \varrho_1}{\partial t} = -\nabla \cdot (\varrho_0 \mathbf{u}_1) , \quad (1.4.28f)$$

$$\frac{p_1}{p_0} = \gamma \frac{\varrho_1}{\varrho_0} . \quad (1.4.28g)$$

If we suppose the solution to be a plane wave like (1.4.17) we can substitute temporal derivative and the nabla operator as follow

$$\frac{\partial}{\partial t} \rightarrow -i\omega \quad \nabla \rightarrow i\mathbf{k} . \quad (1.4.29)$$

so that we can rewrite, where is necessary, the fluctuating quantities as:

$$i\mathbf{k} \times \mathbf{B}_1 = \mu_0 \mathbf{j}_1, \quad (1.4.30a)$$

$$\mathbf{k} \times \mathbf{E}_1 = \omega \mathbf{B}_1, \quad (1.4.30b)$$

$$i\mathbf{k} \cdot \mathbf{B}_1 = 0, \quad (1.4.30c)$$

$$-i\omega \varrho_0 \mathbf{u}_1 = -\nabla p_1 + \mathbf{j}_1 \times \mathbf{B}_0, \quad (1.4.30d)$$

$$\omega \varrho_1 = \mathbf{k} \cdot (\varrho_0 \mathbf{u}_1). \quad (1.4.30e)$$

An important class of waves are the Alfvén waves, these are transversal waves propagating parallel to the magnetic field, thus their formation depends on the degree of magnetization of the system defined by parameter

$$\beta = \frac{p}{p_{mag}} = \frac{nT}{B^2/2\mu_0}.$$

From the previous equations set, it is possible to show that the dispersion relation of an Alfvén wave is given by:

$$\omega^2 = \frac{B_0^2}{\mu_0 \varrho_0} k^2. \quad (1.4.31)$$

We can easily see solving equation (1.4.18) and (1.4.19) for (1.4.31) that group and phase velocity are the same and they are equal to the Alfvén speed

$$v_A = \frac{B_0}{\sqrt{\mu_0 \varrho_0}}, \quad (1.4.32)$$

this property means that the wave is not dispersive. Another important aspect of Alfvén speed is that it is the fastest perturbation that can propagate along the magnetic field so that if a disturbance goes faster a shock wave arise. Unfortunately laboratory observation are quite difficult due to the long wavelength of the Alfvé wave given by

$$\lambda_{\parallel} = 2\pi \sqrt{\frac{m_i}{\mu_0 e^2 n}},$$

for example in Njord with a density of  $10^{16} \text{m}^{-3}$  and  $m_i = m_{H^+}$  we get  $\lambda_{\parallel} = 14 \text{m}$  that is much longer of the 1.5m length we have in Njord.

### 1.4.1 Ion Cyclotron Waves

Ion cyclotron waves are longitudinal oscillation of ions in a magnetized plasma moving almost perpendicular to the magnetic field axis. The dispersion relation is given by

$$\omega^2 = k^2 v_s^2 + \omega_{ci}^2, \quad (1.4.33)$$

where we use the sound speed  $v_s$  defined as

$$v_s = \sqrt{\frac{\gamma p_0}{\rho_0}}.$$

The two terms on the right hand side of the equation (1.4.33) can be explained separately. The first one is derived from equation (1.4.28e) considering only the pressure gradient term so that we can write

$$\rho_0 \frac{\partial \mathbf{u}_1}{\partial t} = -\nabla p_1. \quad (1.4.34)$$

Now we can apply to (1.4.34) the transformation of equation (1.4.29) obtaining

$$\omega \rho_0 \mathbf{u}_1 = \mathbf{k} p_1, \quad (1.4.35)$$

isolating term  $\mathbf{u}_1$  in equation (1.4.28f) and term  $p_1$  in equation (1.4.28g). Now substituting them in equation (1.4.35) we get

$$\frac{\omega^2 \rho_1}{k} = k \gamma p_0 \frac{\rho_1}{\rho_0}. \quad (1.4.36)$$

Using the  $v_s$  definition given above we can write the dispersion relation as

$$\omega^2 = k^2 v_s^2. \quad (1.4.37)$$

This is an Ion-Acoustic Wave. Now the introduction of a magnetic field creates a difference between those ions that move along the magnetic field and those who move perpendicular to it. The former one will be not affected by the Lorentz force, while the latter will suffer a gyrate motion. We can understand these waves as the superposition of two motions. The Ion-acoustic wave creates regions of compression and rarefaction, the magnetic field force them into elliptical orbits instead of moving along a straight line. Under these condition two restoring forces act on the ions generating two superimposed frequencies [7].

In space plasma, electrostatic ion cyclotron waves have been observed in several occasions, in particular associated with magnetic-field-aligned currents, up-flowing ion beams and optical emission of auroral arc; but it is still unclear what the driving mechanism of such waves is. Laboratory experiments have discovered connection with the current-driven electrostatic

ion cyclotron instability. Those have been studied in Q-machines and their connection to ion heating, transverse ion heating and anomalous resistivity has been shown. In some laboratory experiments, the observation of Ion Cyclotron Waves connected with three-dimensional double layer of which we will talk in the next section has been reported.

### 1.4.2 Double Layer

An electric double layer (DL) is a narrow localized potential region within a plasma, not directly attached to a wall, which can sustain a large potential difference [5, 8].

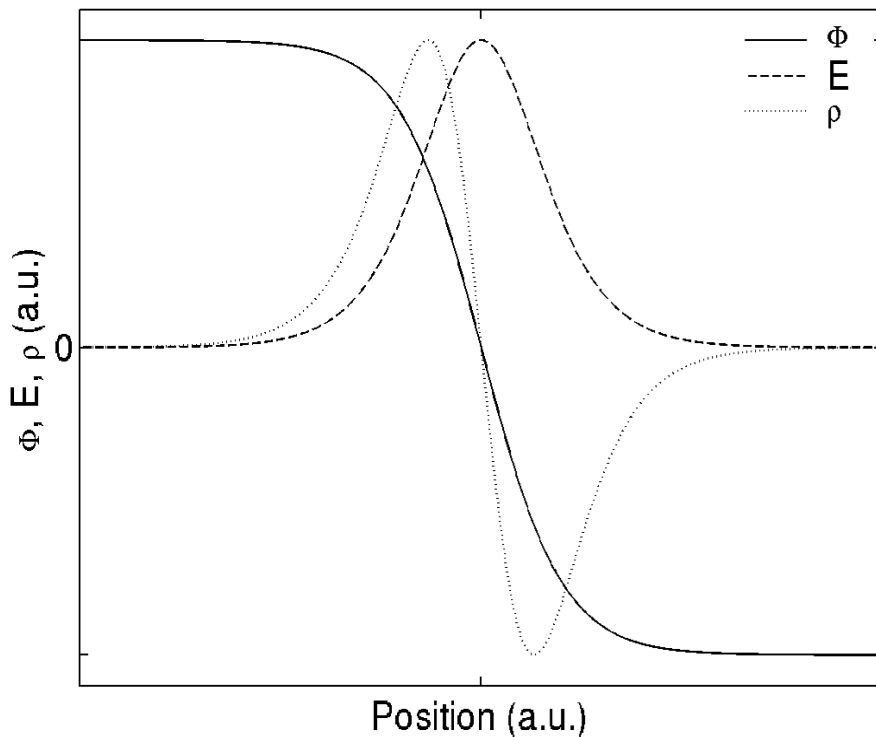


Figure 1.3: Potential (solid), Electric field (dashed) and charge density (dotted) in a double layer. Credit: A.Meige, Ph.D Thesis, ANU, 2006.

Although globally a double layer has no net charge and the surrounding plasma has no significant electric field, the quasi-neutrality within the double layer is not satisfied. We can imagine it as composed of a layer of positive

charge, wrapping the plasma potential like a normal sheath, and a layer of negative charge (see figure 1.3), wrapping the plasma potential back in the other direction, in order to join to the null-electric-field plasma. On each external side of the double layer the plasma may suffer some kind of perturbation due to the extended pre-sheaths, the border condition of a double layer edge is like the one of a normal sheath.

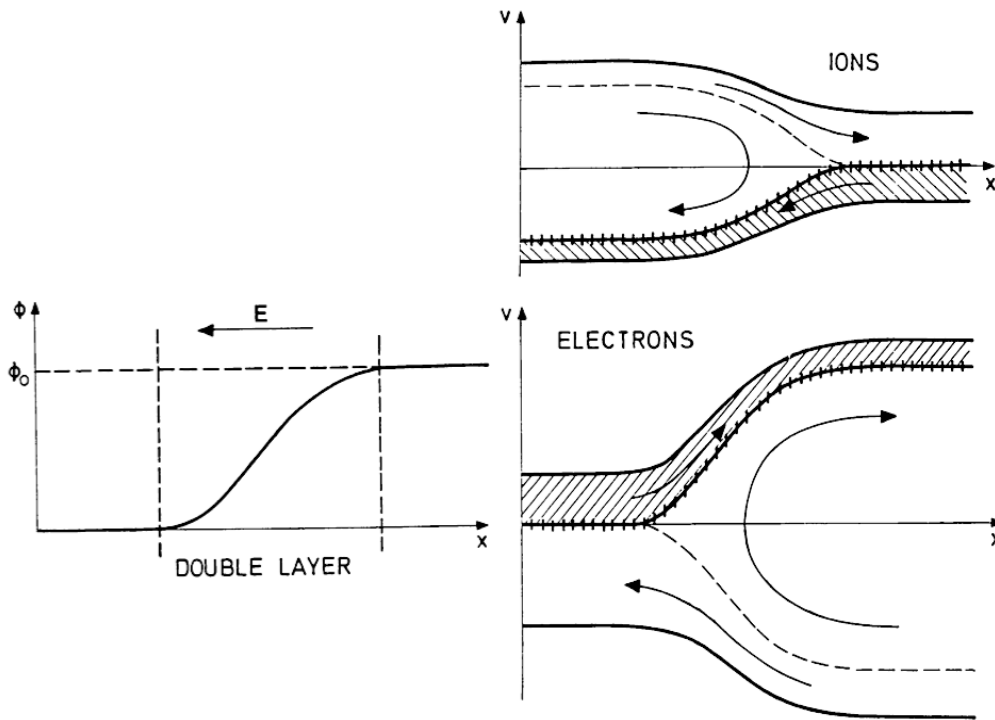


Figure 1.4: On the right: potential distribution of a double layer, on the left: phase space plot in which the different families, hatched and clear areas, are recognizable . Credit: A.Meige, Ph.D Thesis, ANU, 2006.

Double layers can be classified with different methods; the most important is based on the ratio between the potential drop and the plasma thermal potential  $e|\Phi_{DL}|/k_B T_e$ . For high values of this ratio the double layer is said to be strong, in this case the positive and negative charge into the double layer can be subdivided in four families. As in shock theory the two side of the double layer are called upstream (high-potential side) and downstream (low-potential side), ions in the upstream and electrons in downstream side are accelerated through the potential drop on the opposite side, see figure (1.4). If they are instead in the "wrong" side of the double layers, charged

particles will lose energy due to the potential drop. Depending on particle energy and strength of the double layer we could have all or some particles reflected back by the potential barrier. The weaker the double layer is, the higher the number of particles that are able to cross the it will be. It is clear how the four particle families arise and how two different plasmas face each other at the boundary. It's therefore possible to imagine the double layer as a sheet that plasma creates to shield itself from others kinds of plasmas, as, it happens, in presence of a chamber wall<sup>6</sup> [5]. Another way to classify double layers consider the presence of a driving current. For decades, laboratory experiments have been successfully demonstrated the case of current-driven DL, the main production methods are by means of gas-discharges, double plasma machine and plasma expansion in diverging magnetic fields. Lately some experiments had show current-free double layers in plasma expansion regions with high velocity ion beams in the downstream regions, those structures have interesting application in material etching, ion thrusters and provide explanation for ion acceleration in the aurora zone. Bernstein-Greene-Kruskal proved the existence of a class of solution [9] (BGK solution) to the Vlasov equations containing potential structures satisfying the condition shown before that we summarize here:

- $\Phi_{DL} > k_B T_e / e$  where  $\Phi_{DL}$  is the potential drop and  $T_e$  the electron temperature in the downstream.
- The electric field is much higher inside than outside the double layer, with a zero net charge considering the whole system.
- Quasi-neutrality violation at the double layer.

The BGK solution considers the case of four particle families, while for weak double layers the solution is satisfied for three only. The simplest case of the BGK solution was constructed by Langmuir and predicts that to ensure neutrality the electron and the ion current had to be related by

$$I_e = \sqrt{\frac{m_i}{m_e}} I_i ,$$

from the complete BGK solutions is valid only for strong double layers and is not stable.

The most definitive proof of double layers in space came from Viking satellite which measures the differential potential structures in the magnetosphere

---

<sup>6</sup>The theory of sheet formation at plasma boundary will be treated in chapter 3.1, pag. 49



with probe tips mounted 80m apart. These double layer structures usually have an extent of 100 m (a few tens of Debye lengths in space). Magnetospheric structures have an approximately strength ratio of about 0.1, thus they are considered weak double layers and as we said they are considered to play a fundamental role in particle acceleration in the aurora zone. Moreover for explaining ion acceleration and heating in the solar chromosphere it has been proposed that double layers could be a mechanism for energy release in solar flares. Laboratory experiments on double layers have been widely studied on different machines. Double, triple, Q-machine, discharge tube and arc plasma columns are a few examples, theory on double layers have found experimental verification on this devices<sup>7</sup>.

---

<sup>7</sup>A complete review of laboratory experiments on double layers has been written by N.Hershkowitz, *Review of recent laboratory double layer experiments*. Space Science Reviews, 1985



# Chapter 2

## Machine

Njord is a double plasma device since it consist of two different sources. The first one is a hot-filament discharge placed in the main chamber section, while the second one is an RF helicon source placed in the antenna section. In this chapter we will describe the Njord apparatus. In the first section we will focus on the description of the main chamber, the dome, and the DC source. In the second section we will discuss some vacuum technique principles, the pumping system implemented on Njord and the pressure monitoring and control apparatus. In the third section we will describe the theory of helicon waves, the antenna section of the machine and its power system. In last section we will describe the coils system present on Njord and some simulation of the magnetic field generated.

### 2.1 Main Chamber

In figure (2.1) we can see the later section of a model of Njord. All the principal component are visible. The chamber can be divided in three main pieces starting from the right we have the main section, the dome and the antenna. The main section is a stainless steel cylinder with 308mm and 300mm external and internal radius respectively and a total length of 1260mm. At the rear end there is a flange of 344mm that closes the cylinder. Along the sides of the cylinder there are 12 flange openings; they are placed, 3 on each side, on what we will call from now on the bottom, the top and the lateral sides of the cylinder. The eight standard DN 40 conflat flanges (CF) are at 300mm from the two endings while the four DN 100 CF are in the middle of each side (630mm from the two endings). On the rear cap we have a central DN 100 CF and around it six DN 40 CF.

In front of the rear DN 100 CF is mounted a grid for creating a bias

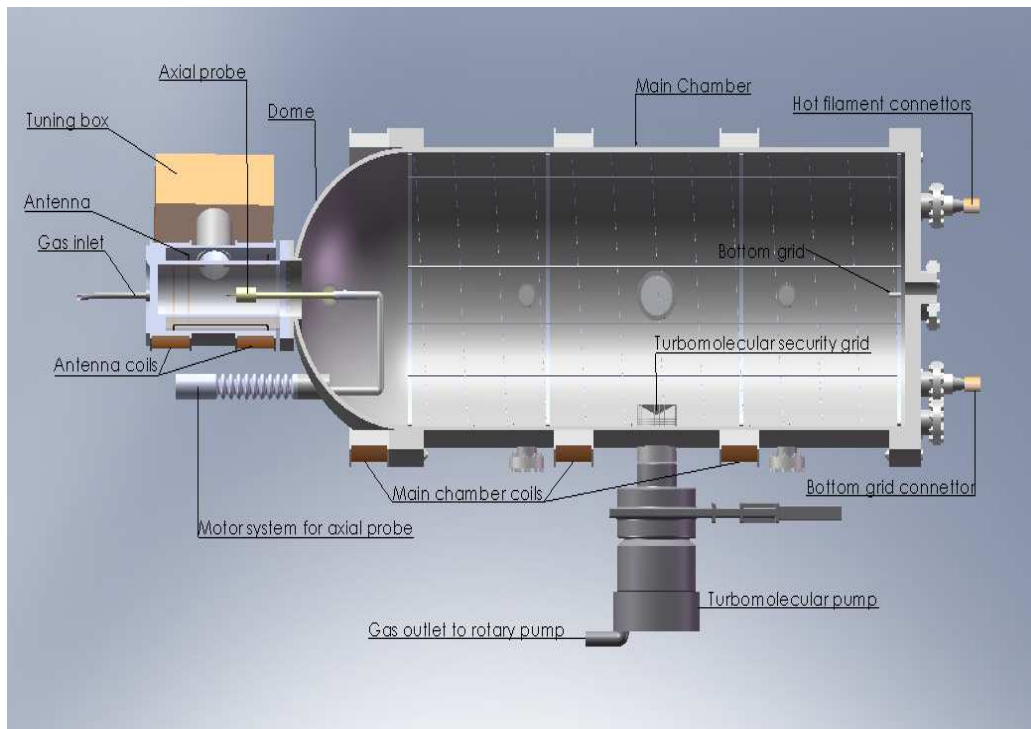


Figure 2.1: Lateral section of Njord

along the main axis of the chamber, the electrical connector to this grid is mounted on one of the rear DN 40 CF. The pressure gauge system and a valve for refill the chamber with air, are mounted on the rear top DN 40 CF, see figure (2.2). All the non used DN 40 CF are temporarily closed waiting for an eventually use in the future.

On the bottom side the DN 100 CF flanges is mounted the turbomolecular pump; inside the chamber, to protect the pump, a circular net with a concave cover has been placed over the flange. Even if this system is probably slowing down the pumping speed, it is necessary to avoid large pieces to fall into the pump and cause serious damage. The two lateral DN 100 CF, and the one mounted on the rear cap are equipped with windows. In particular the one mounted on the rear cap is useful, when the plasma is switched on, for checking the position of the radial probe, and the angular position of the axial one. The dome, on the front side of the main section, is connected with the main chamber by another flange of 344mm radius. The dome is also made of stainless steel and it is a half spherical shell of respectively 300mm and 295mm external and internal radius. There are four DN 40 CF on the dome. With the exception of the one mounted on the bottom side, that is

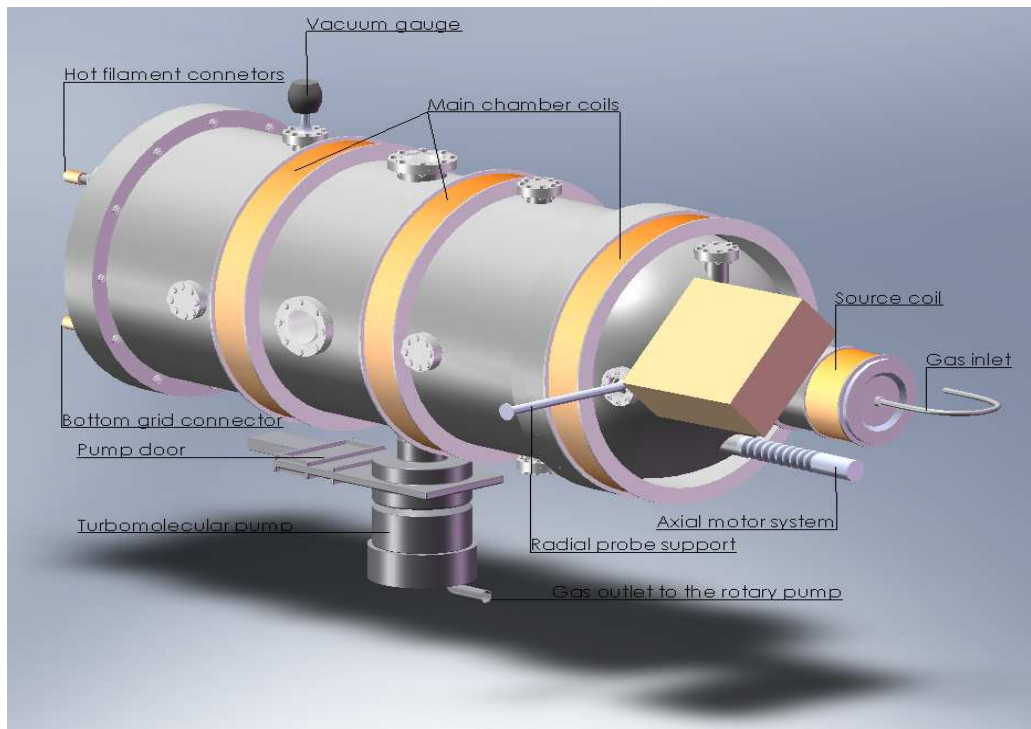


Figure 2.2: Model of Njord with main elements visible

facing on the same direction of the main section axis, the other three are directed radially. The bottom flange is used for inserting the axial probe while the one on the sides can be used for inserting the radial probe<sup>1</sup>. On the front of the dome there is another flange for mounting the antenna<sup>2</sup> with a diameter of 254mm.

## 2.2 Vacuum and pressure control

To produce a laboratory plasma it is necessary to reach work condition with a pressure lower than the normal atmospheric pressure. We must then use vacuum chamber, one or more vacuum pumps and tubes to link all these components. Starting from the pumping speed and the volume of the chamber it's possible estimate the time necessary to reach a pressure value and other parameters.

It's possible to distinguish five different ranges of vacuum:

<sup>1</sup>For more details on probe support see section 3.4.1, page 70.

<sup>2</sup>For more details on antenna lodging see section 2.3.2 page 34.

- from atmospheric pressure down to 1 mbar: low vacuum,
- from 1 mbar down to  $10^{-3}$  mbar: medium vacuum,
- from  $10^{-3}$  mbar down to  $10^{-8}$  mbar: high vacuum,
- from  $10^{-8}$  mbar down to  $10^{-12}$  mbar: ultra-high vacuum,
- under  $10^{-12}$  mbar: extremely high vacuum

During test we were able to reach down to  $10^{-6}$  mbar so that we were able to reach the high vacuum range. To reach this range in vacuum it is necessary to use different vacuum pump, since not all pumps are capable to reach high vacuum, and moreover pumps constructed for high vacuum are unusable at atmospheric pressure. For this reason the pumping system in Njord is composed of two pumps; the first one is a rotary pump that reduce pressure in the vacuum chamber from atmospheric pressure down to  $10^{-1}$  mbar, the second is a turbomolecular pump for higher vacuum. The latter cannot start pumping until the former has reduce the pressure enough to enter the operating range of the turbomolecular pump, in this case the rotary pump is also called backing vacuum pump. Both pumps are controlled in remote by a computer. When we want start pumping an first we shuld start the rotary pumo. In this way we reduce the pressure inside the chamber. After we reach the working pressure of the turbomolecular pump can be swithced on and the gate valve open.

### 2.2.1 Rotary pump

The simplest model of rotary pump is shown in figure refrotative.eps, it consist of a cylindrical chamber (Stator) inside which a piston (Rotor) rotates with a slightly inferior radius to the one of the chamber.

Inside the pistons are mounted two blades connected with a spring that keep the blades in contact with the chamber walls. The inlet port is connected to the vacuum chamber, the gas we want to expel through this outlet, flow into the rotative pump. The blades rotating are able to compress the gas in the small volume between the rotor and the chamber wall. When this volume reaches the exhaust valve the gas is expelled and the total amount of gas in the vacuum chamber is reduced. The system is put into an oil bath for multiple reasons. It is useful as seal between the exterior and the cylindrical chamber, in particular where the motor connect to the rotor, and is also useful as a lubricating and cooling system. The presence of the oil has some disadvantage, in fact some oil gas can flow into the stator chamber

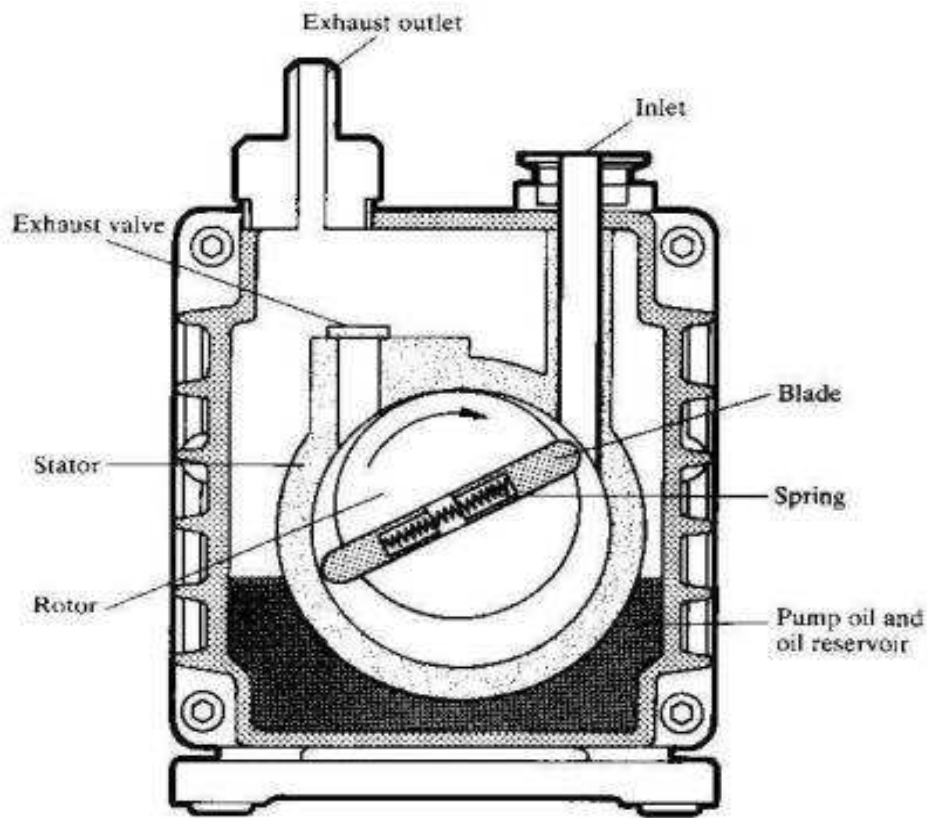


Figure 2.3: Rotative pump section

and from here flow back into the turbomolecular pump and up into the vacuum chamber. The rotative pump used is a Boc Edwards E2M28 with a peak pumping speed of  $0.45 \text{ m}^3/\text{sec}$ , a base pressure of  $10^{-3}$  mbar and a rotor speed of 1500 rpm. The rotative pump is controlled by a computer that open and close an electric valve, mounted on top of the Boc Edwards pump, between the rotary to the turbomolecular pump. When we want to start pumping the computer first switches on the rotative pump and opens the valve so that we decrease the pressure into the chamber to obtain the working pressure of the turbomolecular. When we want stop pumping the electrical valve close immediately to avoid backstream of oil into the vacuum chamber or into the turbomolecular pump.

### 2.2.2 Turbomolecular pump

The pumping system of a turbomolecular pump is based on moment exchange between the rotating blades and the singular gas molecules, this is possible only for angular velocity of the blades comparable to the thermal speed of the molecules.



Figure 2.4: Turbomolecular pump section

The inner structure of a turbomolecular pump is a chamber with multiple stages consisting of rotor/stator pairs mounted in series (Figure 2.4). Gas entering by the upper stages is pushed into the lower stages and successively compressed to the level of the fore-vacuum pressure. As the gas molecules enter through the inlet, the rotor, on which are mounted a number of angled blades, impacts on the molecules. Thus the momentum of the blades is transferred to the gas molecules and those have a lower probability to be reflected back by the blades than going forward. With this newly acquired momentum, the gas molecules enter into the stator. The stator function is



to slow down the molecules coming from the rotor in the smallest space as possible without decreasing the conductance of the system. Reducing the molecules speed is necessary for the next rotor to be effective and maintain a good compression ratio. For obtaining the maximum pumping speed it's necessary to have a small angle blades so that the conductance remain large, on the other side for performing a good compression ratio is necessary to have a large angle blades. To fulfill both these requirements the angle of the blades increase from the high vacuum to low vacuum zone, as visible in example figure (2.4).

Turbomolecular pumps must operate at very high speeds, and the friction heat buildup imposes design limitations. Some turbomolecular pumps use magnetic bearings to reduce friction and oil contamination. Because the magnetic bearings and the temperature cycles allow only for a finite clearance between rotor and stator, the blades at the high pressure stages are somewhat degenerated into spirals. The turbomolecular pump used is a Leybold 361C with a peak pumping speed of  $0.4 \text{ m}^3/\text{secm}$  a base pressure of  $10^{-10}$  mbar, a starting fore-pressure of  $10^{-3}$ - $10^{-2}$  mbar and a rotor speed of 45000 rpm. The control system of the pump is a Leybold Turbotronik NT20, a electronic frequency converter for remote and process control via analog and programmable control inputs and outputs. This system reads the pressure with its own vacuum gauge and when entering into the correct pressure range, it opens the gate with a pneumatic control. A thin membrane and a valve at the exhaust are present to protect the turbomolecular pump from excessive back pressure (i.e. after a power failure or leaks in the backing vacuum).

### 2.2.3 Pressure measurement and flow control

For measuring pressure inside the vacuum chamber we use a Boc Edwards WGR-S wide range vacuum gauge. This system is equipped with two different measurement method. The first one is a Pirani gauge for low vacuum pressure level while the second one for higher vacuum level is an inverted magnetron. The Pirani gauge consist of a wire heated by a current. The gas molecules that hit the wire cool down the wire, the amount of cooling is therefore proportional to the number of molecules, thus to the pressure in the chamber. The resistance of in a wire is proportional to its temperature, so that by measuring the resistance it is possible to evaluate the pressure. This type of measuring system is reliably good down to about  $10^{-3}$  mbar.

The inverted magnetron belongs to the family of the ionization gauges. Those gauges measure pressure indirectly by measuring the charged ions produced when the gas is bombarded with electrons and collected by a properly bias voltage. The lower the pressure is the lower will be the number of ions

produced. There are two different ways of creating electrons. In the hot-cathode they are created by thermionic emission, while in the cold-cathode by a high-voltage discharge. The inverted magnetron belongs to the cold-cathode group and can operate down to  $10^{-9}$  mbar. Such gauges cannot operate if the ions generated by the cathode recombine before reaching the anodes. If the mean-free path of the gas within the gauge is smaller than the gauge's dimensions, then the electrode current will be vanishingly small. This is the reason for using on the low-vacuum range another gauge system, the upper-limit to the detectable pressure is on the order of  $10^{-2}$  mbar. On the other side, the  $10^{-9}$  mbar operating limit is reached when the near-absence of a gas makes it difficult to establish an electrode current.

The flow control is performed by a Omega FMA 5400/5500 series capable of a max flow of  $20\text{cm}^3\text{min}^{-1}$ . The flow control is driven remotely by the computer. On the computer is possible to set up value of the flow and read the pressure change by the vacuum gauge. With this method it's often necessary to check the pressure and manually adjust the value for the flow control.

## 2.3 Antenna section and RF source

The main method for creating plasma in Njord is an RF source based on helicon waves. Experiments concentrating on plasma production with this method started with Boswell [16, 17] and double saddle coil antenna has been widely used in helicon wave research since the beginning. All experimental systems, including the antenna configuration, were empirically designed. How different antenna geometry excite different modes, in order to efficiently couple power to the plasma, is still being studies. In this section we will start with the main theory about helicon waves starting with a general description for waves in plasma [7]. We will then describe the antenna we used in Njord, it's housing and the tuning system. In the end we will briefly explain the secondary method for creating plasma in Njord

### 2.3.1 Helicon waves

We want to find the dispersion relation for helicon waves, let us consider an homogeneous cold plasma with  $s$  different species. As we made in section 1.4 we will use the common small-amplitude perturbations theory, where  $\mathbf{B}$  and  $n$  are the zero order quantities and the first order ones vary as  $e^{i(\mathbf{k}\cdot\mathbf{r}-\omega t)}$ . The electric displacement, according to Ampere's law, is defined as

$$\mathbf{D}(\omega, \mathbf{k}) = \boldsymbol{\epsilon}(\omega, \mathbf{k}) \cdot \mathbf{E}(\omega, \mathbf{k}) = \epsilon_0 \mathbf{E}(\omega, \mathbf{k}) + \frac{i}{\omega} \mathbf{j}(\omega, \mathbf{k}) , \quad (2.3.1)$$

where  $\boldsymbol{\epsilon}(\omega, \mathbf{k})$  is the dielectric tensor defined in term of the susceptibility  $\boldsymbol{\chi}(\omega, \mathbf{k})$ :

$$\boldsymbol{\epsilon}(\omega, \mathbf{k}) = \mathbf{1} + \sum_s \boldsymbol{\chi}_s(\omega, \mathbf{k}) . \quad (2.3.2)$$

For solving Maxwell's equations it is necessary to express the plasma current density

$$\mathbf{J} = \sum_s \mathbf{J}_s = \sum_s n_s q_s \mathbf{u}_s \quad (2.3.3)$$

in terms of the electric field  $\mathbf{E}$ . We can do this through  $\boldsymbol{\chi}_s$ :

$$\mathbf{J}_s = \boldsymbol{\sigma}_s \cdot \mathbf{E} = -i\omega\epsilon_0 \boldsymbol{\chi}_s \cdot \mathbf{E} . \quad (2.3.4)$$

To determine  $\boldsymbol{\chi}_s(\omega, \mathbf{k})$  and  $\boldsymbol{\epsilon}(\omega, \mathbf{k})$  we start from Lorentz equation for a generic species  $s$

$$m_s \frac{d\mathbf{u}_s}{dt} = q_s (\mathbf{E} + \mathbf{u}_s \times \mathbf{B}) , \quad (2.3.5)$$

that can be written at first order of approximation, using equation (1.4.29) as:

$$-i\omega m_s \mathbf{u}_{s1} = q_s (\mathbf{E}_1 + \mathbf{u}_{s1} \times \mathbf{B}_0) . \quad (2.3.6)$$

As usual we consider the magnetic field in the  $z$  direction so that  $\mathbf{B}_0 = \hat{\mathbf{z}}B_0$  and we break the projection of  $\mathbf{u}$  and  $\mathbf{E}$  on the  $xy$  plane into left and right circularly polarized waves.

$$u^\pm = \frac{1}{2}(u_x \pm iu_y) , \quad E^\pm = \frac{1}{2}(E_x \pm iE_y) . \quad (2.3.7)$$

For  $\omega > 0$ , the  $+$  mode is the left-hand circularly polarized amplitude and the  $-$  mode is the right-hand circularly one. Now we can solve equation (2.3.6) for  $u_s$  getting:

$$u_s^\pm = \frac{iq_s}{m_s \omega \mp \omega_{cs}} E^\pm , \quad u_{zs} = \frac{iq_s}{m_s} \frac{E_z}{\omega} . \quad (2.3.8)$$

Using equations (2.3.3) and (2.3.4) we obtain the susceptibilities

$$\chi_s^\pm = -\frac{\omega_{ps}^2}{\omega^2 \mp \omega\omega_{cs}} , \quad \chi_{zz,s} = -\frac{\omega_{ps}^2}{\omega^2} . \quad (2.3.9)$$

Now using equation (2.3.7) we can from the first equation of (2.3.9) get the remaining matrix component of the susceptibility tensor:

$$\chi_{xx} = \chi_{yy} = \frac{\chi^+ + \chi^-}{2}, \quad (2.3.10)$$

$$\chi_{xy} = -\chi_{yx} = \frac{i(\chi^+ - \chi^-)}{2}, \quad (2.3.11)$$

that leads us to write the cold-plasma dielectric tensor

$$\epsilon = \begin{pmatrix} S & -iD & 0 \\ iD & S & 0 \\ 0 & 0 & P \end{pmatrix} \quad (2.3.12)$$

using the following definition for S (sum) and D (difference):

$$S = \frac{1}{2}(R + L), \quad D = \frac{1}{2}(R - L). \quad (2.3.13)$$

For L (left) and R (right), with regards to the polarization of the wave

$$L = 1 + \sum_s \chi_s^+ = 1 - \sum_s \frac{\omega_{ps}^2}{\omega^2 - \omega\omega_{cs}}, \quad (2.3.14)$$

$$R = 1 + \sum_s \chi_s^- = 1 - \sum_s \frac{\omega_{ps}^2}{\omega^2 + \omega\omega_{cs}}, \quad (2.3.15)$$

and for P (plasma)

$$P = 1 - \sum_s \frac{\omega_{ps}^2}{\omega^2} \quad (2.3.16)$$

Now combining Faraday and Ampere's laws we obtain the wave equation for homogeneous plasma

$$\mathbf{k} \times (\mathbf{k} \times \mathbf{E}) + \frac{\omega^2}{c^2} \epsilon \cdot \mathbf{E} = 0, \quad (2.3.17)$$

that could be rewritten as

$$\mathbf{n} \times (\mathbf{n} \times \mathbf{E}) + \epsilon \cdot \mathbf{E} = 0, \quad (2.3.18)$$

using the dimensionless vector  $\mathbf{n} = \mathbf{k}c/\omega$ , that has the magnitude of the refractive index. Now defining  $\theta$  as the angle between the  $\hat{\mathbf{z}}$  direction, i.e. with the  $B_0$  field, and the  $\mathbf{n}$  vector. Considering the case in which  $\mathbf{n}$  lay in the  $xz$  plane we can write

$$n_{\parallel} = n \cos \theta, \quad n_{\perp} = n \sin \theta. \quad (2.3.19)$$

Using equation (2.3.12) we can rewrite (2.3.18) in matrix form

$$\begin{pmatrix} S - n_{\parallel}^2 & -iD & n_{\parallel}n_{\perp} \\ iD & S - (n_{\parallel}^2 + n_{\perp}^2) & 0 \\ n_{\parallel}n_{\perp} & 0 & P - n_{\perp}^2 \end{pmatrix} \begin{pmatrix} E_x \\ E_y \\ E_z \end{pmatrix} = 0 \quad (2.3.20)$$

If  $n_{\parallel}$  is set by plasma parameter the it's possible to solve equation (2.3.20) for  $n_{\perp}$  by setting the determinant of the matrix equal to zero. The solution is given by

$$An_{\perp}^4 + Bn_{\perp}^2 + C = 0 \quad (2.3.21)$$

Where we defined

$$A = S,$$

$$B = (n_{\parallel}^2 - S)(S + P) + D^2,$$

$$C = P[(n_{\parallel}^2 - S)^2 - D^2].$$

The solution of equation (2.3.21) are found via the general quadratic solution

$$n_{\perp}^2 = \frac{-B \pm \sqrt{B^2 - 4AC}}{2A},$$

when  $B^2 \gg 4AC$  we get two real and distinct solutions. This correspond to slow ( $n_{\perp s}$ ) and fast ( $n_{\perp f}$ ) waves expressed by

$$n_{\perp s}^2 = \frac{-P}{S}(n_{\parallel}^2 - S) - \frac{D}{S}, \quad (2.3.22)$$

$$n_{\perp f}^2 = \frac{D^2 - (n_{\parallel}^2 - S)^2}{(n_{\parallel}^2 - S) + D^2/P}. \quad (2.3.23)$$

The helicon wave is a fast wave with a high index of refraction (i.e.  $n_{\parallel}^2 \gg S, D^2/P$ ) and its frequency lies between the ion cyclotron frequency and the electron cyclotron frequency ( $\omega_{ci} \ll \omega \ll \omega_{ce}$ ). We can then from equation (2.3.23) obtain the dispersion relation

$$n_{\parallel}^2 n_{\perp f}^2 + n_{\parallel}^4 = D^2 \approx \left( \frac{\omega_{pe}^2}{\omega \omega_{ce}} \right)^2, \quad (2.3.24)$$

that can be written in terms of the wave number

$$k_{\parallel}^2 k_{\perp f}^2 + k_{\parallel}^4 = \left( \frac{\omega \omega_{pe}^2}{\omega \omega_{ce} c^2} \right)^2. \quad (2.3.25)$$

### 2.3.2 Njord antenna

The housing of the antenna is mounted on the lange of the dome. The two flanges are not in direct contact, they are divided by 10mm lock washer so that air can flow inside the antenna and cool down the entire system. The housing is made of alluminium and consist of a cylinder of 300mm length, 120mm outer and 117mm inner radius. On the outside of the cylinder are mounted two coils<sup>3</sup> that we will call source coils (to distinguish them from the chamber coils). On the outside at in the middle of the cylinder, we have the support for the tuning box, see figure (2.5), which contains the tuning system. Through this cylinder pass the two connectors of the antenna. On the inner side of the flange mounted into the dome is present an o-ring with a diameter of 150mm. On this o-ring is mounted the pyrex tube which will maintain the vacuum into the source.

Pyrex is a brand name for a heat-resistant glass, it is necessary to use this kind of glass due to the high temperatures we will have into the source. The cooling system for this tube is ensured, as mentioned, by the 10mm lock washer that keep the antenna apart from the flange of the dome, letting ambient air flowing inside. On the other side of the antenna with respect to the flange we have the backplate. This is made in aluminium and, as the dome flange, has an o-ring mounted internally to close the pyrex tube and seal the vacuum. When the pumping start it is necessary to check that this component is well inserted otherwise some leak could arise. At low pressure is the vacuum itself to keep the backplate in position and guarantee the vacuum. In all our further measurement the inside face of this backplate, is considered as the zero position for the z-axis that runs along cylinder axis of Njord. In the center of the back plate we have a hole that we use as gas inlet, it is closed by a manual valve which is followed by the flow meter we described in section 2.2, page 25.

The double saddle antenna we use on Njord consists of two current loops on either side of the vacuum tube. The shape of the main body of the antenna

---

<sup>3</sup>For a complete description of coils mounted on Njord see section 2.4, page 41.

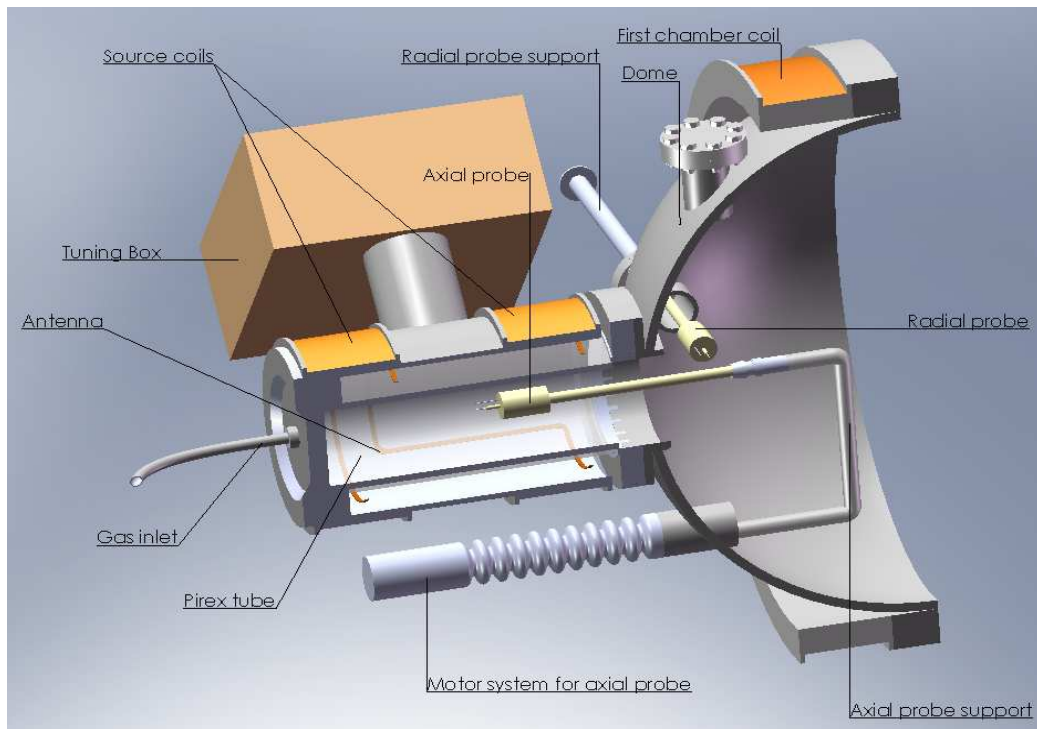


Figure 2.5: Njord antenna lodging lateral section

is sketched in figure (2.6).

The entire body, and also the connectors with the tuning box are made of copper. In our sketch we changed the color of those connectors to make the double saddle shape more visible. The width of the antenna wire is 5mm while the length of one saddle ring is of 230mm. The two saddles are not facing each other, watching the antenna from a frontal view and taking the zero angle at the connector position, the center of first saddle is at  $-45^\circ$  while the second one is at  $90^\circ$ . The diameter circumscribed by the antenna is 170mm. In the point where the two rings meet it is necessary to insert a teflon spacer to keep them well separated, during the preliminary test arcing was noticed (i.e. at plasma ignition some discharges were audible and the plasma light was quivering). This phenomenon was due to two screws mounted inside the teflon, for keeping it close to the antenna. Those screws were too long and extruding from the teflon, being exposed to the RF current they were creating arc discharges between the pyrex tube and the steel chamber. Since those discharges could become dangerous for the pyrex integrity the spacer was dismantled and modified to ensure a better coverage of the two screws.

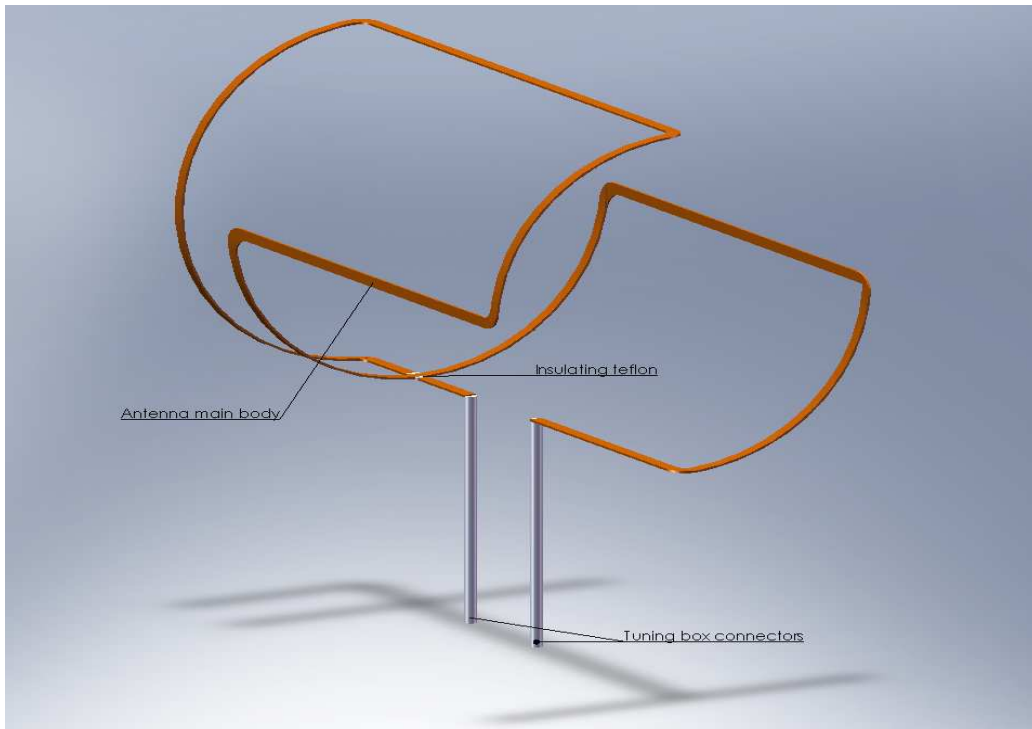


Figure 2.6: Double saddle antenna

On each of the four long side of the antenna, are mounted 2 teflon spacer of about 10mm; those are fixed from the outside of the stainless steel cylinder with screws, to guarantee that the antenna is not going to touch the external wall.

### 2.3.3 Power and tuning system

The power system of the antenna is composed of a wave generator, a pre amplifier and two additional amplifiers. The wave generator is Wavetek-3001 with a generation range between 1 MHz and 520 MHz and a precision of  $\pm 0.001\%$  and a minimum step variation of 1 KHz. The signal out of the generator is fed to the pre-amplifier that is a ENI-411LA with an available band between 150 KHz and 300MHz and an output of 10 W. After this stage we have the first of the two amplifier, which is an Ameritron AL-80B with a frequency band between 1.8 and 21 MHz and a maximum output of 500 W. The second amplifier is a Henry Radio 8K Ultra. The ameritron amplifier is necessary to fed to the Henry Radio amplifier the minimum power input that it needs to work (about 100 W). Is composed of a remote control station,



mounted close to Njord and the previous amplifier, and the amplifier itself mounted on the same rack where we have the power supply for the coils and the filament. This model has a frequency band between 1.8 and 30 MHz and a theoretical output up to 5000 W. Mounted on the remote control station of the Henry Radio amplifier we have a wattmeter MFJ-860 that has been customized to lodge the two buttons that are necessary to power up the antenna. The choice of using two buttons is a security system made to avoid unwanted ignitions of the plasma.

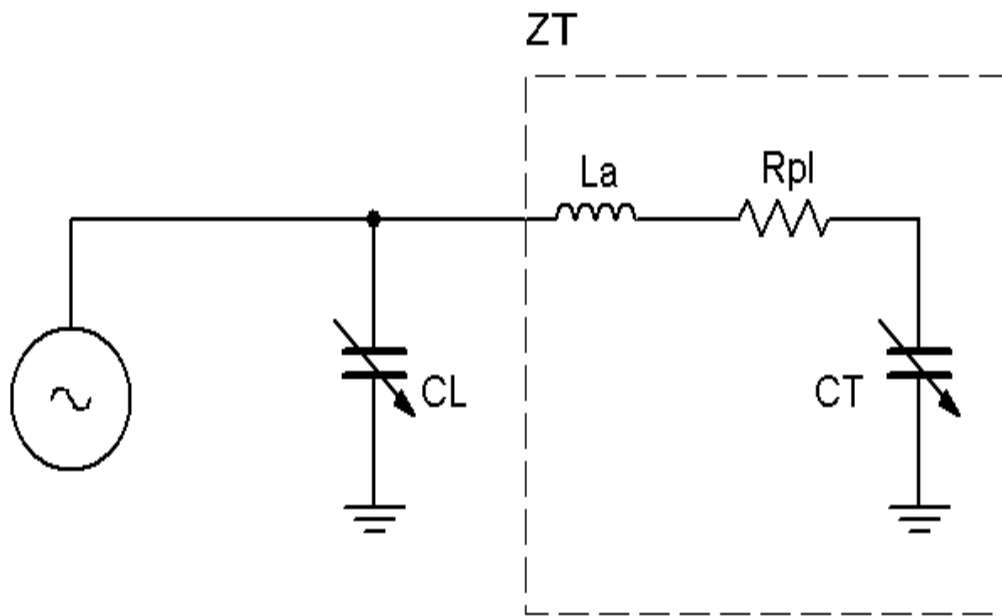


Figure 2.7: Equivalent circuit of the  $\pi$ -network, the two capacitance are mounted into the tuning box

To ensure that the transmission line from the RF transmitter is terminated at its characteristic impedance the antenna is incorporated into a  $\pi$ -network. In figure (2.7) we show the equivalent circuit of the  $\pi$ -network in which: inductance  $L_a$  stands for the antenna, resistance  $R_{pl}$  is the electrical resistance of the antenna when the plasma is switched off, which increases when plasma is on. It is necessary to estimate the load and the tuning capacitance ( $C_L$ ,  $C_T$ ) for better designing the  $\pi$ -network we will use. Let us group  $L_a, R_{pl}$  and  $C_T$  and call them the tune arm. Its impedance is

$$Z_T = i\omega L_a + \frac{1}{i\omega C_T} + R_{pl} , \quad (2.3.26)$$

that can be written dividing real from imaginary part as

$$Z_T = i\tilde{L} + R_{pl} , \quad (2.3.27)$$

where  $\tilde{L}$  is defined as

$$\tilde{L} = \omega L_a - \frac{1}{\omega C_T} . \quad (2.3.28)$$

Now let's assume that the tune capacitance does not completely cancel out the antenna inductance, then the load capacitance can balance the net inductive impedance of the tune arm. The admittance (i.e. the inverse of the impedance) of the tune and load arm can be written as

$$Y_T = \frac{R_{pl}}{R_{pl}^2 + \tilde{L}^2} - \frac{i\tilde{L}}{R_{pl}^2 + \tilde{L}^2} , \quad (2.3.29)$$

$$Y_L = i\omega C_L , \quad (2.3.30)$$

So that the total admittance of the  $\pi$ -network is given by

$$Y_{total} = Y_T + Y_L , \quad (2.3.31)$$

To find values of  $C_L$  and  $C_T$ , we should impose a resonance condition (i.e. along the tuning arm we only see real impedance); we then impose that the total conductance (i.e. the real part of the admittance) will equal the inverse of the total line impedance  $Z_{tot}$ , and the susceptance (i.e. the imaginary parte of the admittance) of the two arms will cancel. These two conditions give us, respectively, the following equations

$$\tilde{L}^2 = R_{pl}(Z_{tot} - R_{pl}) , \quad (2.3.32)$$

$$C_L = \frac{\tilde{L}}{R_{pl}Z_{tot}\omega} . \quad (2.3.33)$$

For the antenna we are using it is possible to assume that  $Z_{tot} \gg R$  so that equation (2.3.32) gives

$$\tilde{L} = \sqrt{R_{pl}Z_{tot}} . \quad (2.3.34)$$

Now combining equations (2.3.33) and (2.3.34) we get the formula for the load capacitance

$$C_L = \frac{1}{\omega \sqrt{R_{pl} Z_{tot}}} , \quad (2.3.35)$$

and substituting equation (2.3.28) into (2.3.32) we get the formula for the tune capacitance

$$C_T = \frac{1}{\omega^2 L_a - \omega \sqrt{R_{pl} Z_{tot}}} . \quad (2.3.36)$$

Taking a typical case with  $L = 0.5 \mu\text{H}$ ,  $R = 1 \Omega$ ,  $Z_{tot} = 50 \Omega$ ,  $\omega = 2\pi f = 85.2 \text{ MHz}$  and using equations (2.3.35) and (2.3.36) we get:  $C_L = 1650 \text{ pF}$  and  $C_T = 330 \text{ pF}$ . In Njord we use two Meiden vacuum variable capacitor, for  $C_L$  we use the model SCV-520M with a variable capacitance between 85 and 2000 pF, a peak working voltage of 3 kVp and a maximum RF current of 100  $A_{rms}$  (at 13.56 MHz). For  $C_T$  we use the model SCV-155M with a variable capacitance between 50-500 pF, a peak working voltage of 9 kVp and the same maximum RF current of  $C_L$ . Both capacitors are mounted inside the tuning box, which is made of copper, so that it acts as a Faraday cage. On one bottom side of the tuning box a 120mm fan is mounted to ensure cooling for the two capacitors.

Measuring the power being coupled into the plasma is very important for defining correctly the plasma parameters we are working with. The antenna radiation resistance is the principle measure of the efficiency of an antenna. The voltage and current on the line are given in terms of forward and reflected voltage and current by the following expression

$$V_{tot} = V_{fwd} + V_{ref} , \quad (2.3.37)$$

$$I_{tot} = I_{fwd} + I_{ref} = \frac{V_{fwd} + V_{ref}}{Z} , \quad (2.3.38)$$

Combining these last two equations we can obtain a formula for  $V_{fwd}$  and  $V_{ref}$  as

$$V_{fwd} = \frac{V_{tot} + ZI_{tot}}{2} , \quad (2.3.39)$$

$$V_{ref} = \frac{V_{tot} - ZI_{tot}}{2} , \quad (2.3.40)$$

from which we get a formula for forward and reflected powers

$$P_{fwd} = \frac{(KV_{fwd})^2}{Z} , \quad (2.3.41)$$

$$P_{ref} = \frac{(KV_{ref})^2}{Z}, \quad (2.3.42)$$

where  $K$  is a calibration factor. If the helicon wave dissipates power into the plasma, i.e. gives energy to the plasma, we should be able to see it as a resistive load on the antenna. To evaluate this load we assume that when plasma is on, as we said, the resistance of the antenna is given by the resistance of the antenna plus that of the plasma

$$R_{tot} = R_{ant} + R_{pl}. \quad (2.3.43)$$

The power dissipated by the antenna is by definition written as

$$I_{ant}^2 R_{tot} = P_{fwd} - P_{ref}. \quad (2.3.44)$$

Measuring  $R_{ant}$  without plasma we find, from the last two equations, a formula for  $R_{pl}$  that is the load of the antenna

$$R_{pl} = \frac{P_{fwd} - P_{ref}}{I_{ant}^2} - R_{ant}. \quad (2.3.45)$$

During measurements we usually read the power on the Henry Radio amplifier remote control panel, common values for forward and reflected power are respectively of about 300 W and 5 W with a pressure of  $5 \times 10^{-4}$  and a magnetic field generated by a current of 4 A.

### 2.3.4 Dc source and biasing

Inside the main section are mounted two stainless steel grids on which two thicker grids of 1mm wolfram wires take place, one on the rear section (from the rear ending to about 600mm) and one on the front section (from 660mm to the front end of the cylinder). These two section are electrically connected with the exterior through two different couple of flanges. The rear section has its connection on the rear flange cap, while the front section has connection with the front DN 40 CF mounted on the top and bottom side of the cylinder. These two sections constitute the DC source of Njord. When a current flow through these wires, and thus heat them due to the Joule effect, they will start to emit thermal electrons, and in presence of a proper bias the walls sputtering off fast electrons, which will be accelerated into the wall the neutral gas and create plasma.

## 2.4 Magnetic field

The magnetic field in Njord is provided by 5 coils. Two of them have a radius of 120 mm while the other three of 340 mm. The small coils, since they are mounted on the antenna lodging, are called source coils; the large ones are mounted on the dome and on the main section and are called chamber coils, see figures (2.1) and (2.2).

The two source coil are 95mm large and 20mm deep, they are made by a 1.8 mm diameter copper wire wrapped around the antenna lodging and connected with a Delta-Elektronika SM 120-25D power supply providing up to 25A at 120V. For knowing the magnetic field generated by this coils, we used an IDL simulation program. It's necessary to set up some parameters in a file named coils.dat, in particular: radius of the coil, current flowing through it, space occupied in  $\hat{z}$  and  $\hat{r}$  directions by the wire, number of wrapping in  $\hat{z}$  and  $\hat{r}$  directions and starting position of the coils. The radius is given by the external radius of the lodging, the current will be changed depending on which condition we want to simulate. To estimate the space occupied by the wire, that has an external diameter (considering the shielding) of 2mm, we should consider that in the  $\hat{r}$  direction the second layers of wires will lay on the gaps of the first layer, thus reducing the effective space occupied to about 1.6mm. On the  $\hat{z}$  direction we use a space of 2.3mm for take into account some gap between them in the wrappings. Considering these two values and the total coil dimension we can assume to have forty wires in the  $\hat{z}$  and twelve in the  $\hat{r}$  direction. Last parameter are the position of the coils, as we said we use the origin of the  $\hat{z}$  axis on the backplate's edge of the antenna. Thus we can consider the first source coil to be at a distance  $z = 0$ mm and the second one at  $z = 210$ mm. The simulation is made over a square that lies on the  $zr$  plane, covering a surface that goes from  $r = 0$ m to  $r = 0.2$ m and from  $z = 0$  m to  $z = 0.6$ m. We choose this dimension for having a better idea of the magnetic field intensity into the dome and into the pyrex tube of the antenna.

In figure (2.8) we plot the contour of the magnetic field intensity using the source coils with a current supply of 6A. In the image we also show the velocity field (white arrow) inside the pyrex tube along the antenna  $\hat{z}$  axis, this additional plot will come on handy when we will have different direction for the magnetic field. The dashed line represents the pyrex tube and the dome perimeter, to have a better idea of the position with respect to the chamber walls.

In this and the following figures the white color represent a saturated magnetic intensity value, the levels for colors has been choose to give as more information as possible in the zone of interest (i.e. on the left of the

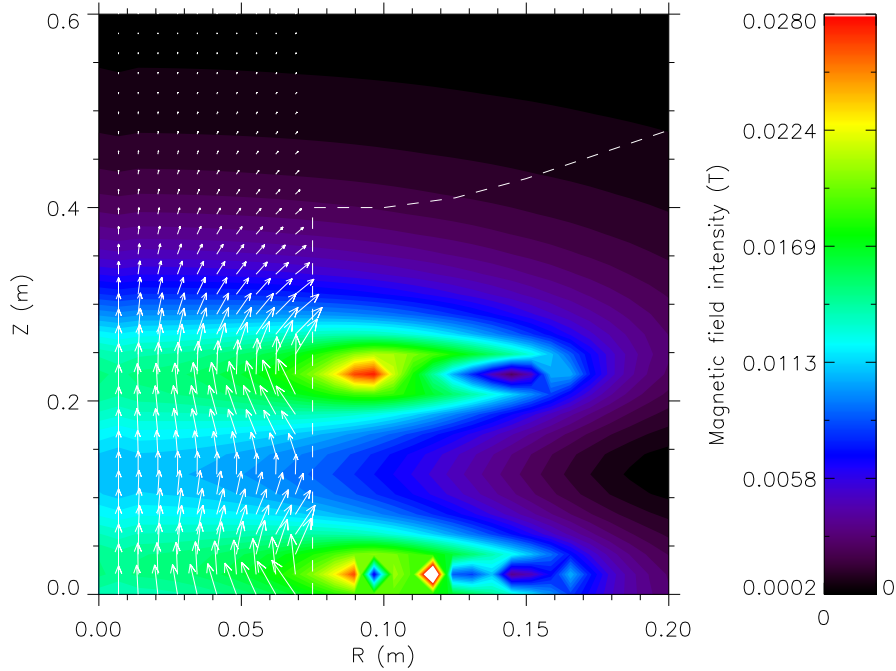


Figure 2.8: Magnetic field generated by source coils supplied by 6A.

dashed line). The magnetic field intensity as we could expect decrease with lower supplied current. In particular we will soon show how, with lower magnetic field, the intensity at the end of the pyrex tube and into the dome is less than 10G.

The first of the chamber coils is mounted on the dome close to the flange connector with the main section, it has 340mm radius, 90mm length and 35mm deep and it's wired with 3.5mm diameter copper wire connected with a Delta-Elektronika SM 120-50 power supply providing up to 50A at 120V. Considering the shielding of the wire (for a total diameter of 3.8mm) and the previous consideration we made, the space occupied by the each wrapping is 4.1mm and 3.1mm respectively in the  $\hat{z}$  and  $\hat{r}$  direction.

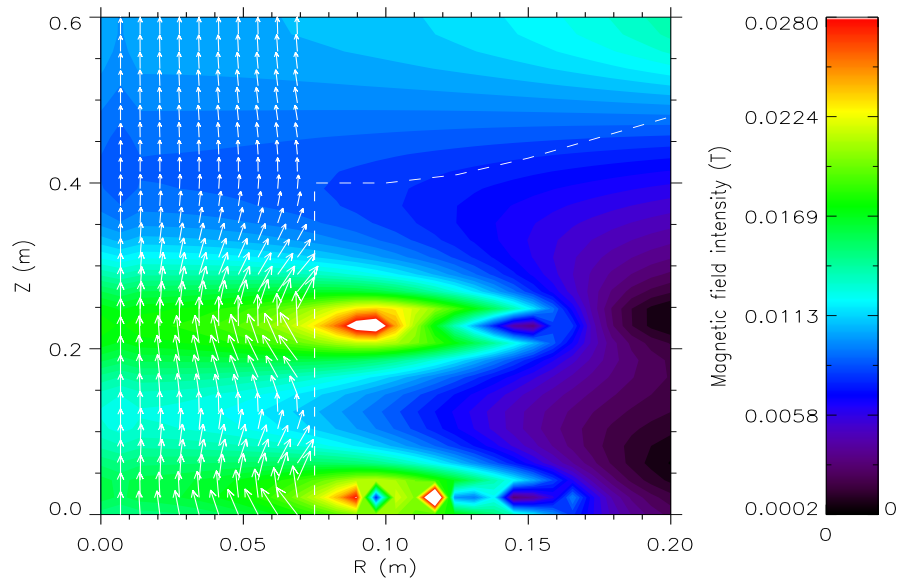


Figure 2.9: Magnetic field generated by source coils (6A) and by chamber coil (20A).

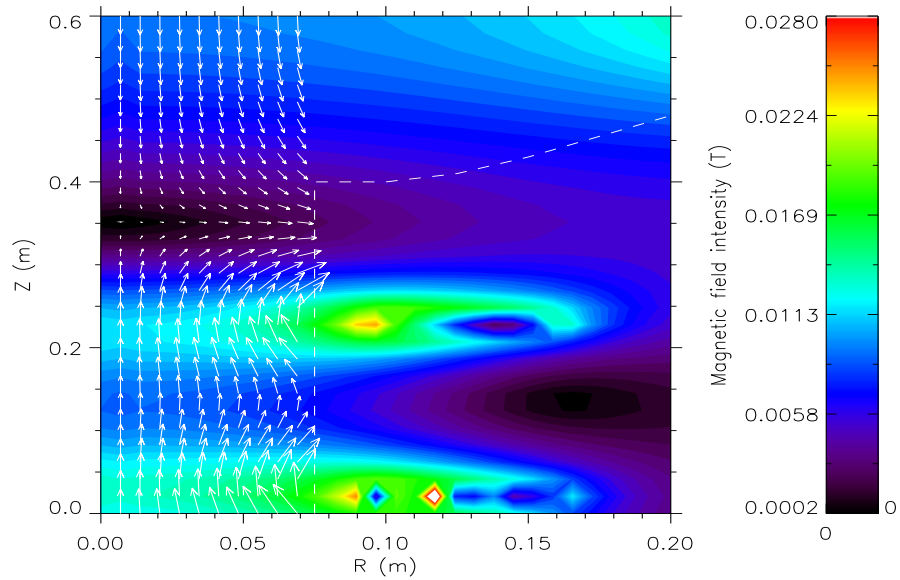


Figure 2.10: Magnetic field generated by source coils (6A) and by chamber coil (-20A).

In figure (2.9) and (2.10) we show the magnetic field intensity for a chamber coil in which respectively flows a 20A and -20A current. On the first case the coil generate a magnetic field with the same direction of the source coils, this configuration is useful to bring plasma outside of the source into the dome. In the second case the field is in the opposite direction, as shown by the white arrows on the left side. As we can see in this configuration we are able to create strong drops in magnetic field along the main axis inside the pyrex tube. Has been shown [?] using plasma simulation software that the the presence of strong and thin drops in magnetic field it's one of the necessary condition for creating double layers. We must point out that with this configuration can occur that along the  $\hat{z}$  axis at the end of the pirex tube the cuspid formed by the magnetic field lines could destroy the plasma confinement.

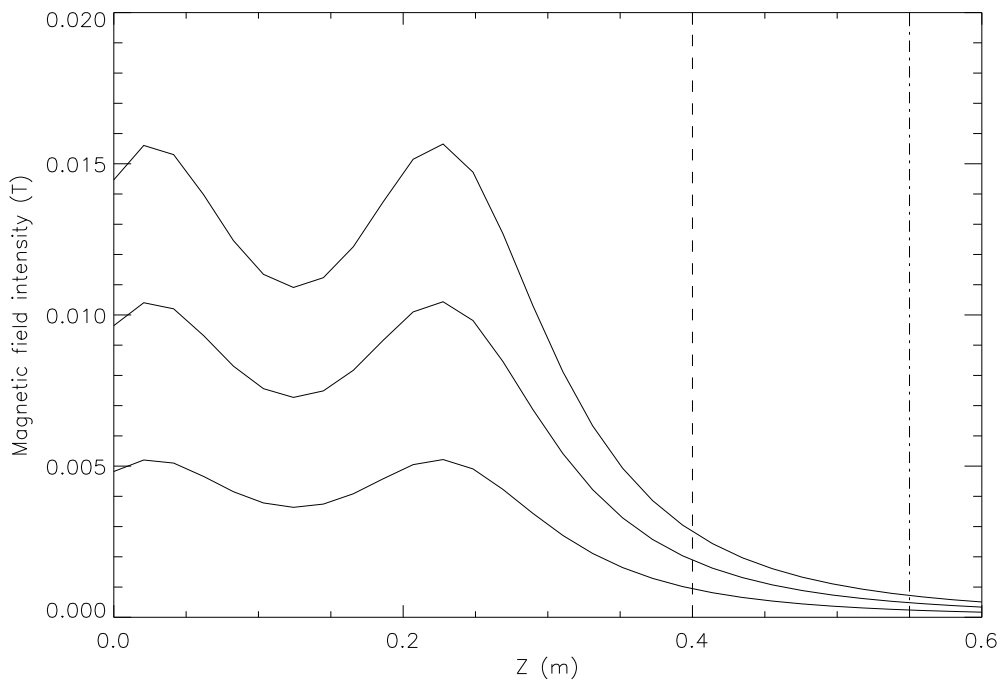


Figure 2.11: Magnetic field along  $\hat{z}$  generated by source coils supplied by 2,4 and 6A

To summarize the results from this simulation we show in figure (2.11) the magnetic field intensity, along the  $\hat{z}$  axis, generated only by the source coils with a current of 2,4 and 6A. The dashed line is the position at which the chamber enlarge into the dome and the dash-dot line is approximately



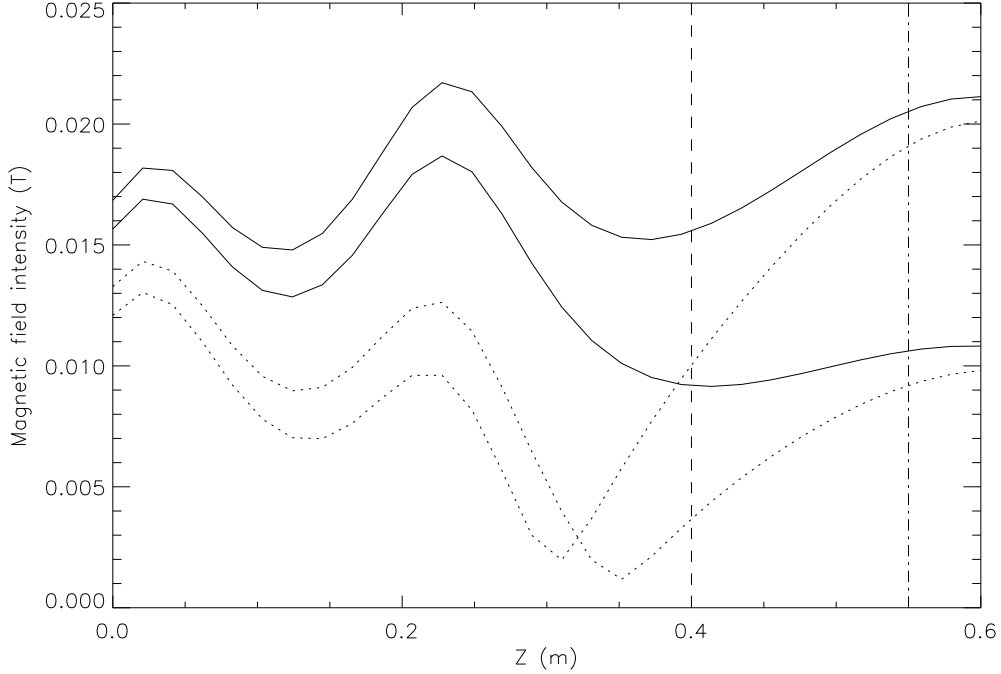


Figure 2.12: Magnetic field along  $\hat{z}$  generated by source coils (6A) and chamber coil: 20,40A (solid line) -20,-40A (dotted)

the position of the dome flanges (i.e. where we perform our radial scan). From this figure is clear how the source coils slightly affect the magnetic field inside the main chamber, even with 6A current the magnetic field is less than 30G at the dome edge and less than 10G where we perform radial measurement. On the second figure (2.12) we show the same plot but adding the first chamber coil, with positive current 20,40A (solid) and negative -20,-40A (dashed). The negative current, as we said above, stand for a opposite direction magnetic field. Adding the chamber coil with a current of 40A the magnetic field into the source is much higher; it has a minimum close to the dome edge and again a maximum close to the radial scan position. While for the 20A case the magnetic field is almost constant at 100G between the dome edge and the radial scan position. For the negative current case, it is easy to see that increasing current on the chamber coil the magnetic field drop will be steeper and will move inside the source toward the zero position of the  $\hat{z}$  axis.

While the heating of the chamber coils is not a problem, for the source

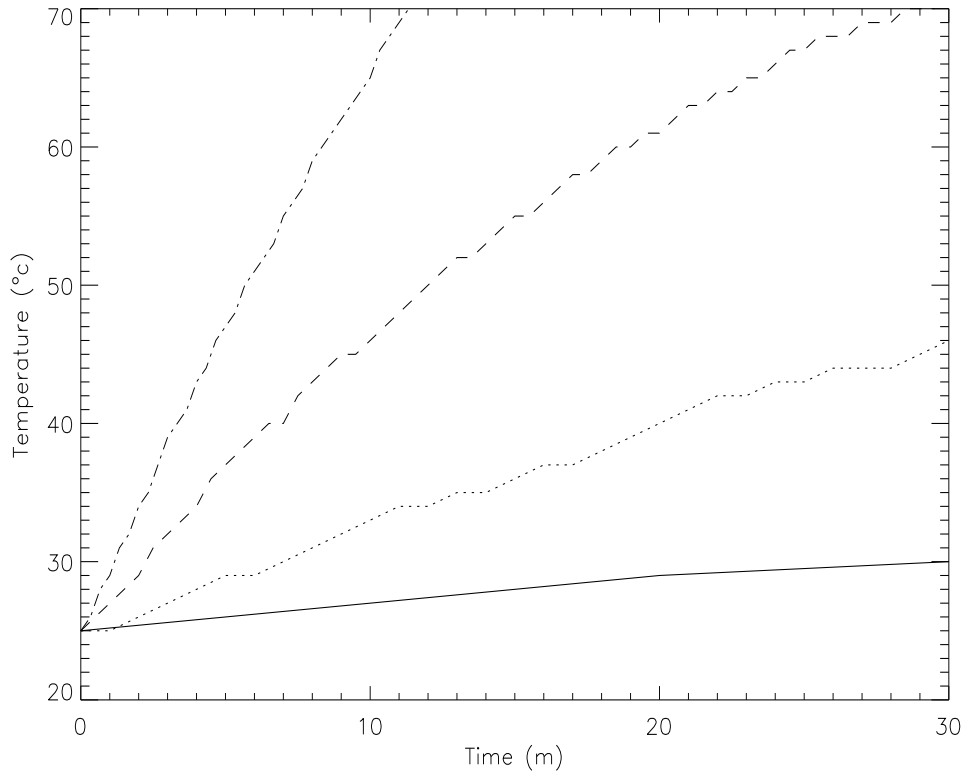


Figure 2.13: Source coils temperature for current equal to 2 (solid),4 (dotted),6 (dashed) and 8(dot-dashed)

coils (due to the smaller dimension and even if we used a lower current) in longer experiments that could become troublesome. Both coils are equipped with a temperature sensor connected with the computer, so that is it possible to read in real time the temperature of both coils. Without any kind of cooling system the temperature has been measured and plotted in figure (2.13) for 2,4,6 and 8A. The wires mounted on the coils are tested up to 130°C. From the figure we can see that performing long experiments at 2A or 4A should not presents any problem since the temperature rises but not enough fast to reach the critical temperature. Anyway, after thirty minutes it seems that in both cases an equilibrium has been reached between the heating from the current and the cooling provided by the room temperature. For 6A the rise in temperature is steeper, after thirty minutes it seem to start an asymptotic behavior so that the system could be used continuously but with a constant monitoring on the temperature after long times. In the 8A

case the temperature goes up much faster and we were not able to perform a thirty minutes test, therefore, if it will be necessary to perform test with this, or higher, current, will be mandatory to let the coils cool down very often. These test have been performed without any kind of cooling system on the source coils, in case a extensive use it might be a good idea to project and build some kind of fan system for allowing more longer experiments or higher current supply.



# Chapter 3

## Diagnostic

For the primary investigation on Njord we used probes since they are easy to implement with respect to others diagnostic techniques (like interferometry for example) and offers lot of different possibility for studying different parameters. The plasma behavior near a probe is similar to its behavior near a material wall in which, due to the collective response of plasma, space charge layers arise and as a rule the general quasi-neutrality of plasma will be no longer fulfilled at such boundary. In this chapter we will first present the sheath theory [10] that describes a space charge layer that forms on the plasma boundary. We will then show the main theory for probes [11, 12] we used and possible extensions to our particular case [15]. In the end we will describe the construction and testing procedure we used for these probes and their movement and acquisition system.

### 3.1 Sheath theory

Let us consider a bulk of plasma, the space potential inside this bulk is called the plasma potential ( $V_p$ ). Consider now an electrode (a probe or a wall) the floating potential ( $V_{fl}$ ) is defined as the potential that the electrode has when it is in contact with the plasma but draws no current. This two potentials are in general not equal, this is due to the difference in mass between the light electrons with respect to the heavy ions. Unless the particular case in which the ion temperature ( $T_i$ ) is much larger then the electron one ( $T_e$ ) the higher mobility of electrons produces a negative charge on the electrode although no net current is flowing through it. The Sheath theory we will describe is simplified to an infinite homogeneous collisionless plasma facing a floating infinite wall that does not emit neither reflect any particles that get in touch with it. As we move from inside the plasma towards the wall, the potential

changes from  $V_p$  to  $V_{fl}$ , that could be a real floating or a externally biased potential. Consistently to the Poisson's law the charge density varies with the potential as

$$\nabla^2 V(x) = -\frac{\rho(x)}{\varepsilon_0} = -\frac{e}{\varepsilon_0}[n_i(x) - n_e(x)] , \quad (3.1.1)$$

so that where the quasi-neutrality exist  $n_i \simeq n_e \simeq n$  there is no electric field and thus no potential variation. Obviously since the plasma is quasi-neutral, small electric fields can arise and form potential variation not greater then the plasma mean energy, which is of the order of the thermal energy  $T_e$ . In section 1.4, page 12 we described a linear model for those small perturbation responsible for electrostatic plasma waves propagation. Here that kind of model is not useful anymore since we need to describe a larger potential variation and thus a nonlinear model is necessary.

### 3.1.1 Collisionless sheath

We will study the problem only in one dimension along the x-axis; we place the  $x = 0$  position where the sheath begins, see figure (3.1), here we still have quasi-neutrality so that we can write  $n_e = n_i = n$ . On the same position ions have a velocity  $u_{i0}$  and we define the potential to be equal to zero. The electrons density distribution in the sheet is described by the Boltzmann relation:

$$n_e(x) = n_{e0} e^{V(x)/T_e} . \quad (3.1.2)$$

The total energy of ion must be conserved so that we can write

$$\frac{1}{2} m_i u_{i0}^2 = \frac{1}{2} m_i u_i^2(x) + eV(x) , \quad (3.1.3)$$

and the ion flux must also be conserved (assuming no ionization process in the sheath) giving

$$n_i(x) u_i(x) = n_{i0} u_{i0} , \quad (3.1.4)$$

where  $n_{i0}$  is the ion density at  $x = 0$ . Eliminating  $u_i(x)$  between (3.1.3) and (3.1.4) we get the ion density distribution as a function of the potential

$$n_i(x) = n_{i0} \left( 1 - \frac{2eV(x)}{m_i u_{i0}^2} \right)^{-1/2} . \quad (3.1.5)$$

Now substituting (3.1.2) and (3.1.5) into (3.1.1) we get

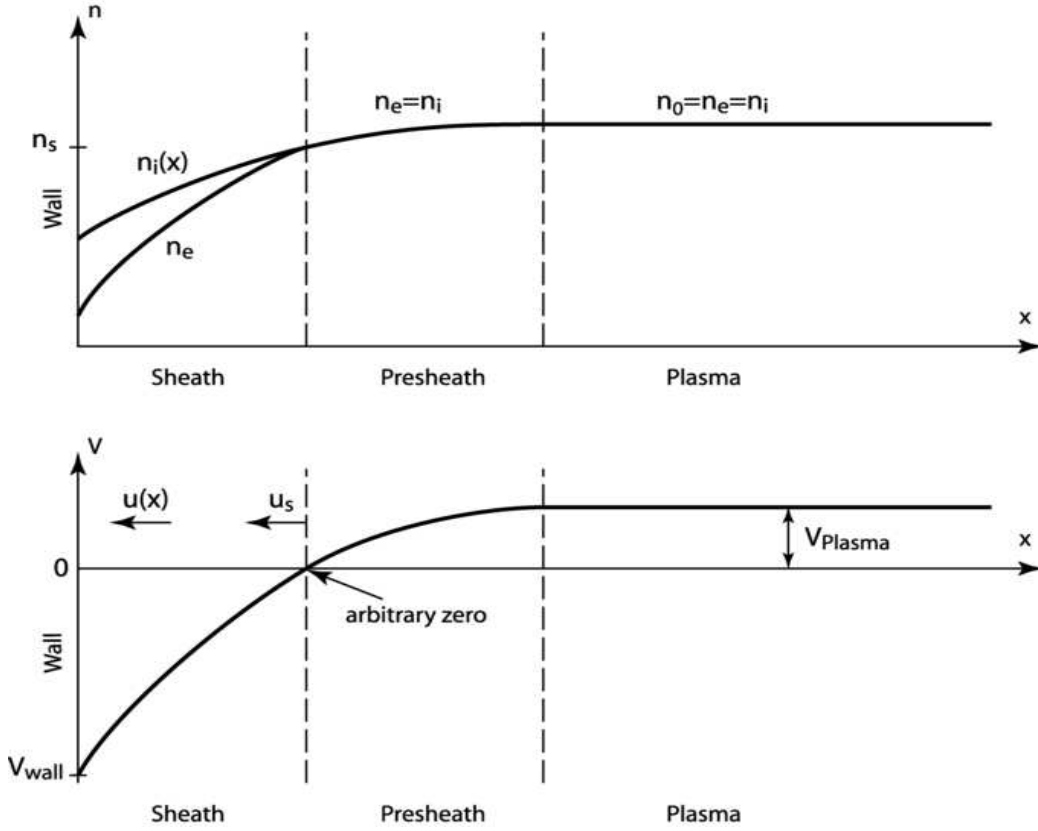


Figure 3.1: Density and potential profile of plasma in presence of a wall.

$$\frac{d^2V(x)}{dx^2} = \frac{en_0}{\epsilon_0} \left( e^{V(x)/T_e} - \left( 1 - \frac{2eV(x)}{m_i u_{i0}^2} \right)^{-1/2} \right). \quad (3.1.6)$$

This is the basic nonlinear equation for sheath description. It is important to notice, and we will show why in the following section, that it depends on the ion velocity at the sheath border  $u_{i0}$ .

### 3.1.2 The Bohm sheath criterion and the presheath

To find a solution of the differential equation (3.1.6) we start looking for the first integral by multiplying both sides by  $dV/dx$  and integrate over  $x$

$$\int_0^V \frac{dV}{dx} \frac{d^2V}{dx^2} dx = \frac{en_0}{\epsilon_0} \int_0^V \frac{dV}{dx} \left( e^{V/T_e} - \left( 1 - \frac{2eV}{m_i u_{i0}^2} \right)^{-1/2} \right) dx. \quad (3.1.7)$$

Now simplifying the dx and use dV as integration variable we get:

$$\frac{1}{2} \left( \frac{dV}{dx} \right)^2 = \frac{en_0}{\varepsilon_0} \left( T_e e^{V/T_e} - T_e + m_i u_{i0}^2 \left( 1 - \frac{2eV}{m_i u_{i0}^2} \right)^{-1/2} - m_i u_{i0}^2 \right), \quad (3.1.8)$$

where we use as border conditions  $V(0) = V'(0) = 0$  since the plasma is assumed to be field free. Equation (3.1.8) can be solved numerically, but for having at least an existence condition we can notice that the RHS must be always positive since the LHS is a squared value. We can thus perform a Taylor expansion on the exponential and on the square root on the RHS, which we can do since we are considering small potential value. We get:

$$\frac{1}{2} \frac{V^2}{T_e} - \frac{1}{2} \frac{eV^2}{m_i u_{i0}^2} \geq 0, \quad (3.1.9)$$

that can be written as a condition on  $u_{i0}$ :

$$u_{i0} \geq \left( \frac{eT_e}{m_i} \right)^{1/2} = u_B. \quad (3.1.10)$$

This is the Bohm sheath criterion, which state that the minimum ion velocity on the sheath border must be at least equal or bigger than the Bohm velocity  $u_B$ . A physical explanation of this condition could be seen if we consider the densities. Going back to equation (3.1.8) having RHS larger than zero, can be seen as a request for the ion density to remain always higher than the electron density.

In figure (3.2) we show in a logarithmic plot the behavior of electron density (solid line), that is exponentially falling according with equation (3.1.2), for equation (3.1.4) the ion density also has to fall since ions are accelerated by the sheath. If the ion velocity is too small at the sheath border they are accelerated more, thus the density falls faster (dashed line) and can become less than the electron density. Thus it is necessary that ions on the border of the sheath already have a minimum velocity so that the ion density curve (dotted line) always remain above the electron density.

Now the main problem is to explain how the ions, that in the bulk of plasma move only due of thermal motion; are able to get a minimum velocity towards the wall before entering the sheath. The idea for solving this problem is that the sheath edge is not sharp, but instead a presheath extend into the bulk of the plasma so that the potential has a small drop capable of accelerating ions towards the wall enough to fulfill the Bohm criterion. The length of this presheath should be in the order of an ion mean free path



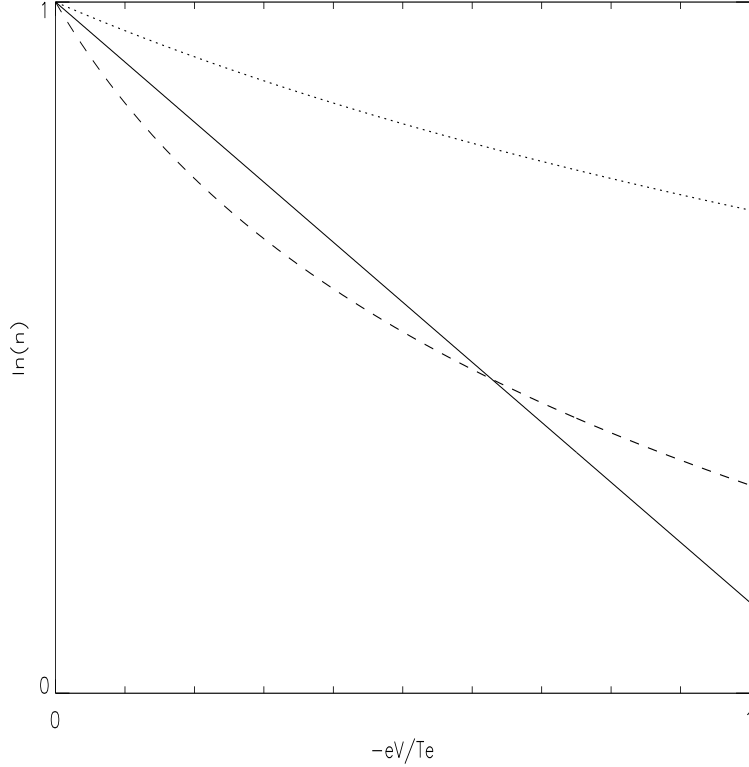


Figure 3.2: Electron density (solid), ion density with  $u_{i0} \geq u_B$  (dotted), ion density with  $u_{i0} < u_B$  (dashed)

while the sheath usually is in the order of few Debye lengths. On such a spatial scale the potential drop in the presheath is sufficient to be half of the electron temperature, and thus still explainable with the linear theory. We should also consider that the model we are analyzing is quite simple and abstract, in nature a system with infinite plasma facing an infinite wall does not exist; thus it is plausible to imagine that in a real system the speed of the ions at the sheath edge is determined also by the other boundaries of the system. We can anyway try to figure out some condition for the presheath, let us start redefining the ion density through the ion current:

$$n_i = \frac{J_i}{eu_i}, \quad (3.1.11)$$

the quasi-neutrality condition can be written as:

$$\frac{J_i}{eu_i} = e^{V/T_e}, \quad (3.1.12)$$

where we used the Boltzmann relation for the electron density. Now evaluating the derivative of the logarithm of equation (3.1.12), we get:

$$\frac{1}{J_i} \frac{dJ_i}{dx} - \frac{1}{u_i} \frac{du_i}{dx} = \frac{1}{T_e} \frac{dV}{dx}, \quad (3.1.13)$$

since ions are accelerated in the presheath up to the Bohm velocity we should impose in equation (3.1.13)  $u_i < u_B$ . This lead us to the condition on the presheath:

$$\frac{1}{u_B} \frac{du_i}{dx} + \frac{1}{T_e} \frac{dV}{dx} < \frac{1}{J_i} \frac{dJ_i}{dx}, \quad (3.1.14)$$

that could be satisfied by:

$$\frac{1}{u_B} \frac{du_i}{dx} + \frac{1}{T_e} \frac{dV}{dx} < 0, \quad \frac{1}{J_i} \frac{dJ_i}{dx} = 0, \quad (3.1.15)$$

that implies some kind of friction in the presheath since for equation (3.1.3) the LHS of equation (3.1.14) is larger than zero. Otherwise it is satisfied by:

$$\frac{1}{u_i} \frac{du_i}{dx} + \frac{1}{T_e} \frac{dV}{dx} > 0, \quad \frac{1}{J_i} \frac{dJ_i}{dx} > \frac{1}{u_i} \frac{du_i}{dx} + \frac{1}{T_e} \frac{dV}{dx}, \quad (3.1.16)$$

that implies ionization phenomena. In both cases it is useful to relate the density on the sheath edge to the density of the plasma bulk. We can assume that the ions are accelerated by a potential drop of:

$$\frac{1}{2} m_i u_B^2 = eV_p, \quad (3.1.17)$$

using the definition of the Bohm velocity from equation (3.1.10) we find:

$$V_p = \frac{T_e}{2}, \quad (3.1.18)$$

that inserted in the Boltzmann relation gives:

$$n_0 = n_b e^{-V_p/T_e} \simeq 0.61 n_b, \quad (3.1.19)$$

where  $n_b$  is the density at the bulk-presheath junction.

### 3.1.3 Child-Langmuir law

Further in our discussion we will meet the necessity to know exactly the probe surface  $A_p$  that is directly exposed to the plasma; thus it is necessary to check that the sheath dimension  $s^2$  is smaller or at least comparable with the probe dimension. If we have the case  $A_p \gg s^2$  the probe theory can be greatly simplified. The Child-Langmuir law gives the current between two electrodes spaced by a distance  $s$  as a function of potential differences between them. Let us consider equations (3.1.3) and (3.1.11), with the initial ion energy  $\frac{1}{2}m_i u_{i0}^2$  small compared to the potential, we get

$$\frac{1}{2}m_i u_i^2(x) = -eV(x) . \quad (3.1.20)$$

$$en_i(x)u_i(x) = J_0 . \quad (3.1.21)$$

Solving for  $n_i(x)$  we obtain:

$$n_i(x) = \frac{J_0}{e} \left( -\frac{2eV(x)}{m_i} \right)^{-1/2} , \quad (3.1.22)$$

now using Poisson equation (3.1.1) we get:

$$\frac{d^2V(x)}{dx^2} = -\frac{J_0}{\varepsilon_0} \left( -\frac{2eV(x)}{m_i} \right)^{-1/2} . \quad (3.1.23)$$

As we made for the evaluation of the Bohm-sheath criterion we multiply by  $dV/dx$  and integrate over  $x$  obtaining:

$$\frac{1}{2} \left( \frac{dV}{dx} \right)^2 = 2 \frac{J_0}{\varepsilon_0} \left( \frac{2e}{m_i} \right)^{-1/2} (-V)^{1/2} , \quad (3.1.24)$$

where again we choose the plasma field free border conditions  $V(0) = V'(0) = 0$ . Of the two square roots we pick up the negative one, since  $dV/dx$  is negative, see figure (3.1); integrating again we get:

$$-V^{3/4} = \frac{3}{2} \left( \frac{J_0}{\varepsilon_0} \right)^{1/2} \left( \frac{2e}{m_i} \right)^{-1/4} x . \quad (3.1.25)$$

Now we just need to define  $V(s) = V_0$  and isolate the  $J_0$  term from last equation to get the Child-Langmuir law.

$$J_0 = \frac{4}{9} \varepsilon_0 \left( \frac{2e}{m_i} \right)^{1/2} \frac{V_0^{3/2}}{s^2} \quad (3.1.26)$$

We can now try to isolate the sheath dimension  $s$  by: substituting the explicit form of the current at the sheath edge  $J_0 = en_{i0}u_B$ , using the given definition of Bohm velocity in equation (3.1.10) and the given definition of Debye length from equation (1.3.11)

$$s = \frac{\sqrt{2}}{3} \lambda_D \left( \frac{2V_0}{T_e} \right)^{3/4} . \quad (3.1.27)$$

In our case  $s \approx 10^{-9} - 10^{-10} V_0^{3/4}$  in square meter, even considering high value for  $V_0$ , the sheath is much smaller than the probe dimension  $A \approx 10^{-6} \text{ m}^2$ .

## 3.2 Probe Theory

### 3.2.1 Langmuir Probe

The most simple probe for studying plasma is the Langmuir probe. It is

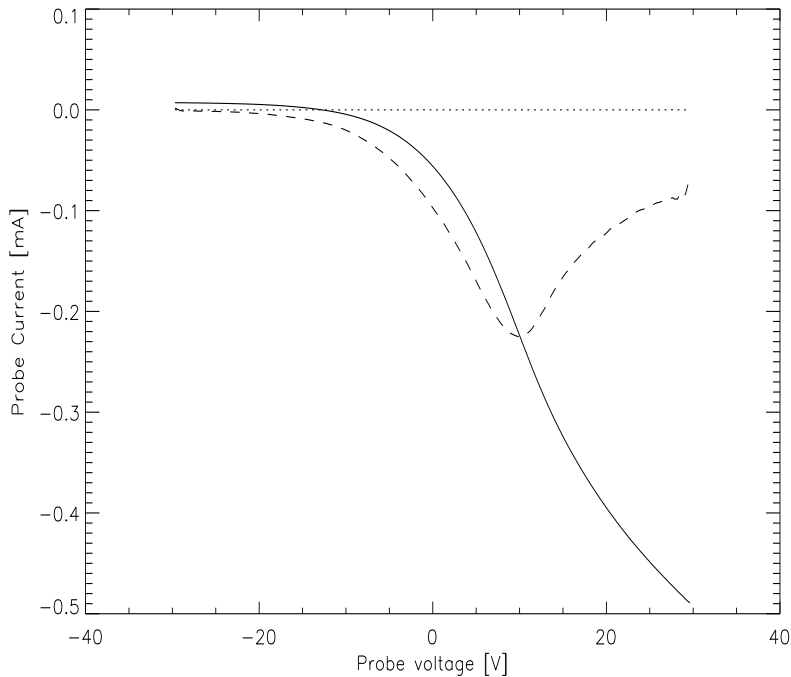


Figure 3.3: An example of Langmuir characteristic (solid) and it's first derivative (dashed)

composed of a metal electrode inserted into the plasma; the current through

the probe is composed of an ion and an electron component, depending on the bias. By varying the bias voltage, a typical Langmuir trace can be measured, as shown by the solid line in figure (3.3). Starting by a negative biased potential, the current drawn by the probe is mainly given by ions (the zero level is marked by the dotted line) and we are in the ion saturation regime. Increasing the bias we reach the floating potential  $V_f$  that is defined as the zero current point of the curve, that is the one in which ion and electron current balance. Then there is the electron retardation exponential part, as the Coulomb barrier is lowered to allow slower electrons in the Maxwellian distribution to penetrate it. In this section the electrons that contribute to the current (thanks to their lighter nature), as we said, are Maxwellian distributed. Thus the current will have the form:

$$I_e = neA_p v_{te} e^{(V_B - V_p)/T_e} , \quad (3.2.28)$$

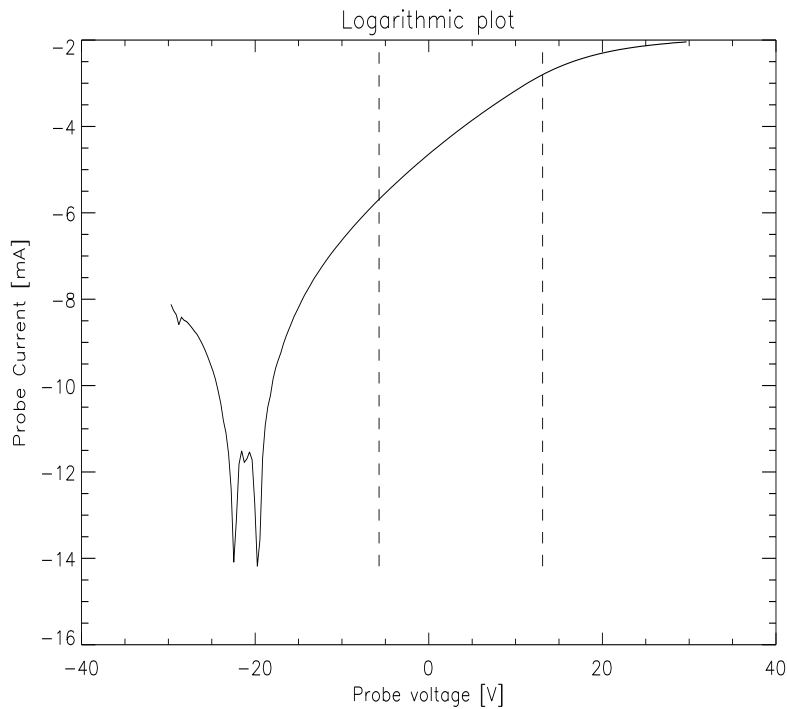


Figure 3.4: Logarithmic plot of Langmuir characteristic (solid),  $V_f$  position (left dashed),  $V_p$  position (right dashed)

where  $v_{te} = (T_e/2\pi m_e)^{(1/2)}$  is the electron thermal speed and  $V_B$  is the probe bias. As we can see from performing the derivative of the curve (the

dashed line) we get in the minimum at  $V_B = V_p$ , from which we can gather information on the plasma potential. At this point the current is mainly composed by electrons, due to their higher mobility. In fact increasing the potential, the curve has a knee, and it start the electron saturation current segment. This knee in RF plasma, as in Njord, is usually not very clear and require some modification to the probe itself that we will explain further on.

Performing the logarithm of the curve, figure (3.4), we can see from equation (3.2.28) that the slope of the exponential segment is proportional to  $1/T_e$ , so that we can have information on the electron temperature, that from equation (3.2.28) is given as

$$\frac{1}{T_e} = \frac{1}{V_B - V_P} \ln \left( \frac{I_e}{neA_p v_{te}} \right) \quad (3.2.29)$$

In the figure the two vertical line are the floating and the plasma potential, so that is easier to recognize where the exponential part of the Langmuir characteristic should be.

### 3.2.2 Compensated probe

We saw in section 2.3, page 30 that the source we are using drives sinusoidally fluctuating waves at 13.56 MHz in the plasma potential; the sheath that forms around the probe depends on plasma potential and thus it will also fluctuate and affects the current to the probe. In particular the exponential segment in the Langmuir characteristic is distorted and the floating potential is shifted towards more negative voltage [12, 15]. Let us consider the plasma potential as the superposition of DC and RF voltage:

$$V_p = V_{DC} + V_{RF} . \quad (3.2.30)$$

It is necessary to modify the Langmuir probe so that it will follow the RF oscillations and give the DC signal as a result. Many different methods have earlier been used with other RF plasma sources [13, 14]. We chose to use a method [15] with only passive components, so that it is not necessary to build a complex and expensive active circuit.

In figure (3.5) we can see the equivalent circuit of the Langmuir probe,  $V_p$  as usual is the plasma potential, the sheath impedance consist of the parallel between  $R_{sh}$  and  $C_{sh}$ .  $C_s$  is the stray capacitance of power supply and connecting cables,  $V_B$  is the voltage bias and  $R_m$  is the measuring resistor. Let us first neglect the RF component and consider only the DC signal, the total current drawn by the probe is given by:

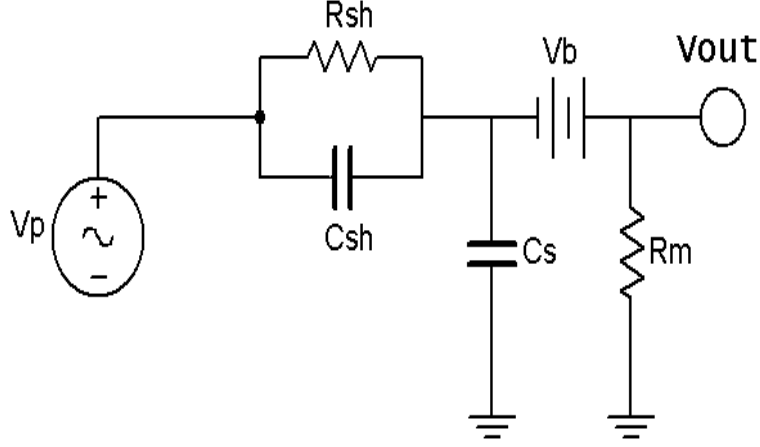


Figure 3.5: Equivalent circuit of a Langmuir probe

$$I = I_i - I_e , \quad (3.2.31)$$

where  $I_i = \frac{1}{2}neA_p u_B$  is the ion current and  $I_e$  is the electron current we defined in equation (3.2.28). When the probe is at the floating potential,  $V_B = V_f$ , it draws no current and therefore  $I_i = I_e$ . Substituting the definition we gave for the two current components we get an equation for the floating potential:

$$V_f = V_{DC} - \frac{T_e}{2e} \ln \left( \frac{2m_i}{\pi m_e} \right) . \quad (3.2.32)$$

The resistance of the probe sheath is given by:

$$\frac{1}{R_{sh}} = \frac{dI}{dV} \approx -\frac{dI_e}{dV} , \quad (3.2.33)$$

the use of  $\approx$  is due to the higher contribution of electrons to the current. Using again the definition of  $I_e$  into the last equation leads us to the definition of the value of the sheath resistance. This will fluctuate since the electric current depends on  $V_B - V_p$ , but at the floating potential the resistance is uniquely defined as:

$$R_{sh}|_{V_f} = \frac{T_e}{eI_i} \approx \frac{2\lambda_D^2}{\varepsilon_0 A_p u_B}. \quad (3.2.34)$$

Let's now reintroduce the RF component, which amplitude  $|V_{rf}|$  may be much larger than the DC signal, so that we can evaluate the dynamic sheath capacitance that is defined as:

$$C_{sh} \equiv \frac{\Delta Q}{\Delta V}, \quad (3.2.35)$$

where  $\Delta V = V_B - V_p$ . The assumption we make for applying the sheath theory discussed before is that the sheath reach an equilibrium at each phase of the RF cycle. This can be considered a good approximation when the RF frequency is much smaller than the ion plasma frequency (1.3.10), under this condition ions have enough time to reach the equilibrium into the sheath. For argon gas and density around  $n = 10^{11} \text{ cm}^{-3}$ , like we have in Njord, the ion plasma frequency is about 67 MHz and therefore the approximation should hold. In section 3.1.3, using the Child-Langmuir law, we have shown that the sheath dimension is much smaller smaller than the probe dimension, thus we can expand last equation and write:

$$\frac{C_{sh}}{A_p} = \frac{\Delta \varrho_p}{\Delta V} = -\varepsilon_0 \frac{d}{dV} \left( \frac{dV}{dx} \right), \quad (3.2.36)$$

where  $\varrho_p$  is the surface density charge. Now we should find an expression for  $dV/dx$ ; we use again Poisson equation (3.1.1), ion total energy (3.1.3) and flux conservation (3.1.4). Combining all these and multiplying by  $dV/dx$ , we obtain:

$$\frac{dV}{dx} \frac{d^2V}{dx^2} = -\frac{en_{i0}}{\varepsilon_0} \left( 1 - \frac{2eV}{m_i u_B^2} \right)^{-1/2} \frac{dV}{dx}. \quad (3.2.37)$$

We integrate equation (3.2.37), using the usual border condition  $V(0) = V'(0) = 0$ , and picking up the negative root we get:

$$\frac{dV}{dx} = -2 \left( \frac{n_{i0} m_i u_B^2}{2\varepsilon_0} \right)^{1/2} \left( \left( 1 - \frac{2eV}{m_i u_B^2} \right)^{1/2} - 1 \right)^{1/2}. \quad (3.2.38)$$

Now performing the derivation with respect to V and substituting in equation (3.2.36) we get:

$$\frac{C_{sh}}{A_p} = \frac{e}{2} \left( \frac{2n_{i0}\varepsilon_0}{m_i u_B^2} \right)^{1/2} \left( -\frac{2eV}{m_i u_B^2} \right)^{-3/4} \left( 1 + \frac{1}{2} \left( -\frac{m_i u_B^2}{2eV} \right)^{1/2} \right), \quad (3.2.39)$$



that can be simplified using the ion current definition given by equation (3.1.11) so that we get:

$$\frac{C_{sh}}{A_p} = \frac{1}{2} \left( \frac{m_i}{2e} \right)^{1/4} (\epsilon_0 J_i)^{1/2} (-V)^{-3/4} \left( 1 + \frac{1}{2} \left( -\frac{m_i u_B^2}{2eV} \right)^{1/2} \right), \quad (3.2.40)$$

where the last term is usually smaller and is considered as a second order correction as shown in [15].

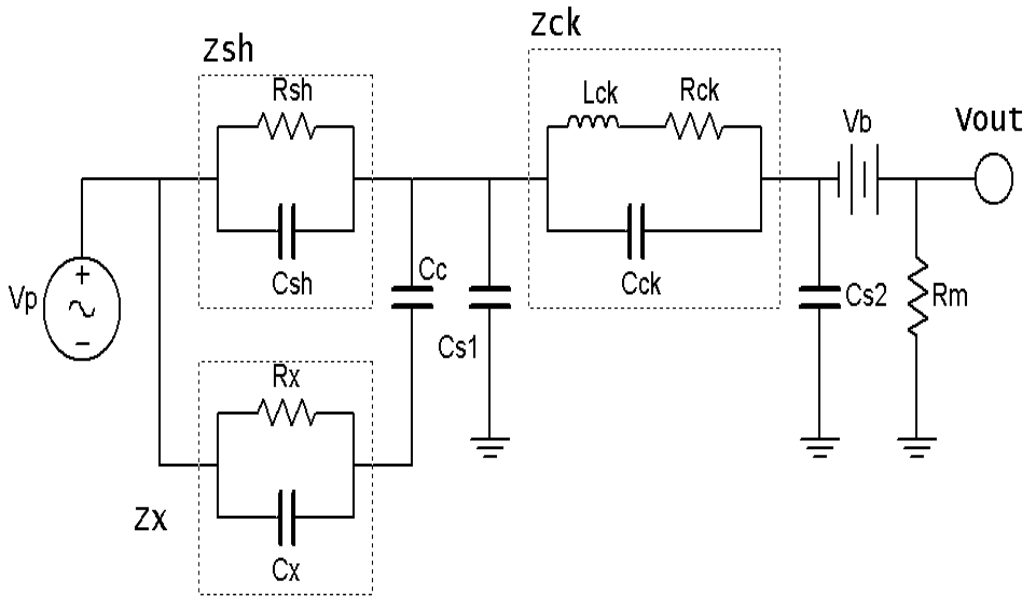


Figure 3.6: Equivalent circuit of compensated Langmuir probe

In figure (3.6) we show the compensating circuit we used. Starting from the left we can see that a new electrode, in contact with the plasma, has been added; its sheath is defined by  $R_x$  and  $C_x$ . This new electrode must have a larger surface  $A_x$  and has to be connected to the probe line with a large coupling capacitor  $C_c$ ; this will let the incoming RF component pass, as if it was a short circuit, but will cut the low-frequency DC component. The presence of this electrode will help the probe tip follow the RF fluctuations, since the resulting impedance  $Z_x$  has identical real and imaginary parts to that of  $Z_{sh}$ , but smaller amplitude.

The group of  $R_{ck}, L_{ck}$  and  $C_{ck}$  (with an impedance  $Z_{ck}$ ) stand for the choke system of the probe. This is the main system responsible for suppressing the

RF signal and consist of a RLC band-pass filter. Varying the value of L and C it is possible to make the filter resonate at the RF frequency, so that the RF component will be damped. The resonating frequency is given by the relation:

$$f_0 = \frac{1}{2\pi\sqrt{LC}}, \quad (3.2.41)$$

while the total impedance of the filter is defined as:

$$Z_{ck} = \frac{1}{\sqrt{\left(\frac{1}{R}\right)^2 + \left(\omega C - \frac{1}{\omega L}\right)^2}}. \quad (3.2.42)$$

The stray capacitance  $C_s$  has been split in two terms. The first one,  $C_{s1}$ , take into account the capacitance between the probe tip and the filter, the second  $C_{s2}$  will have the same role of  $C_s$  as there is no filter. We will see that it is important to keep the choke as close as possible to the probe tip to minimize  $C_{s1}$

To evaluate which impedance values are necessary for our compensated probe to work properly, we should first consider only the normal Langmuir probe, in this case the sheath capacitance  $Z_{sh}$  and the choke capacitance  $Z_{ck}$  form a voltage divider, that gives:

$$V_B = \frac{Z_{ck}}{Z_{sh} + Z_{ck}} V_p \quad (3.2.43)$$

To have a clear Langmuir characteristic despite the RF oscillations, we should require  $V_B - V_p \ll T_e$ , that means:

$$\frac{Z_{ck}}{Z_{sh} + Z_{ck}} |V_{RF}| \ll \frac{T_e}{e}, \quad (3.2.44)$$

or alternately:

$$Z_{ck} \gg Z_{sh} \left( \frac{e|V_{RF}|}{T_e} - 1 \right). \quad (3.2.45)$$

The stray capacitance impedance  $Z_{s1}$  must as well fulfill condition (3.2.45). For large RF potential this may not be possible and this is the reason why the second electrode has to be inserted. The probe tip is forced to follow the RF oscillations due to the (smaller in amplitude)  $Z_x$ , in this way the dominant (i.e the smaller) impedance has to fulfill

$$Z_c \gg Z_x \left( \frac{e|V_{RF}|}{T_e} - 1 \right), \quad (3.2.46)$$

where  $Z_c$  is the smaller between  $Z_{ck}$  and  $Z_{s1}$ .

### 3.2.3 Double probe

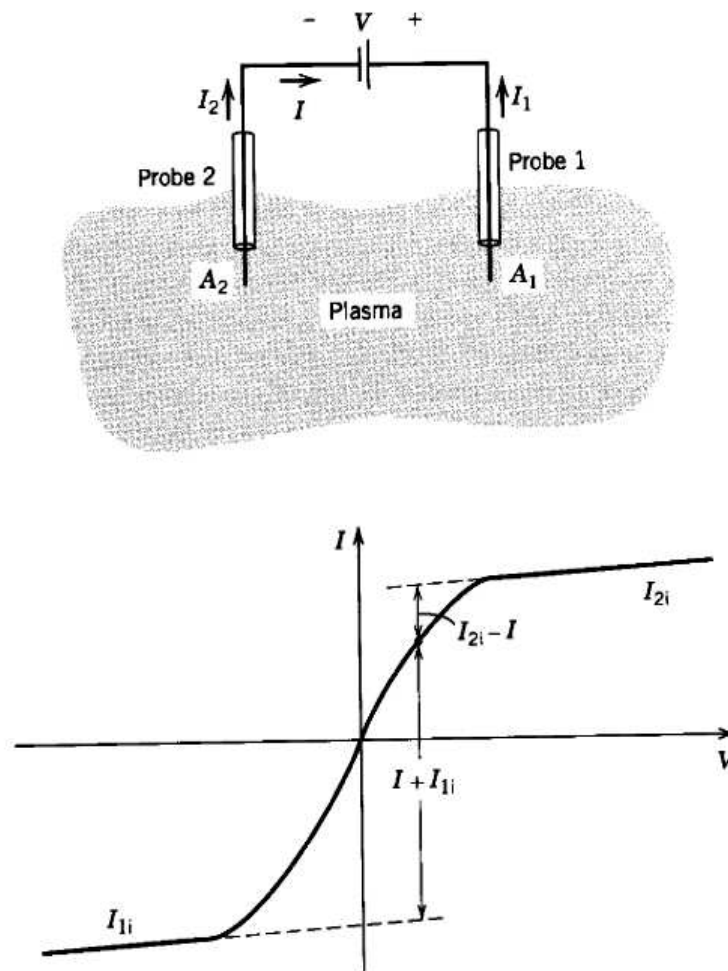


Figure 3.7: Double probe electric scheme (Up), typical I-V characteristic (Down), Credit: [12] page 182.

Another way to solve the problem of the RF oscillations, is to use a double probe configuration. Instead of suppressing the RF oscillations the double probe actually "follow" the oscillations and provide a simple method than the compensated probe. The disadvantage of using this technique is that since the probe follow the potential we don't have any kind of information on floating or plasma potential, as we did in the Langmuir probe. Moreover this probe is able to collect only the high-energy tail of the electron distribution

and these may not be representative of the electron bulk distribution.

Let us suppose to have two probe connected by a bias voltage as in the upper panel of figure (3.7). The four components of the current, given by ions and electrons are:  $I_{1i}$ ,  $I_{1e}$ ,  $I_{2i}$ ,  $I_{2e}$ . In the floating potential we should have no net current flowing through the circuit, thus

$$I_{1i} + I_{1e} + I_{2i} + I_{2e} = 0 , \quad (3.2.47)$$

while the loop current is defined as

$$I_{2i} - I_{2e} - (I_{1i} - I_{1e}) = 2I . \quad (3.2.48)$$

Combining last two equations, we get an expression for the net current passing through the read circuit as

$$I = I_{1e} - I_{1i} = I_{2e} - I_{2i} . \quad (3.2.49)$$

Defining now the two electron currents as:

$$I_{ke} = A_{pk} J_{esat} e^{V_k/T_e} , \quad k = 1, 2 , \quad (3.2.50)$$

where  $A_{pk}$  is the probe surface,  $J_{esat}$  is the random current density and  $V_k$  the probe potential. Now substituting (3.2.50) into (3.2.49) using  $V = V_1 - V_2$  we get

$$\frac{I + I_{1i}}{I_{2i} - I} = \frac{A_1}{A_2} e^{V/T_e} , \quad (3.2.51)$$

which plot is visible in the lower panel of figure (3.7). If  $A_1 = A_2$ , then we can approximate  $I_{1i} = I_{2i} = I_i$  so that equation (3.2.51) can be written as

$$I = I_i \tanh \left( \frac{V}{2T_e} \right) . \quad (3.2.52)$$

Now fitting equation (3.2.52) with the plot in the lower panel of figure (3.7), it is possible to obtain both the electron temperature  $T_e$  and the ion saturation current  $I_i$  that is directly proportional to the density  $n_i = n_e$ .

## 3.3 Construction and testing

### 3.3.1 Compensated probe

On our work on Njord we tried different solutions for the Langmuir probe. The main problem in building our Langmuir probe was given by the filter; as

we said in the previous section it is necessary to place it inside the probe to minimize the distance from the tip. The first step is to evaluate the sheath capacitance of the probe tip and of the second electrode. We used equation (3.2.39) that we rewrite here, isolating  $C_{sh}$ , and defining

$$W_0 = \frac{1}{2}m_i u_B^2 = \frac{T_e}{2},$$

as the starting ion energy and not considering the last term, that, is a correction term which is usually small. The resulting equation is:

$$C_{sh} = A_p \frac{e}{2} \left( \frac{n_{i0} \epsilon_0}{W_0} \right)^{1/2} \left( -\frac{eV}{W_0} \right)^{-3/4}, \quad (3.3.53)$$

Now we predicted some Njord parameters: we expect to have a density  $n \simeq 10^{10} - 10^{11} \text{ cm}^{-3}$ ; an electron temperature  $T_e \simeq 5 \text{ eV}$ , from which we get  $W_0 \simeq 2.5 \text{ eV}$ ; a potential sweep  $V \simeq 30 \text{ V}$  and the probe surface we estimate will be  $A_p \simeq 7.8 \times 10^{-6} \text{ m}^2$ . Inserting these values in equation (3.3.53) we obtain a value for the sheath capacitance of the probe tip of  $C_{sh} \simeq 0.05 \text{ pF}$ . Evaluating the sheath capacitance of the second electrode is quite simple, the only parameter that changes is the probe surface, due to the longer wire. We choose to have a ratio of 5 between the second electrode and the probe tip, thus since the probe tip will be about 5mm long, the second electrode will be of 25mm length and thus a five times larger capacitance  $C_x = 0.25 \text{ pF}$ . The coupling capacitance has been chosen to be much larger than the two sheath capacitance, about 50 pF.

The filter is composed of a capacitor and an inductance. Since the signal we want to read can be quite small the resistor  $R_{ck}$  shown in figure (3.6) is not really mounted; in this way the total impedance of the filter is reduced. To obtain a finer resolution on frequency, we chose to use a trimmer capacitor ranging between 10 and 20 pF with an inductor of 10  $\mu\text{H}$ . First we measured with RLC-meter the real value of the inductor; in most of the cases it result to had a lower value than 10  $\mu\text{H}$ , around 8  $\mu\text{H}$ . With these inductors the theoretical capacitance value should be 17.2 pF, and we used the RLC-meter to trim the capacitance as close as possible to this value.

After soldering the various components together we performed a work-bench test for the filter. We used a wave generator which output is connected to the two electrodes, and then the output of the filter to an oscilloscope for reading the output amplitude of the signal. To have a better knowledge of the filter behavior we performed the test with the entire probe built, mounted on its support and connected to coaxial cable to the oscilloscope. The rest of the probe and the support will be explained further on. To have a complete simulation of the probe circuit, it was necessary to mount two capacitors of

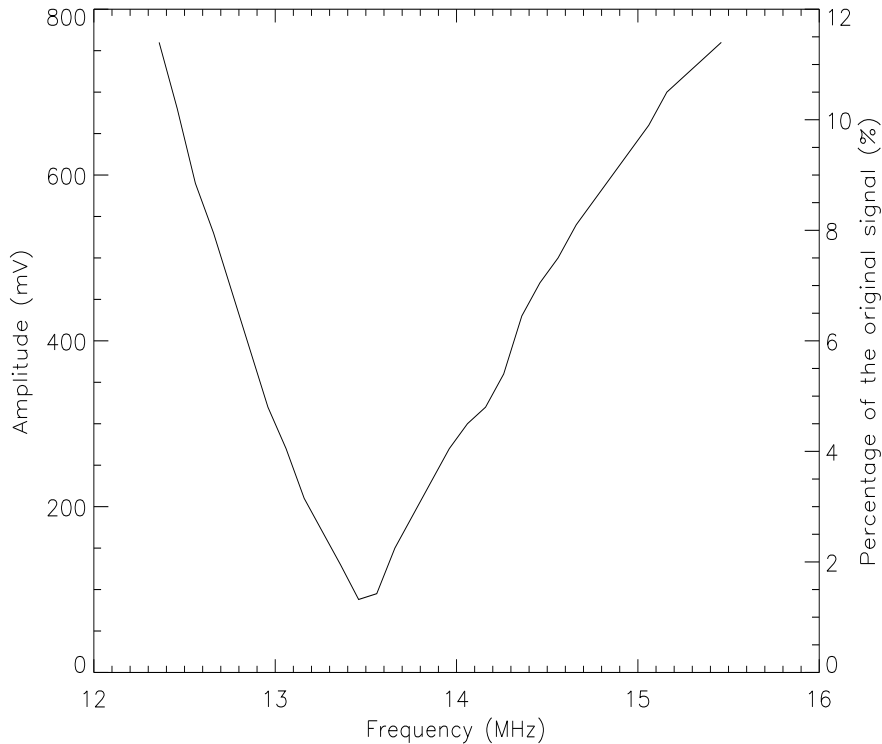


Figure 3.8: Frequency response of the band-pass filter

respectively: 0.05 pF and 0.25 pF, on the electrodes. Those will simulate the different sheath capacitance that the electrodes will exert inside the plasma. Unfortunately those small capacitances were not available, but anyway this workbench test is mean to test the filter frequency response, and not the capacity of the probe to follow the RF oscillation, which is the reason we used the two electrodes. The test results for the first filter we built are shown in figure (3.8). The maximum reduction it is reached at  $f = 13.46$  MHz with 1.2% of the original signal

Now that the filter is build we have to find a way to insert it into the probe. The length of the filter is not a serious problem, since we usually work with probe a of 20-30 cm, the width indeed is a problem. The largest ceramic tube we had has a diameter of about 6mm, while the capacitor is about 5mm. We should also consider that on the capacitor we should mount the inductor, since the circuit required that those component to be in parallel.

The sum of the two, require a diameter of at least 7-8mm for the circuit

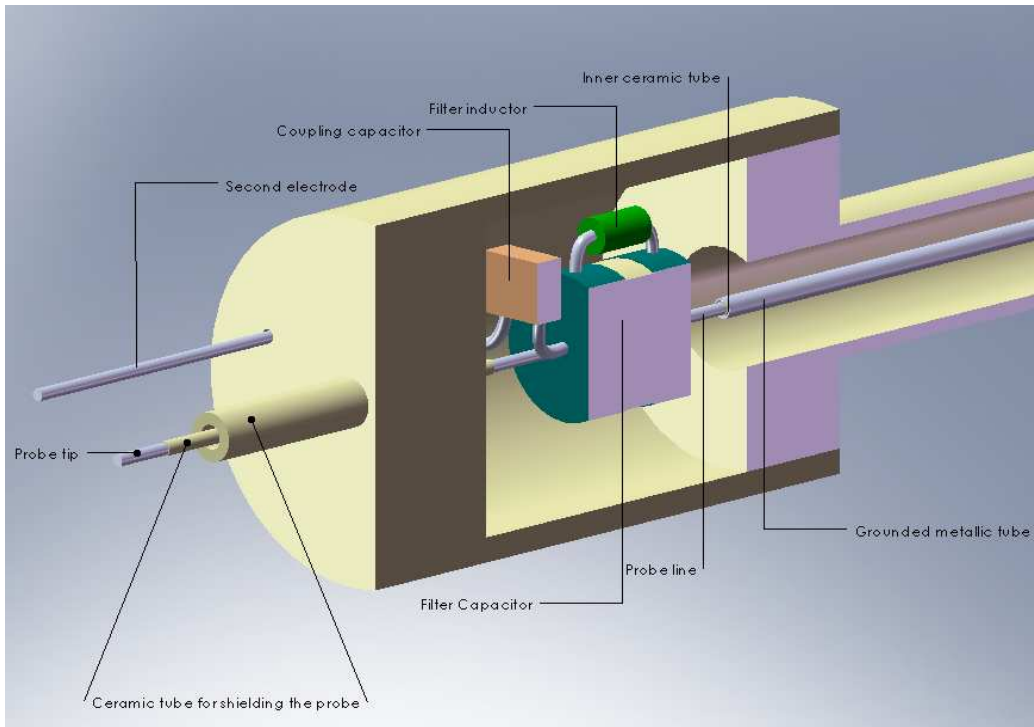


Figure 3.9: Sketch of the compensated probe circuit and housing used in Njord

to fit easily. We also have to consider that, in case of necessity, we should be able to open the probe and extract the filter without causing extensive damage to the filter itself nor to the ceramic tube. The simplest solution was to mount a short ceramic tube on the 6mm tube, customized by us, and wide enough for the filter. This new tube is shown on figure (3.9). For the probe tip we first used orobraz, a gold-nickel alloy (Au 82.5%, Ni 17.5%). Inside the probe tip, exposed to the plasma, arise strong currents due to the RF oscillations. These currents, together with the usual plasma heating, substantially rise the temperature that the probe tip must sustain. Orobraz while it is very easy to solder it has a low melting point 950 K, so that during the first measurements we noticed a progressive reduction of the probe tip length, until it melted completely. We tried with a new probe, that was using the same alloy, to reduce the time of exposure to the plasma. Letting the probe cool down for about 20 minutes every 10 minutes of measurements, we hoped to have enough time to avoid melting problems; unfortunately also this second probe encountered the same difficulty. Moreover in the future it will

be necessary to perform longer test on plasma and therefore we should use a more resistant probe tip. We chose to use wolfram, that has a melting point of 3000 K. The problem in using wolfram is the difficulty on soldering it to the filter circuit. For this reason we solder to the filter a 5mm orobraze wire, then we inserted it together with the 0.5mm wolfram wire into a 1mm diameter and 3mm long cylinder of stainless steel, with the help of an hydraulic press, we squeeze the cylinder to hold together the two wires and have the electrical contact for the probe tip. It is necessary to point out that the rest of the probe wiring is still made in orobraze. Is useful, as we did, to check the electric connection of the soldering point every time the seal is broken and the machine opened. Once the connection was complete we inserted the filter into the ceramic tube, taking care to insert the two electrodes in the right front holes. We then introduced two smaller ceramic tube, with an internal diameter of 0.6mm, around the two electrodes, for holding the wires still and obtaining a better shielding. Adding some ceramic glue was also necessary to reduce the possible movement of the electrodes. In the end we measure the length of the electrodes and cut away the rest to obtain a probe tip length of 5mm and a secondary electrodes length of 25mm, so that we fulfill the requirements for a larger surface of the secondary electrodes, as we explained in section 3.2.2, page 58.

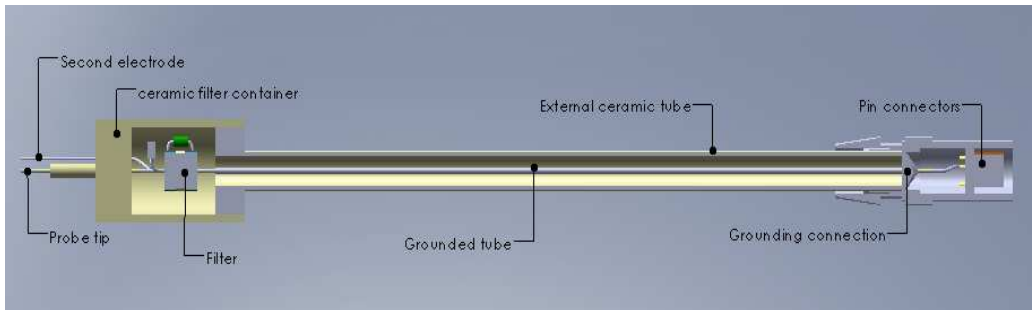


Figure 3.10: Compensated probe sketch used in Njord

On the other side of the filter with respect to the probe tip, we have the main body of the probe, see figure (3.10). As we mentioned earlier the external ceramic tube has a diameter of 6mm, inside it there is another ceramic of 2mm external and 0.8mm internal diameter, within which the 0.5mm orobraze wire is inserted. Between the two ceramic tubes we inserted a copper screen taken from a coaxial cable, to provide RF shielding. Looking on the right side of figure (3.10) the external connector of the probe (the lodging of the high temperature pins connector) is grounded. In the place



where the connector hold the ceramic tube we cut the copper screen, bent and wrapped it around the outside side of the external ceramic tube. In this way we guarantee the presence of a grounding tube all the way into the probe main body. To avoid contact between the grounded screen and the signal line we wrapped the latter in teflon tape from the inner ceramic tube to the pin connectors. On the other side, near the filter, the copper screen is cut before reaching the filter position, and also here some teflon tape is added to avoid accidental contact between the signal line and the ground potential.

### 3.3.2 Double probe

The construction of the double probe is less troublesome than the compensated probe. The absence of the filter allow us to use a simple ceramic tube for all the probe main body. This ceramic is 6mm diameter and 240mm long. Inside it, we inserted a copper screen taken from a coaxial cable, to provide RF shielding. The two lines, from the pin connectors to the probe tips, are inserted into two 0.8mm radius ceramic with a length of 250mm. For the probe tips we used wolfram to avoid the same melting problems we encounter with the compensated probe. We have anyway to face the soldering difficulties with wolfram. That is why we inserted, on the pin connectors side of the 0.8mm ceramic tubes, a 150mm orobraze wire. This wire is actually soldered to the pins and together with the wolfram wire, into the ceramic tube, guarantee us the electrical connection between the probe tips and the connectors.

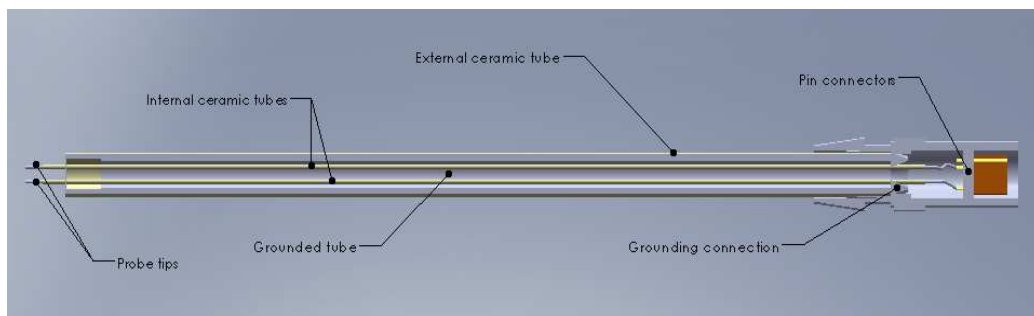


Figure 3.11: Double probe sketch used in Njord

The results is shown in figure (3.11). On the top of the wolfram tips, we inserted two 0.6mm ceramic tube for holding still the wires and adjust the tips length. In the end we choose to have the same tip length of 5mm and 0.5mm diameter as for the compensated probe. Some ceramic glue was added

to keep still the two inner ceramic tubes with respect to the main body of the probe. In the end the total probe length is 280mm (27mm shorter than the compensated one). Since on the pin connectors are available 4 pins, we connected two of them to each probe pins. We tested electrical connection and since no frequency response was needed no further benchmark test has been effectuated.

## 3.4 Diagnostic external hardware

### 3.4.1 Probes support and motor system

As we said in section 2, that we have to main ways for inserting probe into Njord. The first is along the radial direction ( $\hat{\mathbf{r}}$  in our cylindrical reference system), while the second is along the axial direction ( $\hat{\mathbf{z}}$ ). The radial probe is entering into the chamber through a lateral flange in the dome, the support for this probe is a 500mm long stainless steel rod with 4 different lines. The movement of the probe is manual and some care must be given in not touching the axial probe, when is present in the chamber. The axial direction is accessible through a flange below the antenna housing, and its provided with a motor system (see figures (2.1), (2.2) or figure (2.5)). To reach the central axis of the antenna from the flange, a U-shape connector has been built from a stainless steel tube of 0.7mm diameter. This connector is wired with 4 different lines and uses, as the probe, high temperature connection pins. The two arms of the U-connector which are joint to the probe and to the motor system, respectively 30mm and 55mm long. The "motor arm" has to be longer to guarantee enough space for installing a cylindrical lock; this was mounted for avoiding the U-connector to spin around the motor axis and thus let the probe crush against the dome walls or, even worse, against the pyrex tube. The length of the U-connector its of 188mm. It has been built to be as close as possible to the distance between the central axis of the antenna and the central axis of the motor connection flange. Since most part of the U-connector will be directly exposed to plasma and since the connector itself is grounded; it is necessary to shield the presence of the connector with ceramic. For this purpose we inserted over the entire length a series of short ceramic cylinders to cover as much surface as possible. The motor for the axial movement is controlled via computer with a LabView software written for that purpose. The total distance the probe can move is 230mm with a minimum step of 1mm. To start moving the probe it is necessary to insert the total length we want the probe to cover and the length of each steps. The software automatically evaluate the number of step, and bring the probe back

to the starting position at the end of the movement. For security reason end stop switchers are present, so that the probe cannot move too much inside the source, in which case the U-connector will touch the dome walls. On the terminal side of the motor system, the probe rod on which the U-connector is mounted, is equipped with a manual ring nut that allow the rotation of the the probe around the motor axis. Some care must give to the maximum angle of rotation, otherwise the probe will get in contact with the pyrex tube, or the dome walls. When the probe is inside the pyrex tube, it can be shown by trigonometric evaluation that the maximum angle at which the probe can be rotate, measured from the vertical position, is given by

$$\alpha = \pm \arccos \left( 1 - \frac{r^2}{2d^2} \right) = \pm 26^\circ ,$$

where  $r$  is the pyrex tube radius and  $d$  is the distance between the central axis of the antenna and the central axis of the motor rod. When the probe is outside the pyrex tube inside the dome, instead of the pyrex tube radius, must be used the radial dimension of the dome at the probe tip position.

### 3.4.2 Compensated probe acquisition system

In section 3.2.1 we have shown that to study the plasma with a Langmuir probe it is necessary to vary the voltage  $V_b$  (this operation is said to perform a sweep) on the probe tip and read the current that flows through the probe. Since the plasma potential can change from a few to more than one hundred volts, it is necessary to have as large sweep as possible. In our amplifier the sweep ranges between  $\pm 30V$  (actually could go up to  $\pm 34V$  but the amplification is not linear anymore). Thus, to reach higher plasma potential values is necessary to introduce an offset. That is why we introduce a bias box into the circuit, between the probe and the amplifier and in either case of the axial or the radial probe. This simply consists of 15 9V batteries which can be inserted one by one by means of switches for varying the offset at which we will perform our analysis. It is also possible to change the bias of the probe, from positive to negative simply by inverting the input with output line of the bias box. On the amplifier is possible to vary the measuring resistance  $R_m$ , see figures (3.5) and (3.6). The amplifier is then connected to the computer using a digitizer board. The software for performing the sweep has been written for that purpose, and also controls the section on the movement of the axial probe we described in the previous section. This software creates a digital sweep (that will be converted and amplified by the amplifier box into an analogical one), it is possible to change the amplitude of the sweep, the number of digital steps that composed the ramp and the

number of measurements that will be taken for each step (to create a sort of noise suppressing average).

### 3.4.3 Double probe acquisition system

The acquisition system for the double probe, is slightly more complicated than the one for the standard Langmuir probe. The main difficulties arises in having a good floating of the circuit with respect to ground.

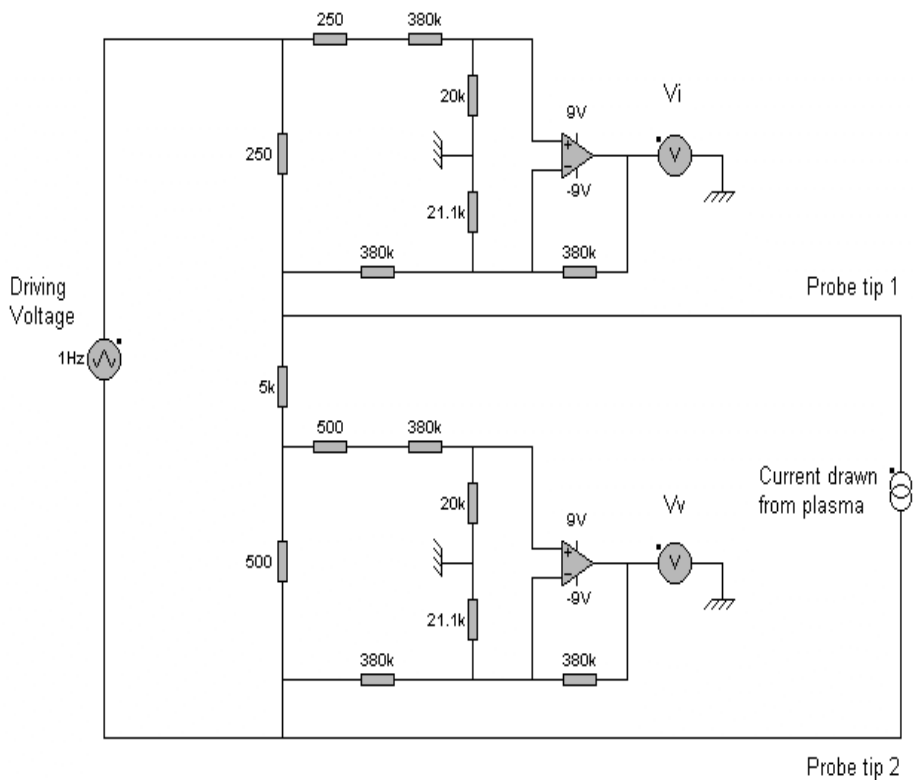


Figure 3.12: Typical double probe acquisition system circuit. Credit: C.Watts, UNM.

In figure (3.12) we see a typical double probe acquisition system. The op-amps are AD629ANs and they are powered using a set of batteries. The driving voltage come from a signal generator with certain parameters. A triangle wave with 50% symmetry and frequency of 99 – 101 Hz, (using a 100Hz the results characteristic is split into bands, probably due to some kind of resonance). The amplitude of the signal is of 4V so that going through the

amplifier we get a  $\pm 40V$  sweep. The output signal, using a digitizer board, is sent to the Pc, where a LabView program process it. This program uses a Levenberg-Marquardt algorithm to fit the I-V trace and, automatically, handles the data and error analysis showing on real time the results. These method is therefore much more faster to use, moreover it's possible to change parameters like pressure, magnetic field and position and see directly on the Pc monitor how this changes affect the I-V trace and thus the output data.



# Chapter 4

## Data analysis

### 4.1 Compensated probe analysis software

In section 3.4.2, we described the hardware that constitute the acquisition system that is controlled by a LabView program in the computer, which handles the acquisition and the probe movement. It is possible to perform measurements in two different modes. The first one automatically, performs a measurement for every step performed by the motor. The motor can move the probe to the next position either automatically after data is acquired, or by manually pushing a "button" in the interface. All the data from the measurements are saved in as single .txt file, each one with the corresponding motor position at which the sweep has been performed. In the second mode, it is possible to take single measurements without changing the motor position, the output data will be saved in a .txt file, but in this case it is necessary to create different .txt files to perform a different measurement. In both cases the output data has the same format and thus can be treated with the same analysis software. The output txt file is composed of a header section with various information, the most relevant are the sweep amplitude, the number of ramp steps and the number of measurements for each step. This quantities are saved into variables and are common for all the data of the txt file. After the header section starts the data section in which we have for each measurement the position of the motor and then three columns containing respectively the values of the bias potential, the output potential from the probe ( $V_b$  in figure 3.5) that should be divided by the measuring resistor, to obtain the probe current and finally the standard deviation of the second column. This last column actually has to be divided by the square root of number of measurements taken at each point (usually we used 200) to obtain the standard deviation of the mean value. The program language

use to perform analysis is IDL v6.5. Due to the fact that we used both the acquisition method we described above, we subdivide the analysis program in a upper and in a lower level. The upper level, called `Langmuir_multi`, is changing depending on the format of the file, i.e. more measurements on a single file, or more files with a single measurement. In any case the upper part send to the lower part (or `Langmuir_core` as we called the function) a single measurement for analysis. Both programs are visible in appendix A.

The lower level of the program start defining some fundamental quantities and constants, electron charge and mass and so on. After that, the position of the probe tip, relative to the chamber  $\hat{z}$  axis, is evaluated. It is necessary to change here the probe length value when a new probe is mounted Then we start a section of data "clean-up": the firsts and lasts data (just a few points) are cut away, usually these area are not interesting and presents spikes in voltage that could disturb the search for minimum and maximum of the function or of its derivative. Then the data is smoothed using a average box with the formula

$$V_i = \frac{1}{n} \sum_{j=0}^{n-1} V_{i+j-n/2} , \quad (4.1.1)$$

and  $n = 13$ . This smoothing is the largest source of error in potential measure as we will explain later. After smoothing the curve we create a four times more thicker sampling of the voltage, we interpolate the old current data with the new voltage sampling, to obtain a new thicker current vector. This operation ends the "clean-up" section. We now take the derivative of the current vector to find the minimum from which we get the plasma potential value. Then the floating potential is found looking for those points that are closest to the zero current, in plus and minus sign, and averaging their position. For the electron temperature evaluation we start removing the ion saturation current, then we perform the logarithm (we are looking in the exponential arm of the Langmuir characteristic) of the curve and we look for the linear segment. The inverse of the slope is equal to the electron temperature, see equation (3.2.29). Knowing the electron temperature it is possible to evaluate the density using

$$n = \frac{I(V_p)}{qA_p} \left( \frac{qT_e}{2\pi m_e} \right)^{-1/2} , \quad (4.1.2)$$

where  $I$  is taken at the plasma potential and  $T_e$  is measured in eV. As we explained in section 3.4.2, it is necessary to introduce a batteries between the bias circuit and the probe to reach higher plasma and floating potential values. The acquisition system is not able to track the number of batteries



we introduce for each measurement. It is therefore necessary to introduce this number at the end of the analysis, so that the software can add the right offset both to the plasma and to the floating potential.

The error evaluations for the two potentials is quite similar. For the plasma potential the largest error is given by the sampling rate of the acquisition system. So that if we have a sweep of  $\pm 30\text{V}$  composed of two hundred steps the minimum step would be  $0.3\text{V}$ . At this starting error we should add, with usual error propagation theory, the error given by the smoothing operation. Moreover since the values of the batteries inserted is not always equal to  $9\text{V}$ , we measure the voltage provided by each battery and evaluate average and standard deviation. This error must be considered since most of the plasma and floating potentials is made by the offset and not by the sweep itself. So depending on the number of batteries the error on potentials range from slightly more than one to a few volts. For the floating potential we thought to use the standard deviations values provided by the acquisition system. We took the current curve and create two others curves made by the original curve plus and minus the error at each point. We used then the distance, between the points in which these two curves cross the zero axis, as the error for the floating potential<sup>1</sup>. The results using this method were always quite smaller than the minimum step error mentioned above, anyway the software compare the two errors and keep the largest one. For the electron temperature the error is evaluated performing thirty times the selection, by the user, of the linear section. This measure on temperature has shown to be quite problematic. The main reason is that the sweep we used, of  $\pm 30\text{V}$ , in most of the cases is too small for clearly cover all the Langmuir characteristic, from the ion saturation zone to the plasma potential point. If the ion saturation zone is not well defined, subtracting its value become troublesome. If we then add the non perfect compensation of the RF signal, that tend to distort the exponential arm; we obtain a non perfectly linear section after we perform the logarithm of the characteristic. This is why we believe, that repeating a large number of times the selection of the zone where the slope has to be measured, is a good estimator of the electron temperature error. The density error is evaluated with the usual theory on error propagation, and since it depends on temperature, we obtain larger error on these two than in the potential measurements. The entire procedure to evaluate errors is much longer then a normal procedure for evaluate just the measurements values. For this reason we performed error analysis only on a smaller, and more significant, group of data. The two functions for performing the

---

<sup>1</sup>The same scheme is not applicable to the plasma potential, both curves always have the minimum of the derivative in the same position as the original curve.

error analysis are called `Error_analysis` and `Error_analysis_core`. Both programs are visible in appendix A.

## 4.2 Axial scan

Along the axial axis of Njord we performed most of our measurement. In particular we investigate the source area of the antenna close to the edge of the dome. Using the bottom of the antenna housing as the zero point of the  $\hat{z}$  axis, we scan an area between 190mm and 420mm. In figure (4.1) this zone is approximately from the beginning of the second source coil to the dome edge with the antenna housing. We performed measurement both with the compensated and the double probe varying position, pressure and coils current. We will subdivide our analysis in two section, that is, pressure and magnetic field scan.

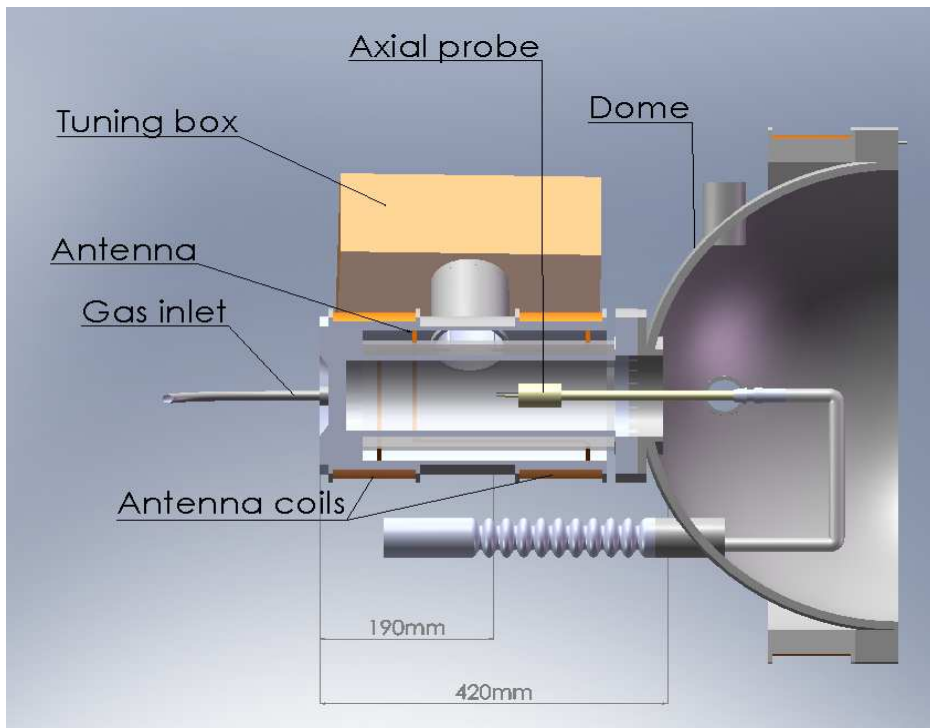


Figure 4.1: Frontal section of the antenna and the dome.

### 4.2.1 Pressure scan

For the pressure scan we analyze the range between  $2\text{-}3 \times 10^{-4}$  mbar and  $1 \times 10^{-3}$  mbar. The main reason we choose this values is that we expect most of the future experiment to be in this pressure range. In any case, for lower pressure the density of neutral particles into the chamber is too low for plasma ignition. On the other side for pressure slightly higher than  $1 \times 10^{-3}$  mbar the vacuum gauge stops working properly due to the transition from the Pirani to the inverted magnetron<sup>2</sup>.

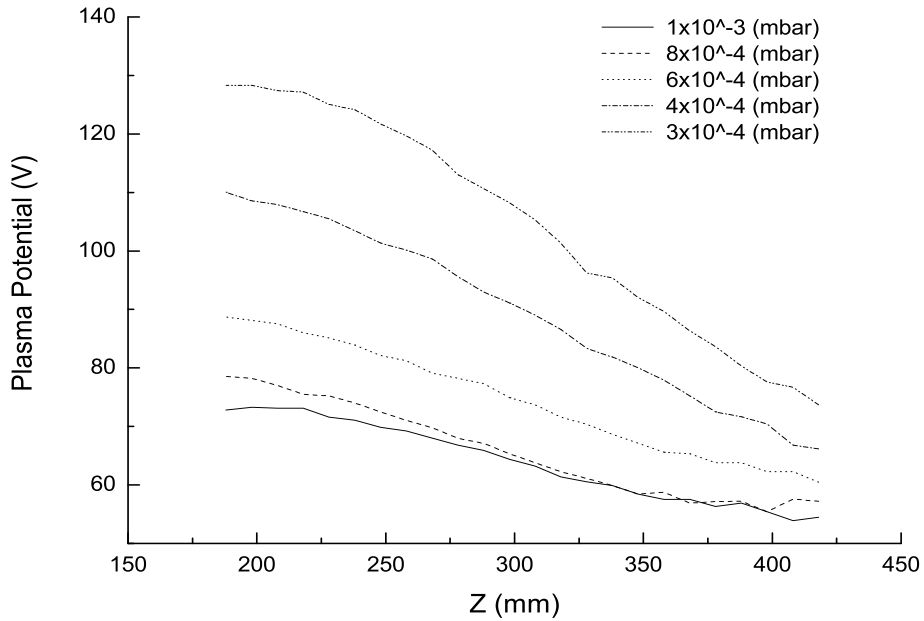


Figure 4.2: Plasma potential as a function of position for different pressure values and source coils current of 6A. Compensated Langmuir probe.

In figure (4.2) we show the plasma potential measured with the compensated probe along the  $\hat{z}$  axis for different pressure values and with a constant source coils current of 6A. It is clearly visible that with decreasing pressure the plasma potential increase. Increasing pressure the number of particles that could be ionized rise; thus the plasma density increase and the sheath thickness at the walls decrease as expressed by the Child-Langmuir law in

<sup>2</sup>See section 2.2.3, page 29 on the vacuum gauge used in Njord.

equation (3.1.27), in which the plasma density is included into the Debye length from equation (1.3.11). We can also notice that going from  $1 \times 10^{-3}$  mbar to  $8 \times 10^{-4}$  mbar the rise is less marked than in lower pressure regime. Moving towards the dome, all curves tend to drop. This behavior is more pronounced with lower pressure and is probably due to the decreasing magnetic field that we have in this region, see figure (2.11) in the range  $z = 0.2\text{m}$  to  $z = 0.4\text{m}$ . The potential drop as we explained in section 1.4.2, is an important parameter for Double Layers creation.

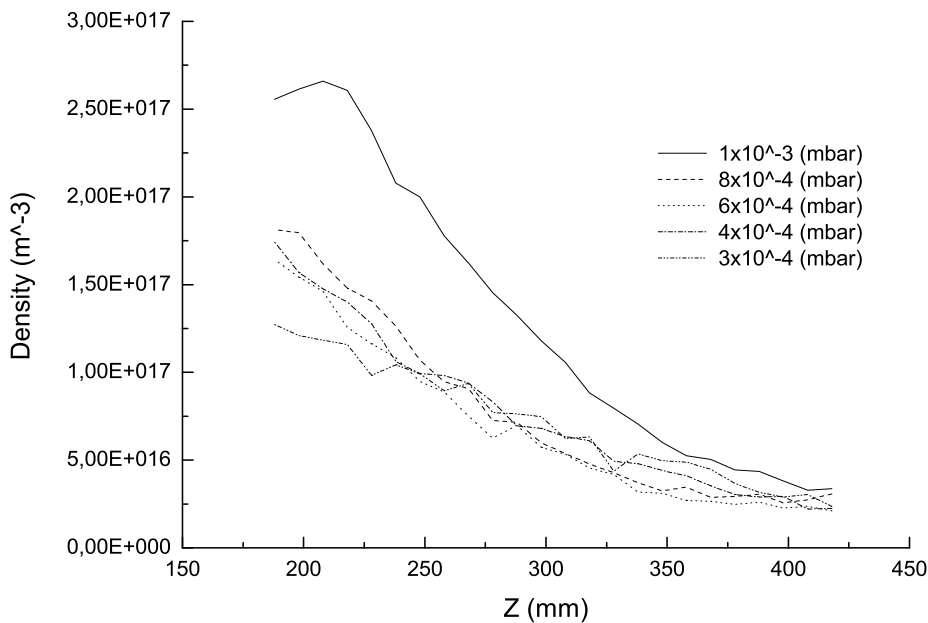


Figure 4.3: Plasma density as a function of position for different pressure values, source coils current 6A, power 600W. Compensated Langmuir probe.

If we plot now plasma density as a function of position for different pressure values, see figure (4.3), we notice that for higher pressure we obtain higher plasma density, (more Argon atoms are available to be ionized) and that density is dropping moving toward the dome due to the magnetic field expansion, that produce a plasma expansion. In this case the curve of  $1 \times 10^{-3}$  mbar and  $8 \times 10^{-4}$  mbar are not as close as they were in the previous plot, it rather seems that except for the highest pressure case all the others are acting almost similar. Examining in detail the curve of the  $1 \times 10^{-3}$  mbar

case it has a maximum at 210mm and then drops. Approximately in the same position we have the maximum of the magnetic field. This explains the drop on the left side of the maximum due as before to plasma expansion. We notice that when referring to the  $1 \times 10^{-3}$  mbar curve, moving towards the dome from higher density values, it approaches the other curves, though remaining always higher. In that region the plasma density seems not to depend anymore on the neutral pressure. As we will see this is probably due to the structure of the chamber at the flange that join the antenna with the dome.

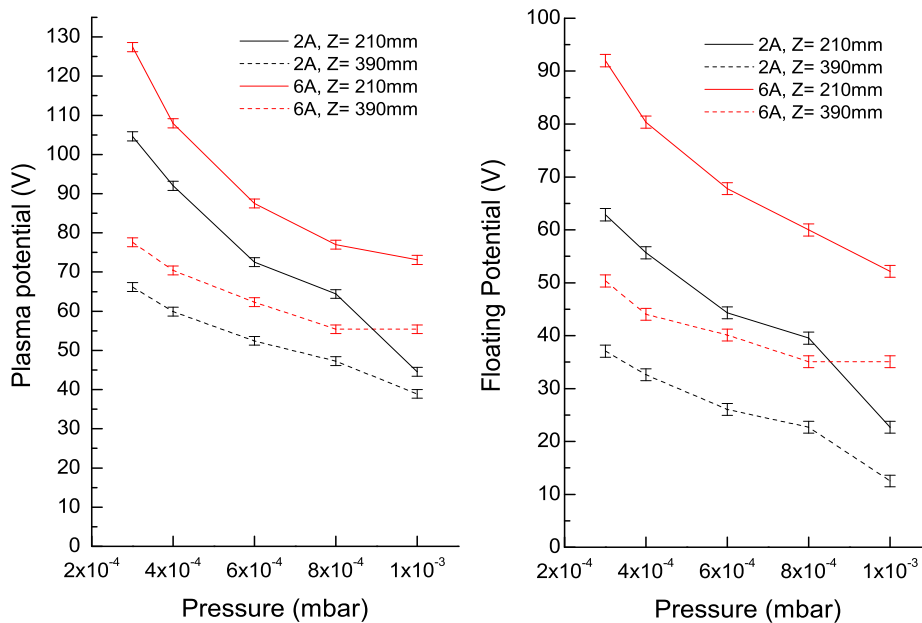


Figure 4.4: Plasma and floating potential as a function of pressure, with source coils current of 2 and 6A and axial position  $Z = 210$  and 390mm. Compensated Langmuir probe.

In figure (4.4) we plot plasma and floating potential varying pressure. The four curves stand for different position and source coils current. In particular red lines are for high source coils current (6A) while black for low current (2A). The solid line stands for an inner position in the source ( $Z = 210$ mm) and the dashed line for an outer position toward the dome ( $Z = 390$ mm). Also here, like in figure (4.2) the drop in plasma potential is significant with

increasing pressure. It is also easy to read the potential drop between the inner position and the outer watching at the difference between the solid and dashed curve (of the same color). As we already mentioned the potential drop reduces with increasing pressure, while, except for the higher pressure range, it does not seem to be dependent on the magnetic field (i.e. the distance between solid and dashed curve is comparable for both high and low coils current). The same pattern is reproduced in the floating potential case.

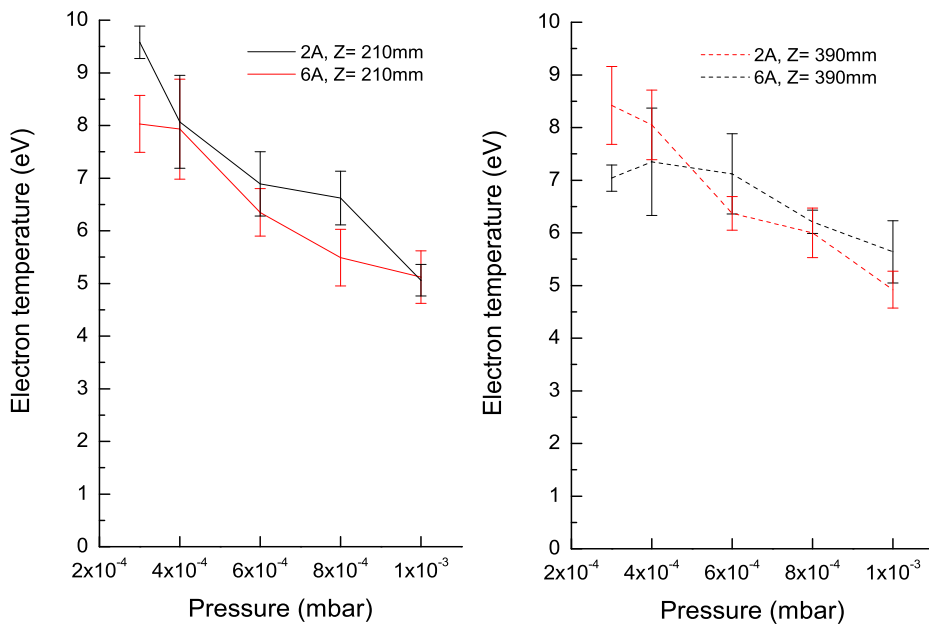


Figure 4.5: Electron temperature as a function of pressure, with source coils current of 2 and 6A and axial position  $Z = 210$  and  $390$ mm. Compensated Langmuir probe.

Looking at the electron temperature, figure (4.5), we obtain what we would expect. The temperature decreases with increasing pressure due to the higher collision rate, which reduces the electron energy and thus its temperature. Inside the chamber (left panel) the temperature drops from about 8-10eV to 5eV. In the high magnetic field case  $T_e$  slightly colder due to the higher confinement of the plasma. Closer to the dome the temperature drop is slightly less marked, from 8-9eV to 5eV. Thus at lower pressure there is a difference between the inside of the source and the outside. This difference is

canceled out in the higher pressure case. Looking at the right panel of figure (4.5) we see that except for the lowest pressures, with a stronger magnetic field the temperature is lower, as we said before due to the better confinement of the plasma. From this consideration we should deduce that the plasma density is actually increasing with a stronger magnetic field. Moreover as we will shortly see this assumption is not verified by the density measure we performed.

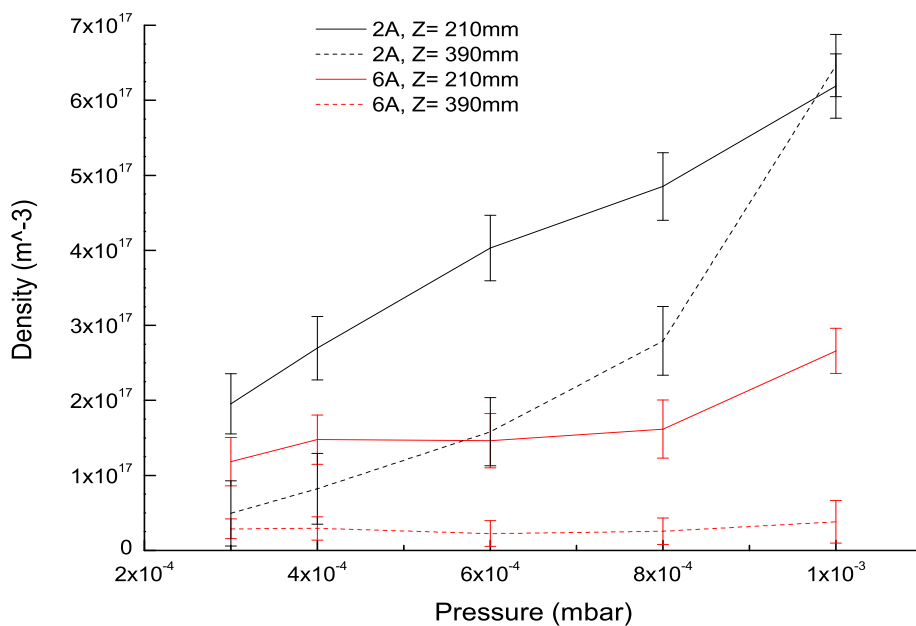


Figure 4.6: Plasma density as a function of pressure, with source coils current of 2 and 6A, axial position  $Z = 210$  and  $390\text{mm}$  and power of  $600\text{W}$ . Compensated Langmuir probe.

In figure (4.6) we show the density varying pressure. At first look it is clearly visible that the density at low magnetic field (black line), is higher than the high magnetic field case (red line); in both the positions inside the source (solid line) and outside (dashed line). Moreover at high magnetic field the density is constant on the dome edge and increases slightly inside. In the low magnetic field case instead the density is strongly increasing, in particular outside the source (where it goes from  $5 \times 10^{16} \text{ m}^{-3}$  to  $6 \times 10^{17} \text{ m}^{-3}$ ).

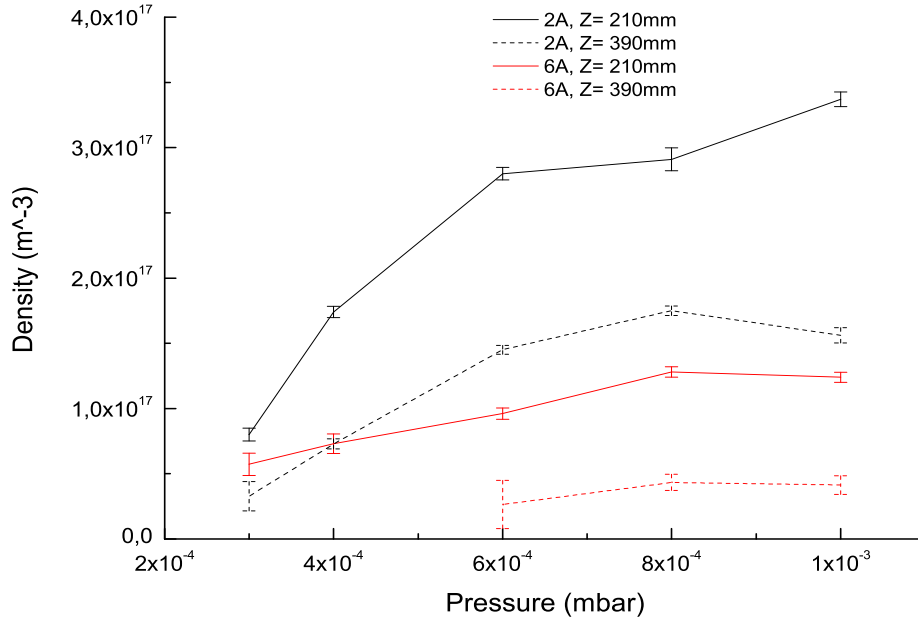


Figure 4.7: Plasma density as a function of pressure, with source coils current of 2 and 6A, axial position  $Z = 210$  and  $390$ mm and power of  $900$ W. Double probe.

To check the goodness of our data we performed density measurements (using the same parameter of pressure, source coils current and position), with a double probe. In figure (4.7) we show the result. As we can see the trend is the same as in the compensated Langmuir probe case. Comparing the two plot we see that the compensated probe seem to be higher of a factor of three with respect to the double probe (taking into account the higher power of the double probe case, see figures captions). Despite of this factor the main trend is the same for all the four curves. In the outside region in particular we have: constant density for high magnetic field and increasing density for low magnetic field, as before. The red dashed curve is incomplete in the low pressure range because the acquisition system of the double probe, was not able to resolve the Langmuir characteristic at this very low density. In our measurements with the double probe technique it was necessary to use a minimum antenna power of about  $900$ W (while we used about  $600$ W for the compensated probe), this higher value is the minimum needed to have



a Langmuir characteristic with the double probe, otherwise the acquisition system was not able to resolve the curve.

Using a simple model for uniform discharge in a electropositive plasma, see [12], we can derive from an energy balance a formula for the plasma density as

$$n = \frac{P_{abs}}{eu_B A_{eff} \varepsilon_T}, \quad (4.2.3)$$

where  $P_{abs}$  is the power coupled from the antenna to the plasma,  $u_B$  is the Bohm velocity (see equation 3.1.10) and  $A_{eff}$  is the effective area of the plasma<sup>3</sup>. The term  $\varepsilon_T$  is the total energy loss per ion lost from the system. Actually if we increase the magnetic field strength the plasma should be more confined and thus less ion should be able to reach the chamber wall and get lost. On this scheme the density should increase with increasing magnetic field. On the other hand, with a stronger magnetic field, the charged particles are more bounded in their gyro-motion around the field lines. Thus if these field lines fall directly into (a region close to) the port wall we will increase the number of particle lost with increasing magnetic field. From figure (4.6) we can see that inside the source density is in both cases (low and high magnetic field) increasing. Outside the source, near the dome edge the density is almost constant with high magnetic field while it strongly increases with low magnetic field. The explanation we propose is that most of the particles are lost in the flange that connects the antenna with the dome. Moving from inside the source toward the main chamber the plasma get in contact with: the pyrex tube in the antenna, see figure (4.1), the 40mm of the flange and the 30mm dome support of the flange. So between the pyrex tube and the dome itself the plasma get in contact with 70mm of grounded walls, in which we suppose most of the plasma gets lost. To let the plasma flow into the main chamber it is necessary to solve this problem. A couple of long term solutions could be arranged in the future. Another pyrex tube can be installed inside the flange, so that it covers the grounded flange and ends directly into the dome. Another long term solution, that could be used in pair with the pyrex tube, is to mount some fixed magnet, or even a small "flange" coil, to keep the plasma away from the walls and let it flow into the main chamber. In my opinion, the second solution seem to be easier to implement and more

---

<sup>3</sup> $A_{eff} = 2\pi R(Rh_R + Lh_L)$ . R and L are respectively the radius and the length of the plasma column. Using a low pressure diffusion model, the ratio between the density at the axial and radial sheath edges and the bulk of plasma can be approximated by:  $h_L = \frac{n_{sL}}{n} = 0.86 \left(3 + \frac{L}{2\lambda_i}\right)^{-1/2}$  and  $h_R = \frac{n_{sR}}{n} = 0.80 \left(4 + \frac{L}{2\lambda_i}\right)^{-1/2}$  in which  $\lambda_i$  is the ion mean free path.

flexible on eventual future modification of the machine.

### 4.2.2 Magnetic scan

In the magnetic scan we analyze data for a range of source coils currents between 2 and 6A. For the lower currents the plasma was having problem on ignition and presents clear instability (mainly glittering), while for higher currents the temperature of the two coils is raising quite fast. With 6A current anyway we get around 160G maximum magnetic field, that is in the range in which Njord will mainly operate (150-200G).

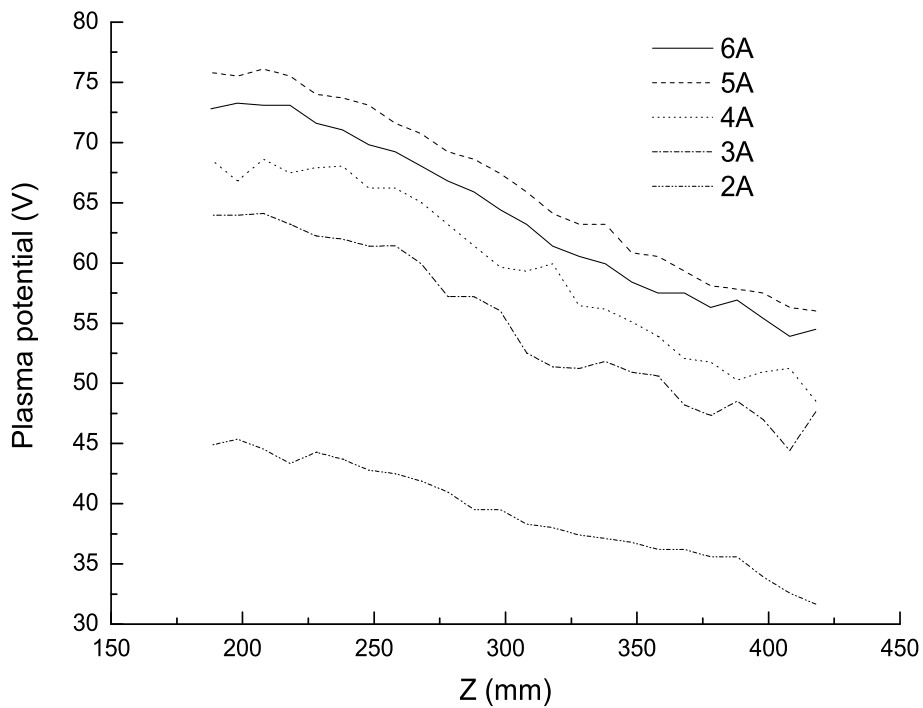


Figure 4.8: Plasma potential as a function of position for different source coils current and a pressure of  $1 \times 10^{-3}$  mbar. Compensated Langmuir probe.

In figure (4.8) we show the plasma potential varying the position along the  $\hat{z}$  axis for different values of the source coils current. Also here, as in the pressure scan case, the potential is dropping moving towards the dome due to the magnetic field expansion. We can also see that increasing the source

coil the potential increases, while with a better confinement we would expect an higher pressure and thus a lower potential. But we have shown that when we increase the magnetic field the density is dropping and therefore this plot is in agreement with the pressure vs. position data we showed in the previous section. What we cannot explain is the strange behavior of the 5A curve that we expect to be at lower potential, with respect to the 6A curve. We can also appreciate how the potential drop between the inner part of the chamber and the outer one seems not to depend on the magnetic field strength.

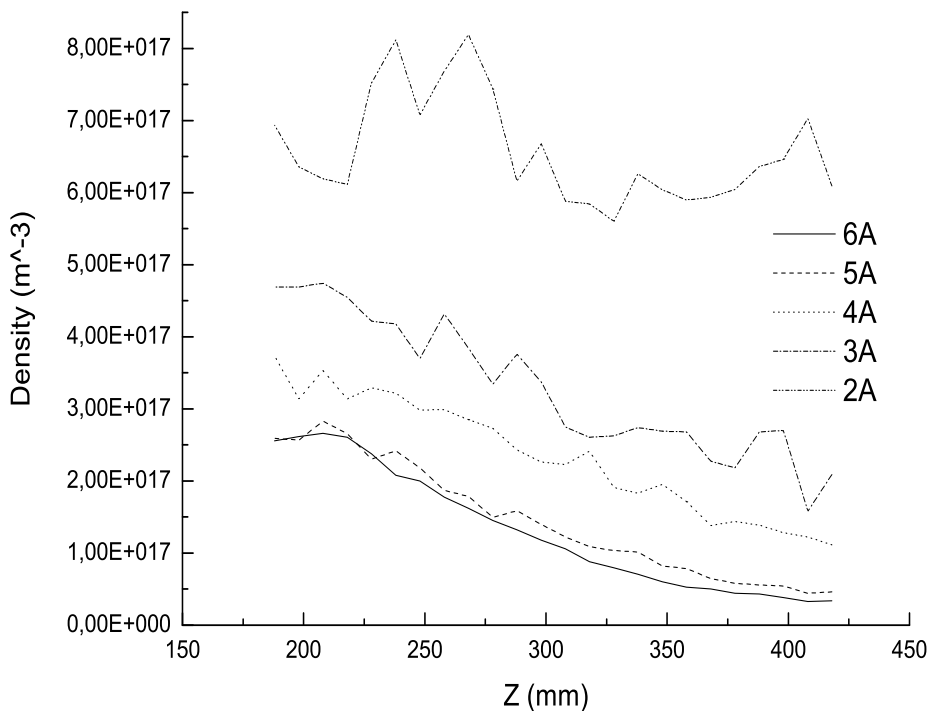


Figure 4.9: Plasma density as a function of position for different source coils current and a pressure of  $1 \times 10^{-3}$  mbar. Compensated Langmuir probe.

In figure (4.9) we show the plasma density as a function of varying magnetic field. In agreement with the previous data the density increase with lower magnetic field. The growth is quite stronger in particular when changing from 3 to 2A in the current. We should point out that the 3 and 2A curves are quite noisy, probably due to the less confinement, with respect to the higher magnetic field case (in particular if compared with the 6A curve

that is quite smooth), thus this stronger growth could be not so relevant.

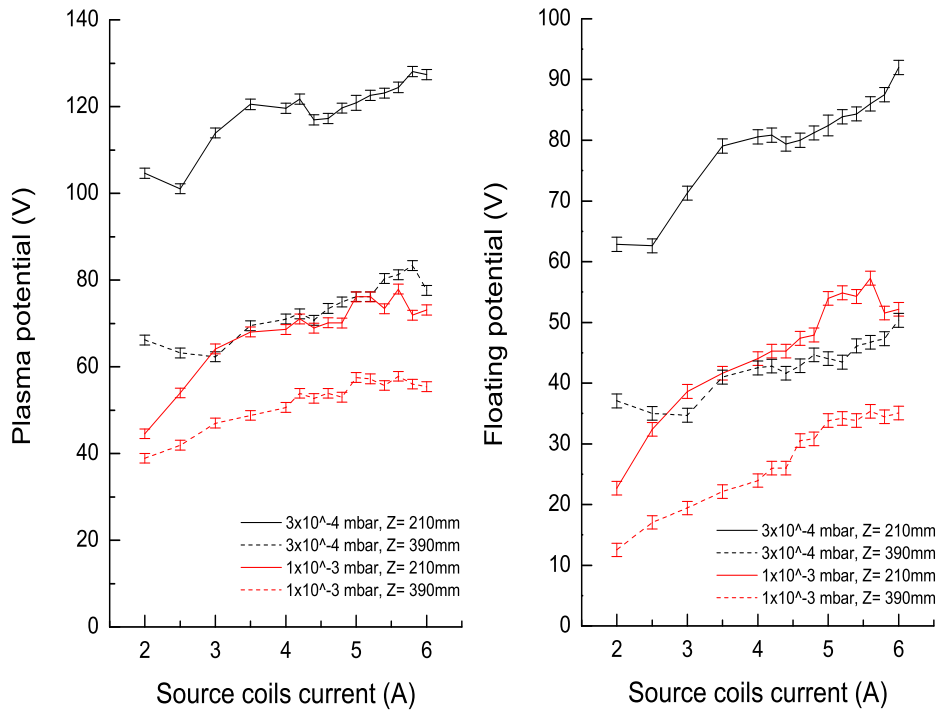


Figure 4.10: Plasma and floating potential as a function of source coils current, pressure from  $1 \times 10^{-3}$  mbar to  $3 \times 10^{-4}$  mbar and axial position  $Z = 210$  and 390mm. Compensated Langmuir probe.

In figure (4.10) we plot, plasma and floating potential as a function of varying magnetic field. As we did in the pressure scan the solid curve stands for an inner position in the source ( $Z = 210$ mm) and the dashed line for an outer position toward the dome ( $Z = 390$ mm). The red color is now used for high pressure ( $1 \times 10^{-3}$  mbar) while black for low pressure ( $3 \times 10^{-4}$  mbar). As we can see in both panels, potential is increasing with increasing magnetic field. We have higher potentials for lower pressure, as we see in the pressure analysis section. Here we can better appreciate the potential drop due to the plasma expansion, i.e. the distance between solid and dashed line of each color. As we pointed out before the lower the pressure is the higher is the potential drop. Except for the lower field and high pressure case, the drop seems not to be dependent of the magnetic field.

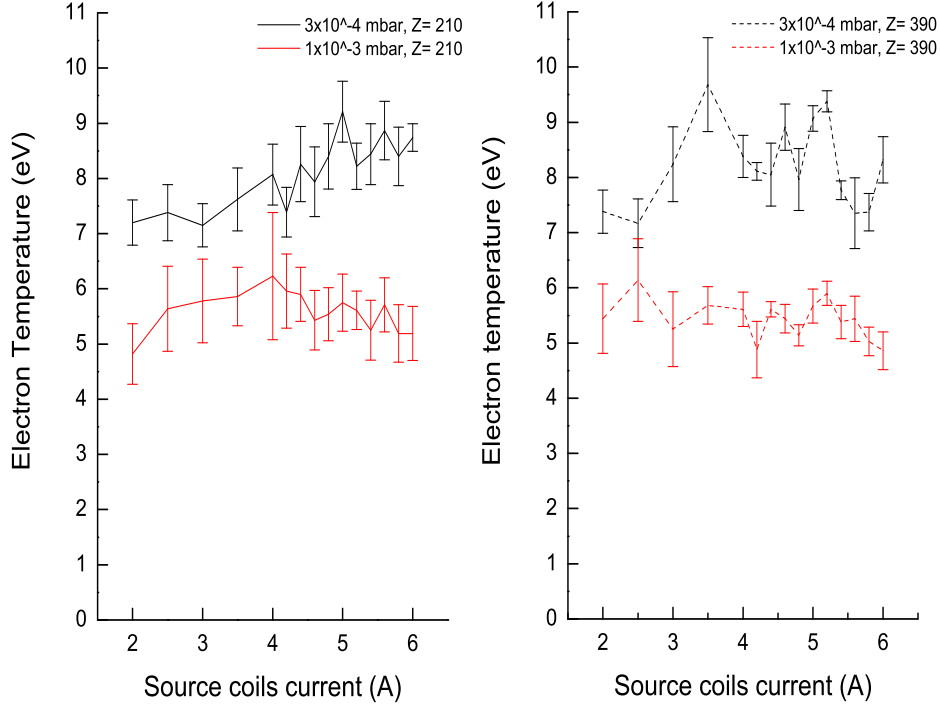


Figure 4.11: Electron temperature as a function of source coils current, pressure of  $1 \times 10^{-3}$  mbar and  $3 \times 10^{-4}$  mbar and axial position  $Z = 210$  and 390mm. Compensated Langmuir probe.

In figure (4.11) we plot the electron temperature both outside and inside the antenna section. As we can see in both cases the temperature does not depend on the magnetic field, and remains almost constant (it seems to slightly increase in the low pressure case). In agreement with the effect of pressure scan on temperature we see that the two temperatures in low pressure cases are clearly higher than the high pressure cases. Comparing the left and right panels we can notice how the temperature seems constant in the two region where we performed the measurements.

In figure (4.12) we plot the densities. As we noticed the density in the low pressure cases are constant, and higher inside than outside due to the plasma expansion (solid and dashed black curves). When the pressure is increased (looking at the red curves) and with a lower magnetic field, the density increases of almost a factor of four, and is equal both inside and outside the

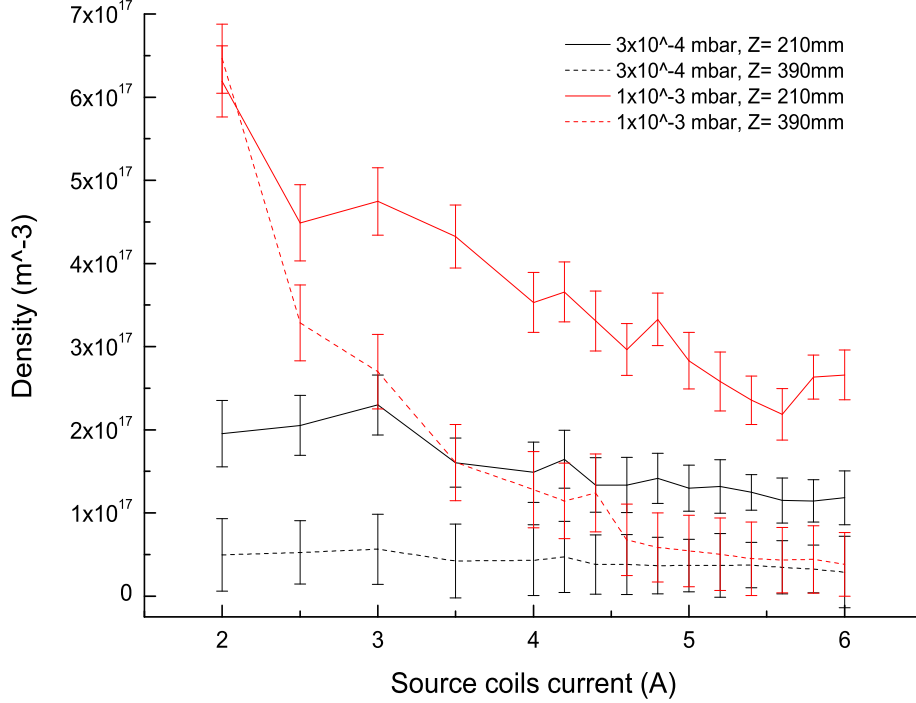


Figure 4.12: Plasma density as a function of source coils current, pressure of  $1 \times 10^{-3}$  mbar and  $3 \times 10^{-4}$  mbar, axial position  $Z = 210$  and  $390$ mm and power of 600W. Compensated Langmuir probe.

source. Following then the two red curves with increasing pressures density drops, much faster outside than inside. While for the flange zone near the dome the density drop could be explained with the simple model we described before. Inside the source the plasma is only in contact with the pyrex tube. A possible explanation for the density drop could be given by a stronger magnetic mirror effect<sup>4</sup>, that pushes away particles towards the dome.

As we did for the pressure scan we perform, using the double probe, a density measure the with same parameters we used for the compensated

<sup>4</sup>The magnetic mirror effect is an application of the first adiabatic invariant. A charged particles, moving towards a stronger magnetic field region, will lose parallel velocity in favor of the gyration velocity. Since at the mirror point the magnetic field is inhomogeneous, the gyration plane is not perpendicular to  $\mathbf{B}$ . The particle is then pushed back into the lower magnetic field region by the restoring force.

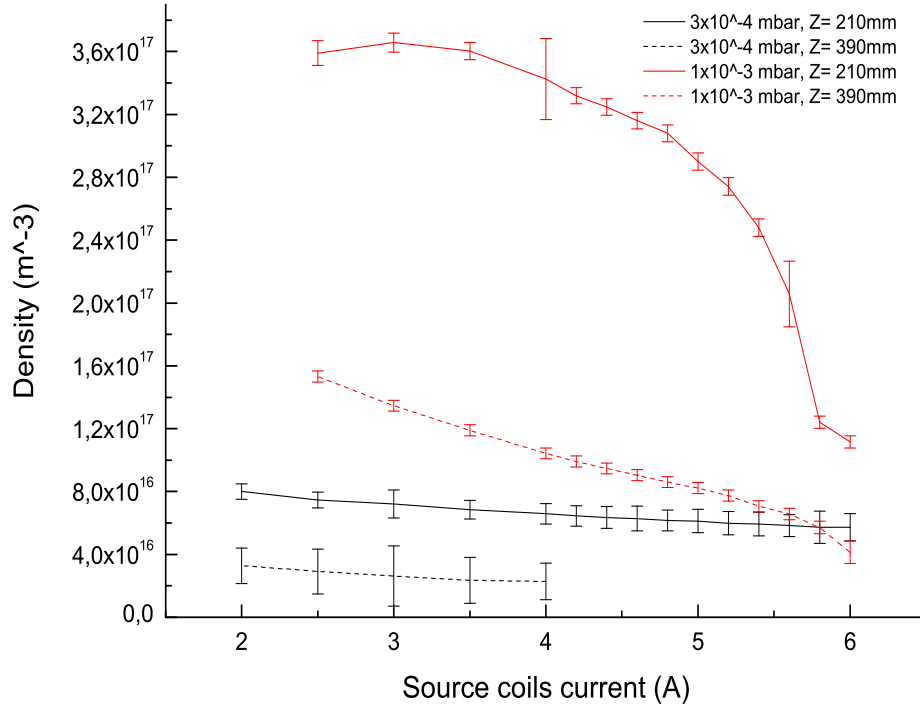


Figure 4.13: Plasma density as a function of source coils current, pressure of  $1 \times 10^{-3}$  mbar and  $3 \times 10^{-4}$  mbar, axial position  $Z = 210$  and  $390$ mm and power of  $900$ W. Double probe.

probe. In figure (4.13) we see the result. The two low pressure curves (black lines) are consistent, counting on the factor of three we found on the pressure scan data, with the compensated probe results. As in the pressure scan the missing data on the dashed-black curve; are due to the low pressure range in which the double probe software is not able to resolve the I-V characteristic. For the high pressure curves, the one taken outside (dashed-red) it's also consistent, while the curve measured inside (solid-red) is not consistent. It is dropping, actually, with increasing magnetic field, but the trend of the curve is different (they have opposite concavity) and in the low magnetic field range it reaches higher values of density.

As we have seen both in the pressure and in the magnetic scan the plasma density is decreasing with increasing magnetic field. In the previous section we tried to give an explanation for this phenomenon, and suggested some

long-term solution. A short term solution we tested is to use the first of the chamber coils to create a stronger magnetic field inside the flange area. In section 2.4 we calculated the magnetic field, in particular in figure (2.12) we plotted the magnetic field intensity with the presence of this coil (with a current of 20,40,-20,-40A). The region of interest is near the dashed line.

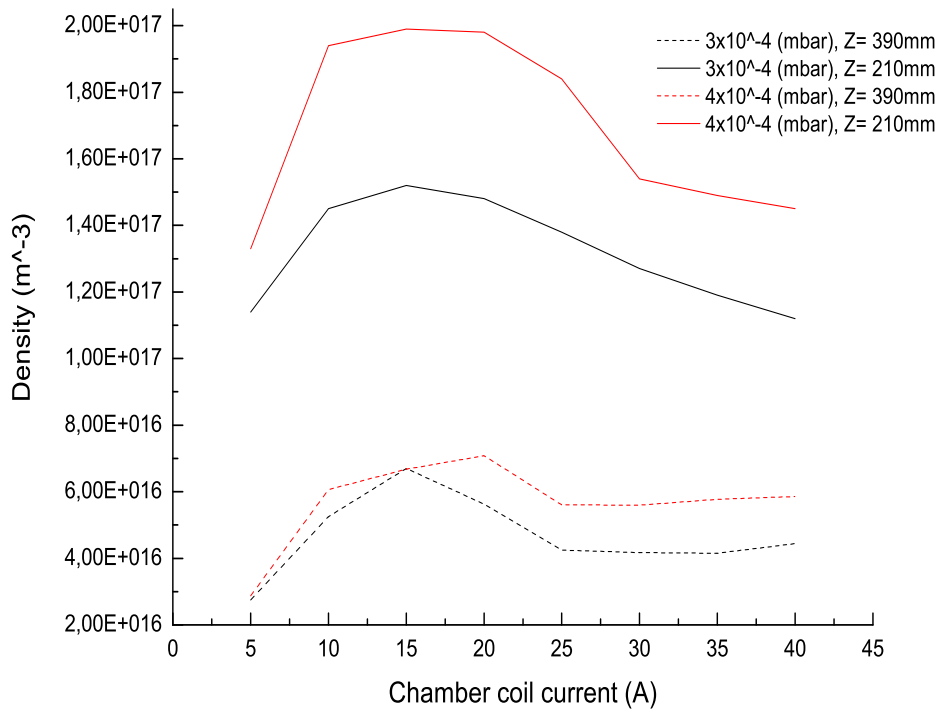


Figure 4.14: Plasma density as a function of chamber coil current, source coils current 6A, pressure of  $4 \times 10^{-4}$  mbar and  $3 \times 10^{-4}$  mbar, axial position  $Z = 210$  and 390mm and power of 900W. Double probe.

In figure (4.14) we plot the results for density while varying the chamber coil current. We used a current of 6A in the source coils, and we measured as before inside (solid) and outside (dashed). Since previously we had problems to obtain some density plots for the low pressure range, see figure (4.7), for this test we performed our measurements at  $3 \times 10^{-4}$  mbar (black lines) and  $4 \times 10^{-4}$  (red lines). As we can see the four curves present all the same trend: first density rise from 0 to 10A, then we have an almost steady zone up to 25A, and then the density drop again. The last drop is due to magnetic



mirror effect but on the other direction, so that particles are pushed into the antenna (the chamber coil magnetic field is now stronger than the source coils magnetic field). While the increase in the dome edge zone (dashed lines) is not marked as inside the source (solid lines); it is, at least, enough to clearly obtain an I-V characteristic. For the two solid curves (inner position) we also plot the density value obtained with zero chamber coil current. As we can see, from 0 to 10A, the density double for the low pressure case and almost triple for the higher pressure case. With this test we want to show that increasing the magnetic field strength in the flange zone could be helpful in increasing the quantity of plasma that could flow into the main chamber. It is our obligation to point out that this "strange" behavior of the plasma density, in relation to the magnetic field intensity, could have a deeper explanation in some particular antenna mode. The description of these modes is far out of the scope of these thesis. For a future better knowledge of plasma behavior in Njord a study of these modes appears to be necessary.

### 4.3 Radial scan

The radial axis on which we performed our measurements is about 550mm from the source bottom, and about 150mm from the antenna and dome edge. The magnetic field in this region, using only the source coils is extremely weak, see figures (2.11) or (2.12) near the dash-dot line. In this condition we expect a low density, and minor radial dependence on the source coils current of our data. Probably due to this lack of magnetic field we encounter more problems in performing the measurements. The main source of this problems what we described in section 4.1. The sweep we used ( $\pm 30V$ ), is barely enough to cover both the ion saturation current regime and the plasma potential point. Moreover when performing the first derivative of the I-V characteristic, the minimum, which gives us the plasma potential, is not defined by a narrow function (as it was in most of the axial measurements). Instead, the minimum is quite wide and forms a kind of plateau in which it is possible to guess the real minimum position, but with a certain amount of error. This is the reason why our radial plots present larger error bars on potential, temperature, and, in particular, density.

In figure (4.15) we show the plasma potential as a function of the radial position<sup>5</sup> for different pressure values (right panel) and source coils currents (left panel). As we noticed in the axial analysis, increasing the pressure

---

<sup>5</sup>The radial position is measured on the radial axis, that is orthogonal to the  $\hat{z}$  axis and lies in the rz plane. The positive direction is, watching from the origin of the  $\hat{z}$  axis, from left to right.

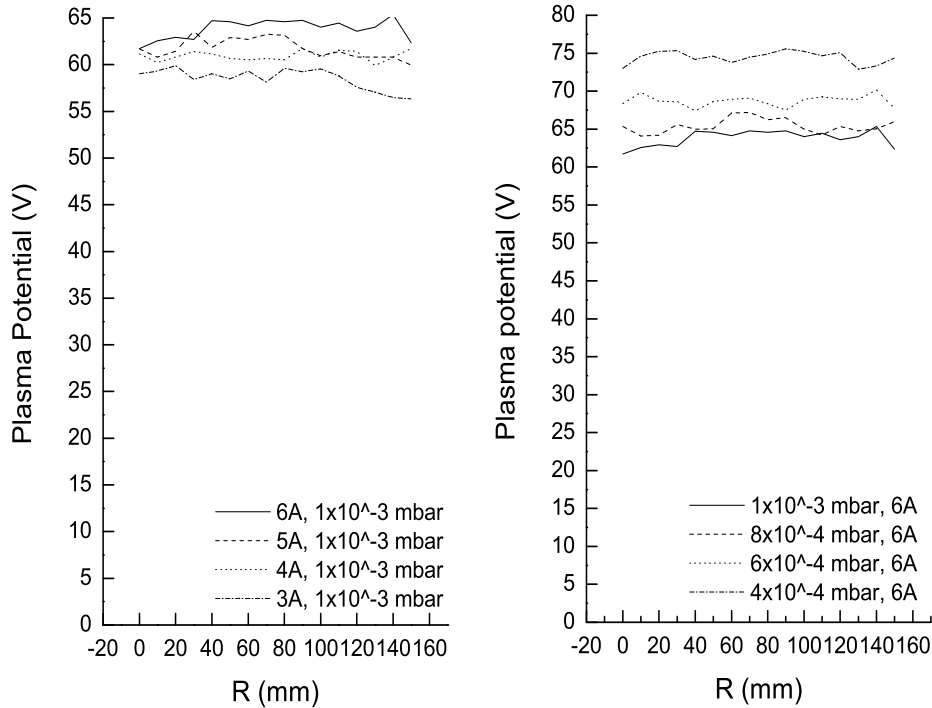


Figure 4.15: Plasma potential as a function of radial position for different values of pressure (right panel) and magnetic field (left panel). Double probe.

results in a lower plasma potential. With respect to the antenna edge, the potential is almost the same, see figure (4.2). This is in agreement with the fact that there is not any more magnetic field expansion, that as we saw is connected to the potential drop. On the left panel we see that when varying the magnetic field, the plasma potential slightly change, with the 3A curve slightly higher than the other curves, see figure (4.8). From both panels we can see that the potential remains almost constant moving along the radial axis. As we said, this is due to the homogeneous and close to zero magnetic field we have, that has spread out in the dome. Reputedly, with a stronger magnetic field from the source coils, a change in potential should be visible at the pyrex tube radial edge position (75mm).

In figure (4.16) we show density profiles along the radial axis, varying pressure (right panel) and magnetic field (left panel). In the pressure panel it is deducible that increasing pressure lead to a higher plasma density. How-

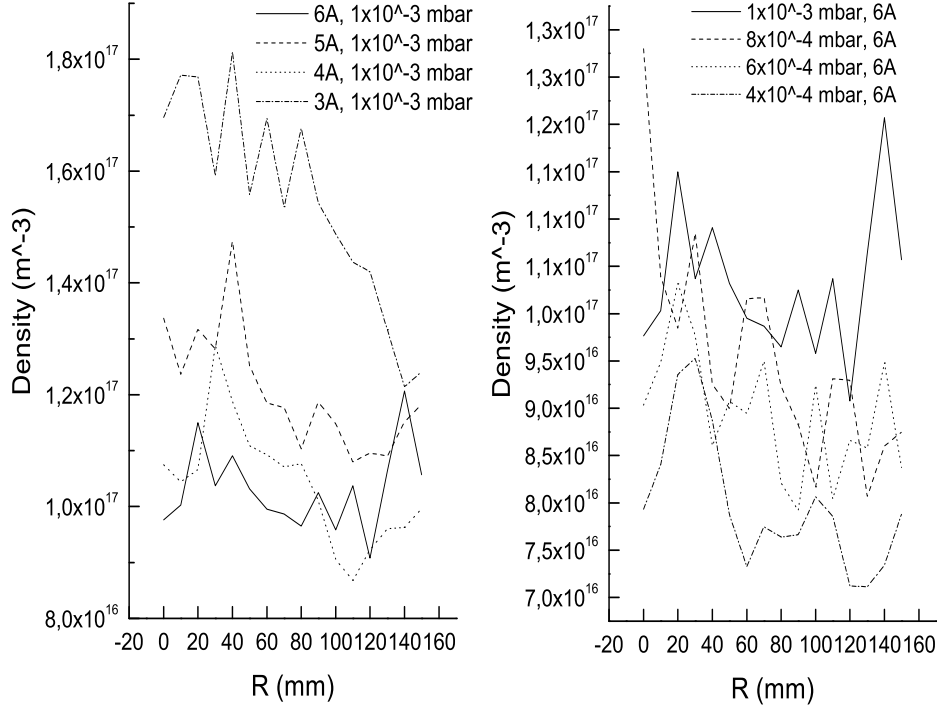


Figure 4.16: Plasma density as a function of radial position for different values of pressure (right panel) and magnetic field (left panel), power of 900W. Double probe.

ever, due to the absence of magnetic field and the difficulties in the sweep we explained before, it is not really possible to extrapolate a certain trend for the curves along the  $\hat{r}$  axis. Looking at figure (4.3) it seems that the density here ( $8.5 - 9.5 \times 10^{16} \text{ m}^{-3}$ ) is slightly higher than at the antenna edge ( $4 - 5 \times 10^{16} \text{ m}^{-3}$ ). On the left panel, as for the right one, the density dependence from radial position is not clear. Only the low current curve (3A) seems to drop moving outwards toward the wall. Looking at figure (4.9) we can see that density is lower on the radial axis than on the antenna edge, ( $1 - 2 \times 10^{16} \text{ m}^{-3}$ ) on ( $3 - 5 \times 10^{16} \text{ m}^{-3}$ ).

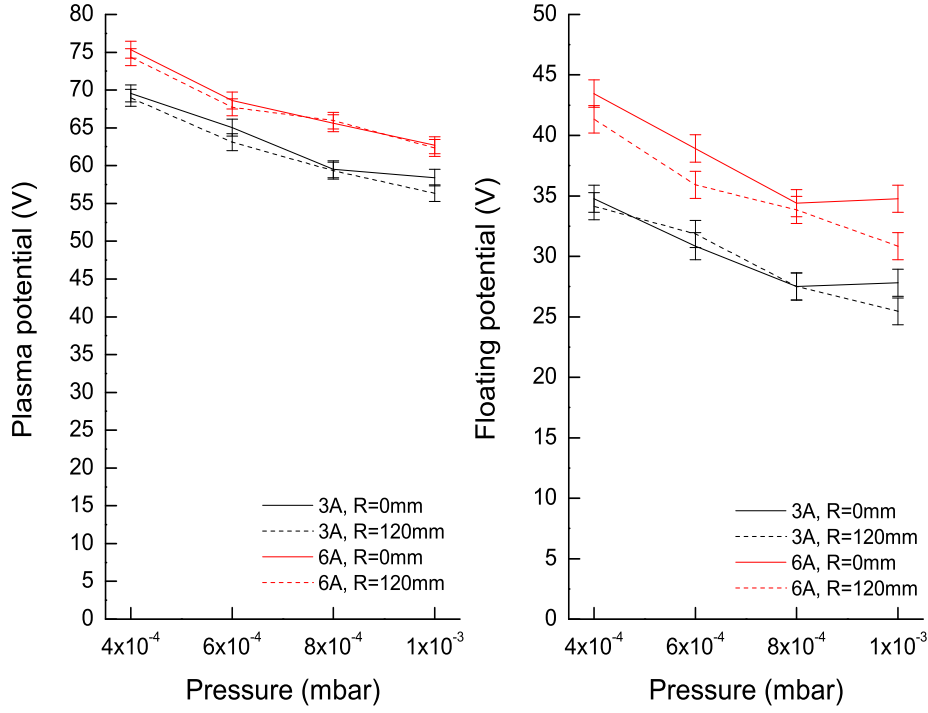


Figure 4.17: Plasma and floating potential as a function of pressure, with source coils current of 3 and 6A and radial position  $R = 0$  and 120mm. Compensated Langmuir probe.

### 4.3.1 Pressure scan

The pressure ranges we used for the pressure scan along the  $\hat{z}$  axis, have been used also for the radial axis analysis. In figure (4.17) we plot plasma and floating potential for two values of source coils current, 3 and 6A (black and red curves) and for two different position  $R = 0$  and 120mm (solid and dashed line). The position  $R = 120$ mm has been chosen on purpose to be outside the pyrex tube column, while obviously  $R = 0$ mm is in the middle. As we said above, the weak magnetic field does not affect the plasma parameters. In both panels, and for both high and low current curves, we can see that the solid and dashed lines are quite close. This means no difference between the plasma in the center of the pyrex tube column and the plasma outside of the column. Instead a drop due to the increasing pressure is visible; even if

here it is of about 10V while in the axial case it is almost the twice as high, around 20V, see figure(4.10).

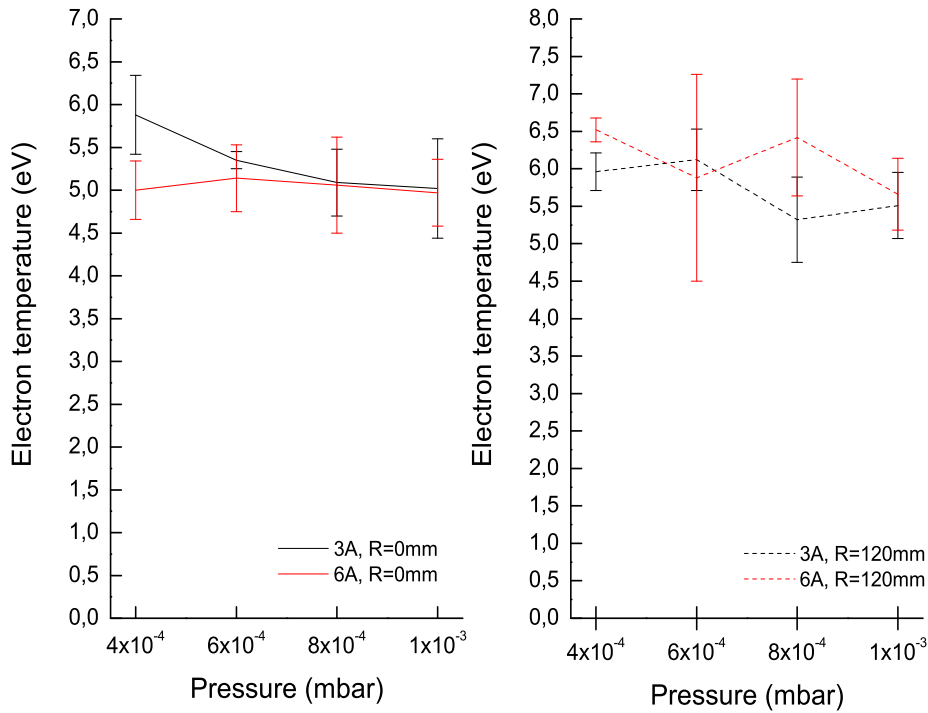


Figure 4.18: Electron temperature as a function of pressure, with source coils current of 3 and 6A and radial position  $R = 0$  and 120mm. Compensated Langmuir probe.

In figure (4.18) we show the electron temperature curves, with the same methodology previously used. Also here the two regions, inside and outside, presents almost the same temperature (dashed and solid line). The drop in temperature we would expect with increasing pressure is not present, as it was in the axial case, see figure (4.5). Moreover, from the same figure, we can compare the temperature here, with the antenna edge area. Only for higher pressure there seem to be an agreement. Evidently, the higher electron temperature in the lower pressure case, at the radial position, has been dissipated somehow.

In figure (4.19) we plot the plasma density as a function of pressure. As we can see, it increases slightly, but as we noticed for the dashed-red curve

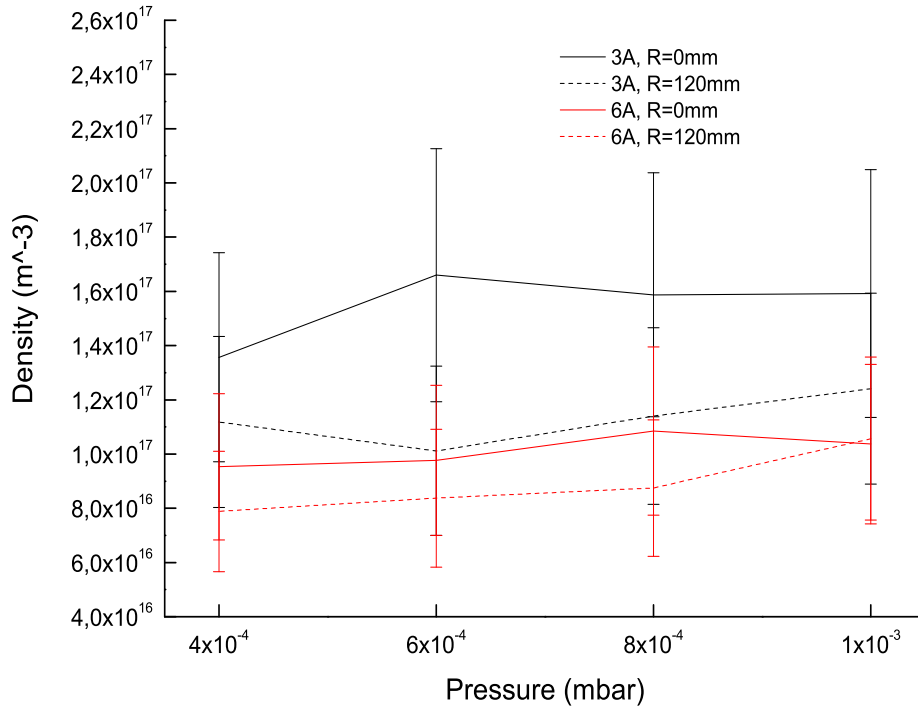


Figure 4.19: Plasma density as a function of pressure, with source coils current of 3 and 6A, radial position  $R = 0$  and 120mm and power of 600W. Compensated Langmuir probe.

of figure (4.6) the density could be considered constant. Most particles has been lost at the dome flange, and in fact the higher density for the lower magnetic field case still persists, as was the case near the antenna. Moreover in the low current case the density near the  $\hat{z}$  axis is higher than the density radially outwards from it. On the other hand for the high current case this difference is much less. It is necessary anyway to point out that the error in these measurements is quite high, as we can see from the error bars.

### 4.3.2 Magnetic scan

On the radial magnetic scan, we increase our lower value from 2 to 3A, since already with 3A the magnetic field where we perform our radial scan is very low.

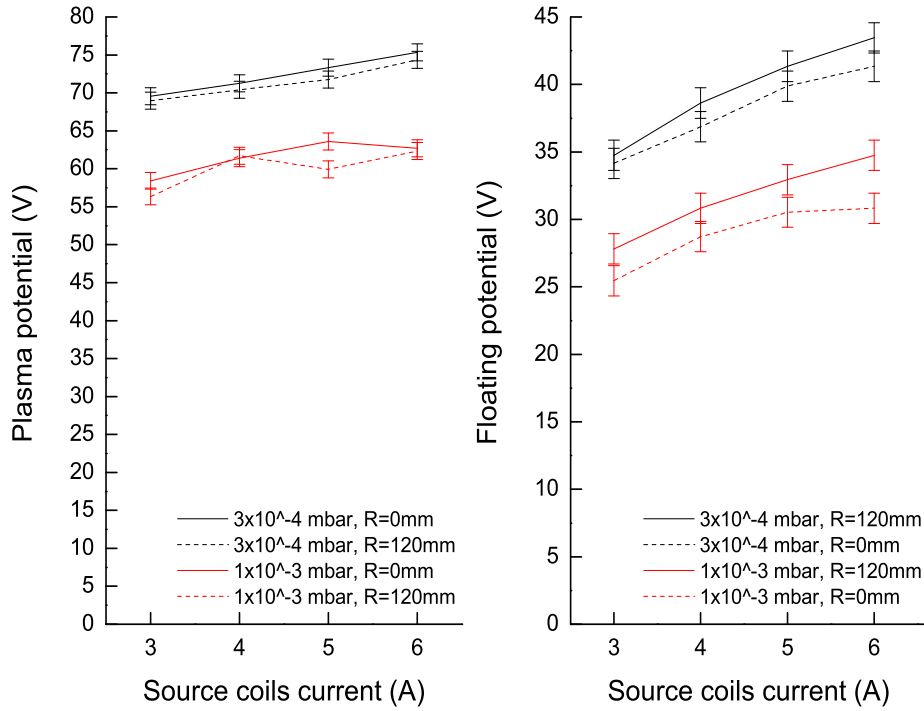


Figure 4.20: Plasma and floating potential as a function of magnetic field, pressure of  $1 \times 10^{-3}$  mbar and  $3 \times 10^{-4}$  mbar and radial position  $R = 0$  and 120mm. Compensated Langmuir probe.

In figure (4.20) we see the plasma and floating potential. As before inner and outer position are very close (solid and dash lines). The potential increases with magnetic field strength and is higher, as expected in the lower pressure case. Looking now at figure (4.10) we can see that the lower pressure case at the antenna edge is in agreement with the value we measured here. The high pressure case instead is lower at the antenna edge and higher here of about 10 – 15 V. The difference between the plasma and the floating potential is in agreement with what we measured on the antenna edge, about

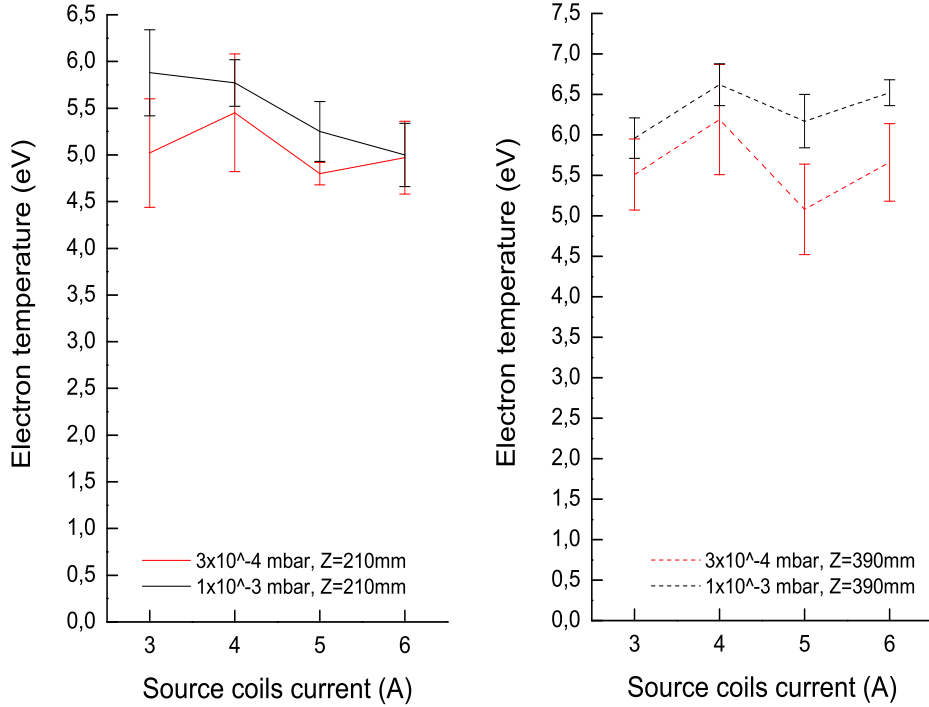


Figure 4.21: Electron temperature as a function of magnetic field, pressure of  $1 \times 10^{-3}$  mbar and  $3 \times 10^{-4}$  mbar and radial position  $R = 0$  and 120mm. Compensated Langmuir probe.

In figure (4.21) we plot electron temperature. As we can see the temperature is almost a constant function of the magnetic field, and radial position (solid and dashed curves are almost equal). Looking at figure (4.11) we see that the high pressure case is in agreement with the temperature we have at the antenna edge. The temperature in the low pressure case instead is higher near the antenna than here. About 2eV of energy are lost by the electrons in the 150mm that separate the two regions.

In figure (4.22) we plot plasma density. As we said before the errors here are quite large, therefore all evaluation of this data must be carefully considered. As usual the density is higher with higher pressure (red curves above the black ones). It decrease with magnetic field, in agreement with all the previous data and is slightly higher near the  $\hat{z}$  axis then away from it. Look-



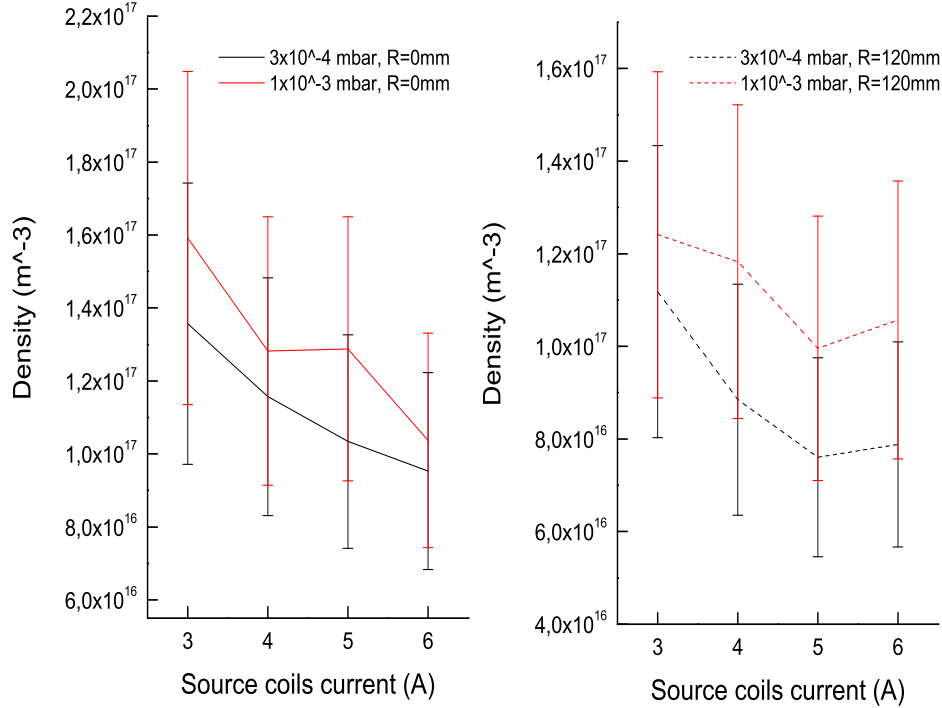


Figure 4.22: Plasma density as a function of magnetic field, pressure of  $1 \times 10^{-3}$  mbar and  $3 \times 10^{-4}$  mbar, radial position  $R = 0$  and 120mm and power of 600W. Compensated Langmuir probe.

ing at figure (4.12) we can see that both the high and the low pressure case are higher near axial position where we performed the radial measurements, then near the antenna edge. But as we said, these measurements are affected by large errors, and should probably need further investigation.

As we did for the axial case, we want to test our short term solution of the antenna flange problem. We performed some measurements along the  $\hat{z}$  axis at position of the radial scan. Using the first chamber coil to increase the magnetic field at the antenna edge we want to avoid losing particles at the flange surface. In figure (4.23) we plot plasma density as a function of the chamber coil current for different pressure values. As we can see, and as was happening in the axial scan (see figure 4.14) we have a maximum near 20A and a strong drop both for lower and for higher currents. The drop in the high magnetic field case is probably due to magnetic mirror effect; the

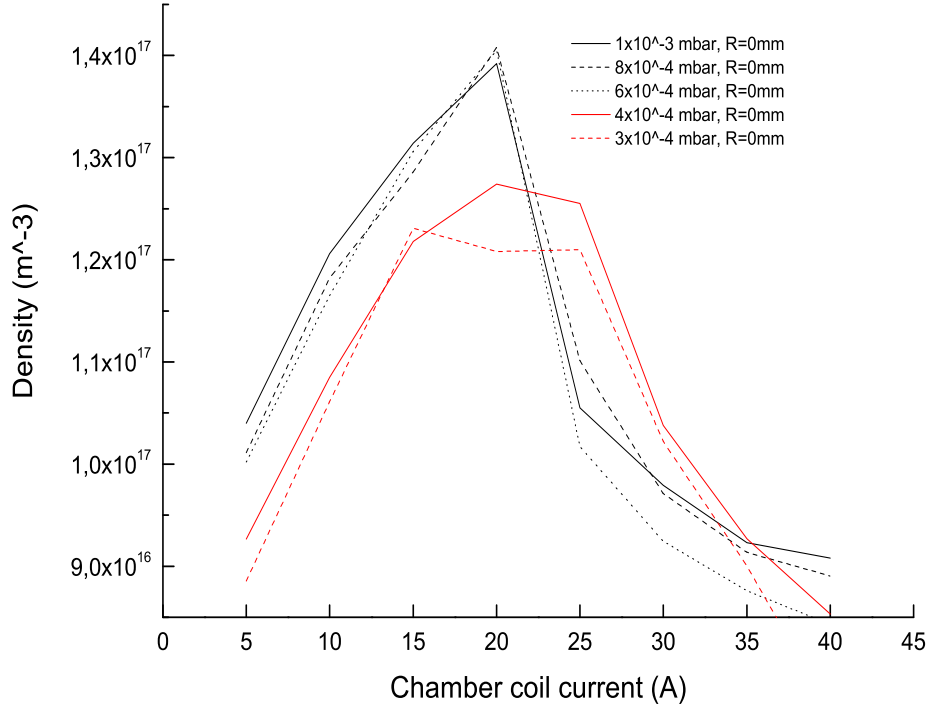


Figure 4.23: Plasma density as a function of chamber coil current, source coils current 6A, pressure of  $3 \times 10^{-4}$  mbar and  $1 \times 10^{-3}$  mbar, radial position  $R = 0$ mm and power of 900W. Double probe.

magnetic field here is stronger than in the antenna, and the particles are pushed back towards the antenna. The three higher pressure curves (black lines) seem to follow the same pattern. While the two lower pressure curves (red lines) seems to have lower peak density. We plotted in different colors so that it is easier to make a comparison with the corresponding axial plot. In figure (4.14) the two dashed curves are measured near the antenna edge, for the same pressures as the red curves in figure (4.23). As we can see comparing them, the density is about two times higher on the radial axis than on the antenna edge. An explanation could still be the magnetic mirror effect, in fact the magnetic field is higher near the antenna edge and can push particles away towards the radial scan position. On the other hand the difference in magnetic field between this two regions is very small (10 – 15G), so that this explanation could not be the correct one.

# Chapter 5

## Conclusion and further improvements

As conclusion of this work, I would like to briefly compare the two probe we used, and propose some measurements and technical improvements that could help on future experiments on Njord.

### 5.1 Diagnostics and further measurements

As we saw in the previous chapter the results obtained by the Langmuir compensated probe and the double probe are quite similar. We notice a factor of three in density that we still cannot explain, but all data trends are perfectly in agreement between them self. From the construction difficulties of the compensated probe, one should immediately prefer the double probe solution. On the other hand the compensated probe gives us useful information, on plasma and floating potential, that are, at this time, not available with the double probe.

The construction difficulties for the compensated probe can be contained in various way, I will give some ideas here:

- Prepare some small electric board, on which, mounting the filter components should be easier. Consider also mounting small clamps to easily connect the probe tip and the probe connectors.
- Look for larger ceramic tube, so that the housing of the filter does not have to be built on purpose.
- Improve the filter using a narrow trimmer capacitor to have a fine precision on cutoff frequency.

- Mount the antenna on a smaller chamber so that it is possible to break the seal, extract the probe, vary the cutoff frequency and pump down again. Njord has a very big chamber and it is necessary to wait at least one day before having good base pressure. Moreover, in a smaller chamber built on purpose, it would be a good idea to have more flanges, so that is possible to test more filter at the same time and with a normal Langmuir probe as a reference.

It must also be considered that the real time result of the double probe is a quite good property, that cannot be achieved easily with the compensated probe. In my idea the best solution would be to use the double probe to have a general idea of how density and temperature changes with parameters (pressure, magnetic field, antenna power). Then if further and deeper information are needed on potential, it could be reasonable to use the compensated probe.

Of all the volume available on Njord in this thesis we only look at a very small portion. An important, but anyway small portion. Other interesting areas could be the zone between the dome flange and the radial axis where we perform our measurements. In particular this area would be interesting after solving the problem of low magnetic field in the flange zone, so that the real plasma expansion would be in this area. Another interesting zone can be more inside the source, but here is necessary to point out some more details, see the following section. And finally deep inside the main chamber, using of course all the three main chamber coils and maybe also the hot-discharge plasma source mounted there.

## 5.2 Suggestion for technical improvements

In this months working on Njord I though about some technical improvements that, in my opinion, could really help to speed up future measurements and experiments. Here I make a list with decreasing importance order:

- Build a new amplifier capable at least of  $\pm 45V$  sweep ( $\pm 60V$  would be even better).
- Change (or at least mount together with the one we already have) the vacuum gauge meter. The combination of Pirani and inverted magnetron fails at  $3 \times 10^{-4}$  mbar, that is an interesting pressure level for our tests.

- Introduce a feedback system in the pressure control; so that the user chose the pressure and the computer handle the flow control to maintain the requested pressure.
- Build a cooling system for source and chamber coils.
- Modify the acquisition system of the Langmuir probe so that it displays automatically the I-V curve and its derivative (to see if the plasma potential point is visible).
- Modify the acquisition system of the Langmuir probe so that is possible to introduce the number of batteries used to create the potential offset directly in the output data file (to avoid the user introduce the number during data analysis).
- Mount a second motor system for the radial scan.
- Introduce in the motor movement program the possibility to pick up a position and stay there until the user want to. Right now when the acquisition system finish to perform the measurements the probe goes back to its original position.
- If higher pressure experiments have to be performed, mount a water cooling system for the turbomolecular pump. The Leybold manual of the pump, suggests water cooling for use at pressure higher than  $10^{-3}$  mbar.
- If further investigation of the inner side of the antenna are needed: move the gas inlet somewhere else, change the back plate and let the probe enters from the other side of the antenna (not from the dome). The compensated probe of 290mm length is already quite heavy, and the ceramic main body has already broke up near the connector, due to the mechanical stress.



# Appendix A

## Programs code

### A.1 Langmuir\_multi

```
;Langmuir multiscan analysis software v0.5

;FORMAT=b###p###th###

@open_experiment
@get_data
@get_nic

; Load predefined color tables from colors1.tbl
loadct,14

; Ensure all file units are close
close,/all

; Physical constant definition
q_electron = 1.6e-19 ; electron charge in Coloumb
m_electron=9.109390e-31 ; electron rest mass in kg
m_proton=1.672623e-27 ; proton rest mass
m_ion=39.948 *m_proton ; Argon mass

; Experiment file path
data_dir=' '
result_dir=' '
; Name experiment
exp_name=''
; Resistor in the probe circuit (ohm)
resistor = '10'
; Probe radius (mm)
radius='0.25'
; Probe Lenght (mm)
length= '5'
; Probe position (mm)
probe_start_pos= '0'
; Batteries used
batteries= '7'
; Data file input path
data_dir = 'C:\Documents and Settings\plasma\Desktop\giulio\dati\03_04_07\'
; Data file output path
result_dir ='C:\Documents and Settings\plasma\Desktop\giulio\dati\03_04_07\'
; Create a string array of dimension ten for widget_base text
```

```

text=strarr(10)
; Create text for previous array
text(0)='IVanalysis'
text(2)='This is a program for the analysis of Langmuir characteristics.'
text(3)='Hardware information
text(4)='For a single file analysis insert: Experiment name, input and output directory. Or click start and pick up a file'
text(5)='For multi file insert input directory, the results will be saved in the same directory'
text(6)='ATTENTION!! Single data analysis will work only if If the following field is empty'
; Create base widget object
base=widget_base(/column,title='IVanalysis',xsize=600,ysize=460)
; Insert previous written text
dum1=widget_text(base,value=text(0:2),xsize=50,ysize=3)
dum1b=widget_text(base,value=text(3),xsize=50,ysize=1)
; Create field for inserting previous experiment variables
dum5=cw_field(base,title='Resistor (ohm):',value=resistor,xsize=4)
dum6=cw_field(base,title='Probe radius (mm):',value=radius,xsize=4)
dum7=cw_field(base,title='Probe length (mm):',value=length,xsize=4)
dum8=cw_field(base,title='Probe position (mm):',value=probe_start_pos,xsize=4)
dum8b=cw_field(base,title='Batteries (##):',value=batteries,xsize=4)
dum1c=widget_text(base,value=text(4),xsize=50,ysize=1)
dum2=cw_field(base,title='Experiment name:',value=exp_name,xsize=60)
dum3=cw_field(base,title='Input data directory:',value=data_dir,xsize=60)
dum4=cw_field(base,title='Output data directory:',value=result_dir,xsize=60)
dum1d=widget_text(base,value=text(5:6),xsize=50,ysize=2)
dum9=cw_field(base,title='Multi input data directory:',value=multi_data_dir,xsize=60)
; Create button labelled 'Start'
but=widget_button(base,value='Start')
; Create button labelled 'Newfile'
but2=widget_button(base,value='New file')
; Display widget_base on screen
widget_control,base,/realize
; Wait for button 'Start' to be pressed
dummy=widget_event(but)
; Store values introduced by the user in variables
INIZIO:widget_control,dum2,get_value=exp_name
widget_control,dum3,get_value=data_dir
widget_control,dum4,get_value=result_dir
widget_control,dum5,get_value=resistor
widget_control,dum6,get_value=radius
widget_control,dum7,get_value=length
widget_control,dum8,get_value=probe_start_pos
widget_control,dum8b,get_value=batteries
widget_control,dum9,get_value=multi_data_dir
; Convert string value 'resistor' in a integer
resistor=fix(resistor(0))
; Convert string value 'radius' in a floating point (TYPE=4) and scale to m
radius=fix(radius(0), TYPE=4)*1.0e-3
; Convert string value 'length' in a floating point (TYPE=4) and scale to m
length=fix(length(0), TYPE=4)*1.0e-3
; Convert string value 'batteries' in a floating point (TYPE=4)
batteries=fix(batteries(0), TYPE=4)

if exp_name(0) eq '' then begin
file_convert=DIALOG_PICKFILE(/READ, filter = '*.txt')
print,file_convert
print,STRLEN(file_convert)
file_convert=STRTRIM(file_convert,0)
print,file_convert
print,STRLEN(file_convert)

file_pos=STRPOS(file_convert,'\b',/REVERSE_SEARCH)
exp_name=STRMID(file_convert,file_pos+1,12)
print,exp_name
data_dir=STRMID(file_convert,0,file_pos+1)
print,data_dir

```



```

endif

;-----SINGLEFILE-----

if multi_data_dir(0) eq '' then begin

output_name=exp_name(0)+'_out'
exp_name=exp_name(0)'.txt'
out_file=result_dir(0)+output_name+'.txt'
; Open the output file and (with APPEND) point for next writing at file end
openw,out_file,out_file,/GET_LUN,/APPEND
; Print on the output file variables name
printf,out_file,' exp_name Pos(mm) Vp(V) Vf(V) Te(eV) n(1/m^3) '
langmuir_core, exp_name,data_dir,out_file,resistor,radius,length,probe_start_pos,V_plasma,V_float,e_temp;,batteries
endif else begin

;-----MULTIFILE-----

multi_file_path= multi_data_dir(0)+'*.txt'
file_list=file_search(multi_file_path,count=n)
print,n

output_name=file_list[0]
output_file=output_name+'multi_out.txt'
; Open the output file and (with APPEND) point for next writing at file end
openw,out_file,output_file,/GET_LUN,/APPEND
; Print on the output file variables name
printf,out_file,' exp_name Pos(mm) Vp(V) Vf(V) Te(eV) n(1/m^3)'
; In experiment name is already save the directory
multi_data_dir(0)=''
for j=0,n-1 do begin
exp_name=file_list[j]
langmuir_core, exp_name,multi_data_dir,out_file,resistor,radius,length,probe_start_pos,V_plasma,V_float,e_temp
endfor

close, /all
endelse
; Wait for button 'new-file' to be pressed
dummy=widget_event(but2)
GOTO, INIZIO

end

;#####_END OF LANGMUIR_MULTI_#####

```

## A.2 Langmuir\_core

```

;Langmuir core analysis software for single and multifile analysis v0.5
pro langmuir_core, exp_name,data_dir,out_file,resistor,radius,length,probe_start_pos,V_plasma,V_float,e_temp;,batteries

; Physical costant definition
q_electron = 1.6e-19 ; electron charge in Coloumb
m_electron=9.109390e-31 ; electron rest mass in kg
m_proton=1.672623e-27 ; proton rest mass
m_ion=39.948 *m_proton ; Argon mass
k_boltzmann=1.38e-23 ; Boltzmann constant

; Using path and experiment name create the file_path to the input file
file_path = data_dir(0)+exp_name(0)
input_file = file_path;+ '.txt'

```

```

; Open the file to read data
openr,1,input_file

; Start file reading
while not EOF(1) do begin
; Create 2 dummy variables
  dum1 =''
  dum2= ''
  ; look for initial input file data, looking for 'Data rec Header' string
  while (strmid(dum1,0,15) ne 'Data rec Header') and (not EOF(1))do begin
  ; Save current string read in dum1
  if not EOF(1) then readf, 1, dum1
  ; Look for 'Numb of chan' string and save the number of channel used
  if (strmid(dum1,0,12) eq 'Numb of chan') then begin
    reads,dum1,dum2,channels,format='(a15,i10)'
    ;print, 'chan=',channels
    if channels lt 1 then read, 'No. of channels:', channels
  endif
  ; Look for 'Smpl freq' string and save the sample frequency
  if (strmid(dum1,0,9) eq 'Smpl freq') then begin
    reads,dum1,dum2,sample_freq,format='(a17,i4)'
    ;print, 'Sampling frequency (KHz)=',sample_freq
    if sample_freq lt 10 then read, 'Sampling frequency (KHz):', sample_freq
  endif
  ; Look for 'Numb of ramp' string and save the length of the ramp
  if (strmid(dum1,0,12) eq 'Numb of ramp') then begin
    reads,dum1,dum2,data_points,format='(a18,i6)'
    ;print, 'length=',data_points
    if data_points lt 100 then read, 'Record length:', data_points
  endif

  ; Look for 'Ramp Amplif' and save gain
  if (strmid(dum1,0,11) eq 'Ramp Amplif') then begin
    reads,dum1,dum2,gain,format='(a20,i5)'
    ;print, 'Gain=',gain
    if gain le 0 then read, 'Ramp gain:', gain
  endif

  endwhile

; Read the variable dum1 (At this point we are reading the line with 'Data rec Header'
; so we ignore the first 25 characters (a25->dum2) and save the probe position in an integer (i5->probe_pos)
  reads, dum1,dum2,probe_pos,format='(a27,i5)'

;offset probe
  l_probe=297;(all following values are in mm)
  ;differential lenght U piece
  l_U_piece=25
  ; probe support lenght
  l_rod=490
  ; distance between the beginning of the source ( the x=0 point )
  ; and the starting position of the motor ( x=0 point for the program)
  d_source_cap=200
  ; total distance between the beginnig of the source and the probe tip
  l_offset=l_rod+l_U_piece-l_probe+d_source_cap
  ; Evaluate the relative position inside the chamber, probe_start_pos...could be taken away.
  ;probe_oos going toward the x=0 position is negative
  chamber_pos=fix(probe_start_pos(0), TYPE=4)+fix(probe_pos(0), TYPE=4)+l_offset
  ; Screen the probe position: absolute and chamber frame
  ;print, 'Position relative to starting point:', probe_pos
print, 'Position relative to the chamber:', chamber_pos
; Create an array for probe tension, current & standard deviation with data_points dimension
  V_probe=fltarr(data_points)
  I_probe=fltarr(data_points)
  sigma=fltarr(data_points)

```

```

; Set dummy variables for data transmit from file to array
V_dum=0.0
I_dum=0.0
sigma_dum=0.0
; Copy data from file to the 3 arrays (we discharge the last two point for avoiding EOF error)
for J=0,data_points-2 do begin
  readf,1, V_dum, I_dum, sigma_dum
  V_probe(j)=V_dum
  I_probe(j)=(I_dum/(resistor*gain)) ;mA The probe read voltage, dividing by resistor, we get current!
  sigma(j)=(sigma_dum/(resistor*gain))*1.e3
endfor

; This and the following mod section allow the program to repeat the last data set analysis when requested
V_probe_temp=V_probe
I_probe_temp=I_probe
sigma_temp=sigma

  if NOT EOF(1) then readf, 1, dummy3

AGAIN:V_probe=V_probe_temp
I_probe=I_probe_temp
sigma=sigma_temp

  ; Inverte current
  I_probe=-I_probe
; Define and set=0 max_index
max_index=0
  ; Evaluate max and min of probe potential
V_max=max(V_probe,min=V_min)
  ; Evaluate a minimum potential step depending on potential scale
V_step=0.01*(V_max-V_min)
  ; Save position of those point for which held -> V_min<V_probe<V_step
min_index=where(V_probe lt (V_min+V_step))
  ; This procedure evaluate the first point less then V_min+V_step
min_index=min_index(where(min_index-shift(min_index,-1) ne -1))
min_index=min_index(0)
; Save position of those point for which held -> V_max>V_probe>V_step
max_index=where(V_probe gt (V_max-V_step))
max_index=max_index(where(max_index-shift(max_index,1) ne -1))
; Check that the highest point is higher than the lowest
if max_index(0) gt min_index then max_index=max_index(0)
; Otherwise it look for the first point higher then min_index even if V_max>V_probe>V_step doesn't held
if max_index(0) le min_index then begin
  i_index=1
  max0_index=0
  while max0_index le min_index and i_index le n_elements(max_index)-1 do begin
    max0_index = max_index(i_index)
    ;print, max0_index, 'max0_index'
    i_index = i_index+1
  endwhile
  if i_index le n_elements(max_index)-1 then max0_index=max_index(i_index)
  if max0_index le min_index then max0_index=data_points-1
  max_index=max0_index
endif
;print, min_index,max_index
; Reduce the data only to the ones between min and max index
I_probe=I_probe(min_index:max_index)
V_probe=V_probe(min_index:max_index)
; Count the new number of points we have with the new data
new_data_points=n_elements(V_probe)
;print,'Number of points= ',new_data_points

; Smooth potential and current with a boxcar avarage with dimension 5
V_probe= smooth(V_probe,5)

```

```

I_probe_smoos= smooth(I_probe, 12)
; Create a new shorter step in potential to obtain a better resolution
V_step=(V_probe(new_data_points-1)-V_probe(0))/(new_data_points*4.0)
; Create a new V_probe array
V_probe_new=indgen(new_data_points*4)*V_step+V_probe(0)
; Create an interpolation for the current using the new potential array
I_probe_new=spline(V_probe,I_probe_smoos,V_probe_new, 1.0)

; Plot Current Vs Potential and oplot insert a horizontal line along y=0 axis
plot, V_probe_new, I_probe_new,title='Pos from start: '+strtrim(string(probe_pos),2)+' mm',$
    xtitle='Probe voltage [V]',$
    ytitle='Probe Current [mA]',TICKLEN = 1
oplot, [-40,+40],[0,0]
; Print the smoothed curve
oplot, V_probe, I_probe_smoos, thick=1, color=200

;;-----;;
;; Take derivative of IV curve to find Plasma potential ;;
;; Define plasma potential by maximum in dI/dV ;;
;;-----;;

; Perform derivative to find plasma potential on I_probe_smoos and I_probe_new
deriv_IV_smoos=deriv(V_probe,I_probe_smoos)
; Plot derivative
oplot,V_probe,deriv_IV_smoos*10.0, thick=1, color=150 ; multiply factor was *3
; Evaluate max position of the derivativ
deriv_max=max(-deriv_IV_smoos(0:181),deriv_max_pos)
; Knowing max position we evaluate the corrispettive plasma potential
V_plasma=V_probe(deriv_max_pos)

;# EPS FILE SAVING#;
Set_plot,'PS'
Device, /Encapsulated
Device, Filename='langmuir.eps'
plot, V_probe_new, I_probe_new,LINESTYLE=0,$
    xtitle='Probe voltage [V]',$
    ytitle='Probe Current [mA]'
oplot,V_probe,deriv_IV_smoos*10.0, LINESTYLE=2 ; multiply factor was *3
oplot, [min(V_probe),max(V_probe)], [0,0], LINESTYLE=1
Device, /Close_File
Set_plot,'WIN'

; Print out plasma potential and ask for istructions
print,' Vp calc: ', V_plasma
answer='y'
print,'Do you want to analyse this record ? y/n '
answer=get_kbrd(1)
if ((answer eq 'Y')OR(answer eq 'y')) then begin
; If the program is not able to define V_plasma ask to user
if (deriv_max_pos eq 0) then begin
    print, 'No plasma potential found, choose Vp'
    ;Print, 'Choose Vp'
    ; Pick up and store only x-coordinates(V_plasmax) discharge y (dum1) (using /data)
    ; waiting for button click (/down)
    cursor,V_plasmax,dum1,/data,/down
    V_plasma=V_plasmax
    print,'Vplasma = ', V_plasma
endif else begin
; if the program finds a V_plasma ask if this is the correct value
    print,'Vp =',V_plasma
    answer='y'
    print, 'Value OK (y/n)?

```

```

    answer=get_kbrd(1)
; if the user doesn't like the V_plasma he choose one using same procedure use before
    While ((answer eq 'N')OR(answer eq 'n')) do begin
        print,'Choose Vp '
        cursor,V_plasmax,dum,/data,/down
        V_plasma=V_plasmax
        print,'Vp chosen = ', V_plasma
        print,'Chosen Vp OK (y/n)? '
        answer=get_kbrd(1)
    endwhile

endelse
; Save aproximate position of plasma potential
V_plasma_index=where(abs(V_probe - V_plasma) le abs(V_probe(2)-V_probe(1)))
;print, 'Plasma index: ',V_plasma_index

;;-----;;
;; Floating potential when probe current is zero          ;;
;; Find the point where lpi just less than                ;;
;; and greater than zero and average                      ;;
;;-----;;

; Evaluate max and min of potential
V_min_new=min(V_probe(0:new_data_points-1),V_plasma_min_index)
V_max_new=max(V_probe(0:new_data_points-1),V_plasma_max_index)
; Evaluate distance between max and min of potential
n=V_plasma_max_index-V_plasma_min_index+1
; Define an array containing n terms of potential with linear growth
T=V_min_new+findgen(n)*(V_max_new-V_min_new)/(n-1)
; Find the position for which I_probe_smoo<0
V_plasma_neg=where(I_probe_smoo lt 0)
; Choose the smallest one->the one that is closest to zero
I_neg=I_probe_smoo(V_plasma_neg(0))
; Copy the corrispettive value of the linear potential
V_float_neg=T(V_plasma_neg(0))
; Find the position for which I_probe_smoo>0
V_plasma_pos=where(I_probe_smoo gt 0)
; Choose the biggest one->the one that is closest to zero
I_pos=I_probe_smoo(n_elements(V_plasma_pos)-1)
V_float_pos=T(n_elements(V_plasma_pos)-1)
; Evaluate floating potential
V_float=(V_float_neg+V_float_pos)/2.

;;-----;;
;;           Wants to calculate Te:                       ;;
;;-----;;

;;-----;;
;; Find the Electron temperature by:                       ;;
;; 1) Remove ion current from the characteristic          ;;
;;    by chosing the ion current contrib with the cursor ;;
;; 2) Plot the logarithm of the el. current vs V_probe   ;;
;;    find the slope by choosing two points on the      ;;
;;    line by the cursor                                 ;;
;; 3) Te=1./a2, where a2 is the slop                     ;;
;;-----;;

; Plot the smoothed current Vs the previously built linear potential
AGAIN2: plot,T,I_probe_smoo(0:n-1),title='Probe caracteristic, Vf, Vp', $
    xtitle='Probe voltage [V]', $
    ytitle='Probe Current [mA]'
; Add horizontal zero line
oplot,[V_min_new,V_max_new],[0,0]

```

```

; Add Vertical line for float and plasma potential
;#W0.3MOD#oplot,[V_float,V_float],[min(I_probe),max(I_probe)]
oplot,[V_plasma,V_plasma],[min(I_probe_smo),max(I_probe_smo)]
; Ask the user to define the x-coordinates which correspond to the ion current contribution
print,'Use the mouse to mark left point of ion current contribution'
cursor, x1,y1, /data, /down
print,'Use the mouse to mark right point of ion current contribution'
cursor, x2,y2, /data, /down
; This if statement avoid putting x1 on the right of x2
if x2 le x1 then begin
x2_temp=x2
x1_temp=x1
x1=x2
x2=x1_temp
endif
; Save potential position less than x1
tmp1=where(V_probe lt x1,indx)
; Control on x1 maximum left position
if indx lt 1 then indx=1
; Take one point less than x1
point1=tmp1(indx-1)
; Save potential position bigger than x2
tmp2=where(V_probe gt x2)
; Take the smallest of those ones saved
point2=tmp2(0)
; Control on left position choosed by the user
if point1 lt 1 then point1=1
; Print the resulting point
;print, 'point1, point2:', point1, point2
answer='n'
while ((answer eq 'N')OR(answer eq 'n')) do begin
; Copy the potential value between the two points choosed by the user
V_local=V_probe[point1:point2]
; Copy the current value between the two points choosed by the user
I_local=I_probe_smo[point1:point2]
; Create a linear fit
linear_fit=linfit(V_local,I_local,yfit=dum1)
; y=A+Bx -> linear_fit(0)=A, linear_fit(1)=B, for the x value V_probe evaluate the y_value
I_linear=linear_fit(0)+linear_fit(1)*V_probe; P
; I have to find where I_linear=0
I_linear_x0=where(I_linear le 0)
; Evaluate distance between the x-position of the plasma potential and the x position
; of the intersection of the linear fit
ionic_offset= V_plasma_index(0)-I_linear_x0(0)
; Add Vertical line for float and plasma potential
oplot,[I_linear_x0(0),I_linear_x0(0)],[min(I_probe),max(I_probe)]
oplot,[V_plasma,V_plasma],[min(I_probe),max(I_probe)]
print,'the offset is of the order:',ionic_offset,' Is small enough (y/n)? '
;print,'Is small enough (y/n)? '
answer=get_kbrd(1)
; i correct the offset only if the user says that's not enough small
if answer eq 'n' then begin
; for correcting the value vertically i have to perform l=m*d*0.4
; the 0.4 is to avoid divergence
offset_correction=linear_fit(1)*ionic_offset*0.4
; I introduce the correction
I_probe_smo=I_probe_smo-offset_correction
endif
endwhile
if answer eq 'r' then begin
GOTO, AGAIN2
endif
;plot the correct linear fit
oplot, V_probe,I_linear
wait,1

```

```

; Subtract from current the ionic offset
I_new=I_probe-smoo-I_linear ;V.04MOD I_probe-smoo -> I_probe
; Print everything again with new current values
plot,V_probe,I_new, $
    xtitle='Probe voltage [V]', $
    ytitle='Probe Current [mA]'
oplot,[V_float,V_float],[min(I_new),max(I_new)]
oplot,[V_plasma,V_plasma],[min(I_new),max(I_new)]
oplot,V_local,I_linear
wait,1

; Now we should repeat the procedure for electronic current using logarithmic plot
I_log=log(abs(I_new))
answer='y'
while ((answer eq 'y')OR(answer eq 'Y')) do begin
    plot,V_probe,I_log,title='Logarithmic plot', $
    xtitle='Probe voltage [V]', $
    ytitle='Probe Current [mA]', TICKLEN = 0.2
    oplot,[V_float,V_float],[min(I_log),max(I_log)]
    oplot,[V_plasma,V_plasma],[min(I_log),max(I_log)]
; Ask the user to define the x-coordinates which correspond to the ion current contribution
    print,'Use the mouse to mark left point of electron current'
    cursor, x3,y3, /data, /down
    print,'Use the mouse to mark right point of electron current'
    cursor, x4,y4, /data, /down
; Take potential value smaller then x3
    tmp1=where(V_probe lt x3, indx)
    ; Choose the biggest one
    point1=tmp1(indx-1)
    ; Take potential value bigger then x4
    tmp2=where(V_probe gt x4)
    ; Choose the smallest one
    point2=tmp2(0)
    ; Evaluate local potential in log
    V_local_log=V_probe[point1:point2]
    ; Evaluate local current in log
    I_local_log=I_log[point1:point2]
    ; Perform linear fitting
    linear_fit_log=linfit(V_local_log,I_local_log,yfit=I_coeff)
    oplot,V_local_log,I_coeff
    ; Evaluate electronic temperature
    e_temp=1./linear_fit_log(1)

; Print results and ask if it's correct
    print,'Electronic temperature= ',e_temp
    print,'Do you want to repeat the line fitting? y/n '
    answer=get_kbrd(1)
endwhile

;# EPS FILE SAVING#;
Set_plot,'PS'
Device, /Encapsulated
Device, Filename='langmuir.eps'
    plot,V_probe,I_log,xtitle='Probe voltage [V]',ytitle='Logarithm probe Current'
    oplot,[V_float,V_float],[min(I_log),max(I_log)],LINESTYLE=2
    oplot,[V_plasma,V_plasma],[min(I_log),max(I_log)],LINESTYLE=2
Device, /Close_File
Set_plot,'WIN'

; Evaluation of electron density, we use -I since on the beginning we invert the current sing ;
Ie=1/(-I_probe-smoo(V_plasma_index))
; Prove area
Ap=2*pi*length*radius
; density
n_electron=1/(Ie(0)*q_electron*Ap*((q_electron*e_temp)/(2*pi*m_electron))^(0.5))

```

```

print,'Batteries used?(##)'
batteries1=get_kbrd(1)
batteries2=get_kbrd(1)
print, 'ola'
batteries=batteries1*10+batteries2
print, batteries
V_plasma=V_plasma+9*batteries
V_float=V_float+9*batteries
print, exp_name, chamber_pos, V_plasma, V_float, e_temp,n_electron
print, 'Do you want to repeat the entire analysis?(y/n)'
answer=get_kbrd(1)
if((answer eq 'y')OR(answer eq 'Y'))then begin
GOTO, AGAIN
endif

printf, out_file, exp_name, chamber_pos, V_plasma, V_float, e_temp,n_electron,format='(A,4F8.2,E12.3)'

endif
endwhile
print, 'End of data'
; in multifile scan i should not close all, otherwise close the output file
; but it should close the input file so that on the second run it can be opened againg
; with the new file
close,1
close,out_file
end

;#####_END OF LANGMUIR_CORE_#####

```

## A.3 Error analysis

```

;Langmuir error_analysis

; FORMAT=b##p###th##

@open_experiment
@get_data
@get_nic

; Load predefined color tables from colors1.tbl
loadct,14

; Ensure all file units are close
close,/all

; Physical costant definition
q_electron = 1.6e-19 ; electron charge in Coloumb
m_electron=9.109390e-31 ; electron rest mass in kg
m_proton=1.672623e-27 ; proton rest mass
m_ion=39.948 *m_proton ; Argon mass

; Experiment file path
data_dir=' '
result_dir=' '
; Name experiment
exp_name=''
; Resistor in the probe circuit (ohm)
resistor = '4.7'
; Probe radius (mm)
radius='0.25'
; Probe Lenght (mm)

```



```

length= '5'
; Probe position (mm)
probe_start_pos= '0'
; Batteries used
batteries= '7'
; Data file input path
data_dir = 'C:\Documents and Settings\plasma\Desktop\giulio\dati\magnetic scan\b60p100th000_out.txt'
; Data file output path
result_dir = 'C:\Documents and Settings\plasma\Desktop\giulio\dati\pressure scan\'
; Create a string array of dimension ten for widget_base text
text=strarr(10)
; Create text for previous array
text(0)='IVanalysis'
text(2)='This is a program for the analysis of Langmuir characteristics.'
text(3)='Hardware information
text(4)='For a single file analysis insert: Experiment name, input and output directory. Or click start and pick up a file'
text(5)='For multi file insert input directory, the results will be saved in the same directory'
text(6)='ATTENTION!! Single data analysis will work only if If the following field is empty'
; Create base widget object
base=widget_base(/column,title='IVanalysis',xsize=600,ysize=460)
; Insert previous written text
dum1=widget_text(base,value=text(0:2),xsize=50,ysize=3)
dum1b=widget_text(base,value=text(3),xsize=50,ysize=1)
; Create field for inserting previous experiment variables
dum5=cw_field(base,title='Resistor (ohm):      ',value=resistor,xsize=4)
dum6=cw_field(base,title='Probe radius (mm):   ',value=radius,xsize=4)
dum7=cw_field(base,title='Probe length (mm):   ',value=length,xsize=4)
dum8=cw_field(base,title='Probe position (mm):  ',value=probe_start_pos,xsize=4)
dum8b=cw_field(base,title='Batteries (##):    ',value=batteries,xsize=4)
dum1c=widget_text(base,value=text(4),xsize=50,ysize=1)
dum2=cw_field(base,title='Experiment name :    ',value=exp_name,xsize=60)
dum3=cw_field(base,title='Input data directory : ',value=data_dir,xsize=60)
dum4=cw_field(base,title='Output data directory: ',value=result_dir,xsize=60)
dum1d=widget_text(base,value=text(5:6),xsize=50,ysize=2)
dum9=cw_field(base,title='Multi input data directory: ',value=multi_data_dir,xsize=60)
; Create button labelled 'Start'
but=widget_button(base,value='Start')
; Create button labelled 'Newfile'
but2=widget_button(base,value='New file')
; Display widget_base on screen
widget_control,base,/realize
; Wait for button 'Start' to be pressed
dummy=widget_event(but)
; Store values introduced by the user in variables
INIZIO:widget_control,dum2,get_value=exp_name
widget_control,dum3,get_value=data_dir
widget_control,dum4,get_value=result_dir
widget_control,dum5,get_value=resistor
widget_control,dum6,get_value=radius
widget_control,dum7,get_value=length
widget_control,dum8,get_value=probe_start_pos
widget_control,dum8b,get_value=batteries
widget_control,dum9,get_value=multi_data_dir
; Convert string value 'resistor' in a integer
resistor=fix(resistor(0))
; Convert string value 'radius' in a floating point (TYPE=4) and scale to m
radius=fix(radius(0), TYPE=4)*1.0e-3
; Convert string value 'length' in a floating point (TYPE=4) and scale to m
length=fix(length(0), TYPE=4)*1.0e-3
; Convert string value 'batteries' in a floating point (TYPE=4)
batteries=fix(batteries(0), TYPE=4)

if exp_name(0) eq '' then begin
file_convert=DIALOG_PICKFILE(/READ, filter = '*.txt')
print,file_convert

```

```

print,STRLEN(file_convert)
file_convert=STRTRIM(file_convert,0)
print,file_convert
print,STRLEN(file_convert)

file_pos=STRPOS(file_convert,'\b',/REVERSE_SEARCH)
exp_name=STRMID(file_convert,file_pos+1,12)
print,exp_name
data_dir=STRMID(file_convert,0,file_pos+1)
print,data_dir
endif

;-----SINGLEFILE-----

if multi_data_dir(0) eq '' then begin

output_name='magnetic_scan'
exp_name=exp_name(0)+'.txt'
out_file=result_dir(0)+output_name+'.txt'
; Open the output file and (with APPEND) point for next writing at file end
openw,out_file,out_file,/GET_LUN,/APPEND
; Print on the output file variables name
;printf,out_file,' exp_name Pos(mm) Vp(V) Vf(V) Te(eV) n(1/m^3) '
error_analysis_core, exp_name,data_dir,out_file,resistor,radius,length,probe_start_pos,V_plasma,V_float,e_temp;,batteries
endif else begin

;-----MULTIFILE-----

multi_file_path= multi_data_dir(0)+'*.txt'
file_list=file_search(multi_file_path,count=n)
print,n

output_name=file_list[0]
output_file=output_name+'multi_out.txt'
; Open the output file and (with APPEND) point for next writing at file end
openw,out_file,output_file,/GET_LUN,/APPEND

multi_data_dir(0)=''
for j=0,n-1 do begin
exp_name=file_list[j]
error_analysis_core, exp_name,multi_data_dir,out_file,resistor,radius,length,probe_start_pos,V_plasma,V_float,e_temp;,batteries
endfor

close, /all
endelse
; Wait for button 'new-file' to be pressed
dummy=widget_event(but2)
GOTO, INIZIO

end

;####_-----END OF ERROR_ANALYSIS_-----#####

```

## A.4 Error\_analysis\_core

```

;Langmuir error_analysis_core
pro error_analysis_core, exp_name,data_dir,out_file,resistor,radius,length,probe_start_pos,V_plasma,V_float,e_temp;,batteries

; Physical costant definition
q_electron = 1.6e-19 ; electron charge in Coloumb

```

```

m_electron=9.109390e-31 ; electron rest mass in kg
m_proton=1.672623e-27 ; proton rest mass
m_ion=39.948 *m_proton ; Argon mass
k_boltzmann=1.38e-23 ; Boltzmann constant

; Using path and experiment name create the file_path to the input file
file_path = data_dir(0)+exp_name(0)
input_file = file_path;+ '.txt'
; Open the file to read data
openr,1,input_file

; Start file reading
while not EOF(1) do begin
; Create 2 dummy variables
dum1 =''
dum2= ''
; look for initial input file data, looking for 'Data rec Header' string
while (strmid(dum1,0,15) ne 'Data rec Header') and (not EOF(1))do begin
; Save current string read in dum1
if not EOF(1) then readf, 1, dum1
; Look for 'Numb of chan' string and save the number of channel used
if (strmid(dum1,0,12) eq 'Numb of chan') then begin
reads,dum1,dum2,channels,format='(a15,i10)'
;print, 'chan=',channels
if channels lt 1 then read, 'No. of channels:', channels
endif
; Look for 'Smpl freq' string and save the sample frequency
if (strmid(dum1,0,9) eq 'Smpl freq') then begin
reads,dum1,dum2,sample_freq,format='(a17,i4)'
;print, 'Sampling frequency (KHz)=' ,sample_freq
if sample_freq lt 10 then read, 'Sampling frequency (KHz):', sample_freq
endif
; Look for 'Numb of ramp' string and save the length of the ramp
if (strmid(dum1,0,12) eq 'Numb of ramp') then begin
reads,dum1,dum2,data_points,format='(a18,i6)'
;print, 'length=',data_points
if data_points lt 100 then read, 'Record length:', data_points
endif

; Look for 'Ramp Amplif' and save gain
if (strmid(dum1,0,13) eq 'No of Average') then begin
reads,dum1,dum2,n_average,format='(a15,i5)'

endif

endwhile
gain=1
; Read the variable dum1 (At this point we are reading the line with 'Data rec Header'
; so we ignore the first 25 characters (a25->dum2) and save the probe position in an integer (i5->probe_pos)
reads, dum1,dum2,probe_pos,format='(a27,i5)'

;offset probe
l_probe=297;(all following values are in mm)
;differntial lenght U piece
l_U_piece=25
; probe support lenght
l_rod=490
; distance between the beginning of the source ( the x=0 point )
; and the starting position of the motor ( x=0 point for the program)
d_source_cap=200
; total distance between the beginnig of the source and the probe tip
l_offset=l_rod+l_U_piece-l_probe+d_source_cap
; Evaluate the relative position inside the chamber, probe_start_pos...could be taken away.
; ;probe_oos going toward the x=0 position is negative
chamber_pos=fix(probe_start_pos(0), TYPE=4)+fix(probe_pos(0), TYPE=4)+l_offset

```

```

; Screen the probe position: absolute and chamber frame
;print, 'Position relative to starting point:', probe_pos
print, 'Position relative to the chamber:', chamber_pos
; Create an array for probe tension, current & standard deviation with data_points dimension
V_probe=fltarr(data_points)
I_probe=fltarr(data_points)
sigma=fltarr(data_points)
; Set dummy variables for data transmit from file to array
V_dum=0.0
I_dum=0.0
sigma_dum=0.0
; Copy data from file to the 3 arrays (we discharge the last two point for avoiding EOF error)
for J=0,data_points-2 do begin
readf,1, V_dum, I_dum, sigma_dum
V_probe(j)=V_dum
I_probe(j)=(I_dum/(resistor*gain))*1.e3 ;mA The probe read voltage, dividing by resistor, we get current!
sigma(j)=(sigma_dum/(resistor*gain))/(sqrt(n_average))
endfor

; This and the following mod section allow the program to repeat the last data set analysis when requested
V_probe_temp=V_probe
I_probe_temp=I_probe
sigma_temp=sigma

if NOT EOF(1) then readf, 1, dummy3

AGAIN:V_probe=V_probe_temp
I_probe=I_probe_temp
sigma=sigma_temp

; Inverte current
I_probe=-I_probe
; Define and set=0 max_index
max_index=0
; Evaluate max and min of probe potential
V_max=max(V_probe,min=V_min)
; Evaluate a minimum potential step depending on potential scale
V_step=0.01*(V_max-V_min)
; Save position of those point for which held -> V_min<V_probe<V_step
min_index=where(V_probe lt (V_min+V_step))
; This procedure evaluate the first point less then V_min+V_step
min_index=min_index(where(min_index-shift(min_index,-1) ne -1))
min_index=min_index(0)
; Save position of those point for which held -> V_max>V_probe>V_step
max_index=where(V_probe gt (V_max-V_step))
max_index=max_index(where(max_index-shift(max_index,1) ne -1))
; Check that the highest point is higher than the lowest
if max_index(0) gt min_index then max_index=max_index(0)
; Otherwise it look for the first point higher then min_index even if V_max>V_probe>V_step doesn't held
if max_index(0) le min_index then begin
i_index=1
max0_index=0
while max0_index le min_index and i_index le n_elements(max_index)-1 do begin
max0_index = max_index(i_index)
;print, max0_index, 'max0_index'
i_index = i_index+1
endwhile
if i_index le n_elements(max_index)-1 then max0_index=max_index(i_index)
if max0_index le min_index then max0_index=data_points-1
max_index=max0_index
endif
;print, min_index,max_index
; Reduce the data only to the ones between min and max index

```

```

I_probe=I_probe(min_index:max_index)
V_probe=V_probe(min_index:max_index)
sigma=sigma(min_index:max_index)
; Count the new number of points we have with the new data
new_data_points=n_elements(V_probe)
;print,'Number of points= ',new_data_points

I_probe_p=I_probe+sigma
I_probe_m=I_probe-sigma

; Smooth potential and current with a boxcar average with dimension 5
V_probe= smooth(V_probe,5)
I_probe_smoo= smooth(I_probe, 12)
I_probe_smoo_p= smooth(I_probe_p, 12)
I_probe_smoo_m= smooth(I_probe_m, 12)
; Create a new shorter step in potential to obtain a better resolution
V_step=(V_probe(new_data_points-1)-V_probe(0))/(new_data_points*4.0)
; Create a new V_probe array
V_probe_new=indgen(new_data_points*4)*V_step+V_probe(0)
; Create an interpolation for the current using the new potential array
I_probe_new=spline(V_probe,I_probe_smoo,V_probe_new, 1.0)
I_probe_new_p=spline(V_probe,I_probe_smoo_p,V_probe_new, 1.0)
I_probe_new_m=spline(V_probe,I_probe_smoo_m,V_probe_new, 1.0)
; Plot Current Vs Potential and oplot insert a horizontal line along y=0 axis
plot, V_probe_new, I_probe_new,title='Pos from start: '+strtrim(string(probe_pos),2)+' mm',$
xtitle='Probe voltage [V]',$
yttitle='Probe Current [mA]',TICKLEN = 1
oplot, [-40,+40],[0,0]
; Print the smoothed curve
oplot, V_probe, I_probe_smoo, thick=1, color=200

;;-----;;
;; Take derivative of IV curve to find Plasma potential ;;
;; Define plasma potential by maximum in dI/dV ;;
;;-----;;

; Perform derivative to find plasma potential on I_probe_smoo and I_probe_new
deriv_IV_smoo=deriv(V_probe,I_probe_smoo)
deriv_IV_smoo_p=deriv(V_probe,I_probe_smoo_p)
deriv_IV_smoo_m=deriv(V_probe,I_probe_smoo_m)
; Plot derivative
oplot,V_probe,deriv_IV_smoo*10.0, thick=1, color=150 ; multiply factor was *3
; Evaluate max position of the derivativ
deriv_max=max(-deriv_IV_smoo(0:181),deriv_max_pos)
deriv_max_p=max(-deriv_IV_smoo_p(0:181),deriv_max_pos_p)
deriv_max_m=max(-deriv_IV_smoo_m(0:181),deriv_max_pos_m)
; Knowing max position we evaluate the corrispettive plasma potential
V_plasma=V_probe(deriv_max_pos)
V_plasma_p=V_probe(deriv_max_pos_p)
V_plasma_m=V_probe(deriv_max_pos_m)

; Print out plasma potential and ask for istructions
answer='y'
print,'Do you want to analyse this record ? y/n '
if (probe_pos(0) eq -20) OR (probe_pos(0) eq -210) then begin
answer='y'
endif else begin
answer='n'
endelse

If ((answer eq 'Y')OR(answer eq 'y')) then begin
; If the program is not able to define V_plasma ask to user
if (deriv_max_pos eq 0) then begin
print, 'No plasma potential found, choose Vp'
;Print, 'Choose Vp'

```

```

; Pick up and store only x-coordinates(V_plasmax) discharge y (dum1) (using /data)
; waiting for button click (/down)
cursor,V_plasmax,dum1,/data,/down
V_plasma=V_plasmax
print,'Vplasma = ', V_plasma

endif else begin
; if the program finds a V_plasma ask if this is the correct value
print,'Vp =',V_plasma
answer='y'
print, 'Value OK (y/n)?'
answer=get_kbrd(1)
; if the user doesn't like the V_plasma he choose one using same procedure use before
While ((answer eq 'N')OR(answer eq 'n')) do begin
print,'Choose Vp '
cursor,V_plasmax,dum,/data,/down
V_plasma=V_plasmax
print,'Vp chosen = ', V_plasma
print,'Chosen Vp OK (y/n)? '
answer=get_kbrd(1)
endwhile

endelse
; Save aproximate position of plasma potential
V_plasma_index=where(abs(V_probe - V_plasma) le abs(V_probe(2)-V_probe(1)))
;print, 'Plasma index: ',V_plasma_index

;;-----;;
;; Floating potential when probe current is zero          ;;
;; Find the point where lpi just less than                ;;
;; and greater than zero and average                      ;;
;;-----;;

; Evaluate max and min of potential
V_min_new=min(V_probe(0:new_data_points-1),V_plasma_min_index)
V_max_new=max(V_probe(0:new_data_points-1),V_plasma_max_index)
; Evaluate distance between max and min of potential
n=V_plasma_max_index-V_plasma_min_index+1
; Define an array containing n terms of potential with linear growth
T=V_min_new+findgen(n)*(V_max_new-V_min_new)/(n-1)
; Find the position for which I_probe_smo0<0
V_plasma_neg=where(I_probe_smo0 lt 0)
V_plasma_neg_p=where(I_probe_smo0_p lt 0)
V_plasma_neg_m=where(I_probe_smo0_m lt 0)
; Choose the smallest one->the one that is closest to zero
I_neg=I_probe_smo0(V_plasma_neg(0))
I_neg_p=I_probe_smo0_p(V_plasma_neg_p(0))
I_neg_m=I_probe_smo0_m(V_plasma_neg_m(0))
; Copy the corrispettive value of the linear potential
V_float_neg=T(V_plasma_neg(0))
V_float_neg_p=T(V_plasma_neg_p(0))
V_float_neg_m=T(V_plasma_neg_m(0))
; Find the position for which I_probe_smo0>0
V_plasma_pos=where(I_probe_smo0 gt 0)
V_plasma_pos_p=where(I_probe_smo0_p gt 0)
V_plasma_pos_m=where(I_probe_smo0_m gt 0)
; Choose the biggest one->the one that is closest to zero
I_pos=I_probe_smo0(n_elements(V_plasma_pos)-1)
V_float_pos=T(n_elements(V_plasma_pos)-1)

I_pos_p=I_probe_smo0_p(n_elements(V_plasma_pos_p)-1)
V_float_pos_p=T(n_elements(V_plasma_pos_p)-1)

I_pos_m=I_probe_smo0_m(n_elements(V_plasma_pos_m)-1)
V_float_pos_m=T(n_elements(V_plasma_pos_m)-1)

```

```

; Evaluate floating potential
V_float=(V_float_neg+V_float_pos)/2
V_float_p=(V_float_neg_p+V_float_pos_p)/2.
V_float_m=(V_float_neg_m+V_float_pos_m)/2.
v_float_err=(V_float_p-V_float_m)/2

;;-----;;
;;      Wants to calculate Te:                ;;
;;-----;;

;;-----;;
;; Find the Electron temperature by:          ;;
;; 1) Remove ion current from the characteristic ;;
;;    by choosing the ion current contrib with the cursor ;;
;; 2) Plot the logarithm of the el. current vs V_probe ;;
;;    find the slope by choosing two points on the ;;
;;    line by the cursor ;;
;; 3) Te=1./a2, where a2 is the slop ;;
;;-----;;

; Plot the smoothed current Vs the previously built linear potential
AGAIN2: plot,T,I_probe_smo0(0:n-1),title='Probe characteristic, Vf, Vp', $
        xtitle='Probe voltage [V]', $
        ytitle='Probe Current [mA]'
; Add horizontal zero line
oplot,[V_min_new,V_max_new],[0,0]
; Add Vertical line for float and plasma potential
;#V0.3MOD#oplot,[V_float,V_float],[min(I_probe),max(I_probe)]
oplot,[V_plasma,V_plasma],[min(I_probe_smo0),max(I_probe_smo0)]
; Ask the user to define the x-coordinates which correspond to the ion current contribution
print,'Use the mouse to mark left point of ion current contribution'
cursor, x1,y1, /data, /down
print,'Use the mouse to mark right point of ion current contribution'
cursor, x2,y2, /data, /down
; This if statement avoid putting x1 on the right of x2
if x2 le x1 then begin
x2_temp=x2
x1_temp=x1
x1=x2
x2=x1_temp
endif
; Save potential position less than x1
tmp1=where(V_probe lt x1,indx)
; Control on x1 maximum left position
if indx lt 1 then indx=1
; Take one point less than x1
point1=tmp1(indx-1)
; Save potential position bigger than x2
tmp2=where(V_probe gt x2)
; Take the smallest of those ones saved
point2=tmp2(0)
; Control on left position choosed by the user
if point1 lt 1 then point1=1
; Print the resulting point
;print, 'point1, point2:', point1, point2
answer='n'
while ((answer eq 'N')OR(answer eq 'n')) do begin
; Copy the potential value between the two points choosed by the user
V_local=V_probe[point1:point2]
; Copy the current value between the two points choosed by the user
I_local=I_probe_smo0[point1:point2]
; Create a linear fit
linear_fit=linfit(V_local,I_local,yfit=dum1)
; y=A+Bx -> linear_fit(0)=A, linear_fit(1)=B, for the x value V_probe evaluate the y_value

```

```

I_linear=linear_fit(0)+linear_fit(1)*V_probe; P
; I have to find where I_linear=0
I_linear_x0=where(I_linear le 0)
; Evaluate distance between the x-position of the plasma potential and the x position
; of the intersection of the linear fit
ionic_offset= V_plasma_index(0)-I_linear_x0(0)
; Add Vertical line for float and plasma potential
oplot, [I_linear_x0(0), I_linear_x0(0)], [min(I_probe), max(I_probe)]
oplot, [V_plasma, V_plasma], [min(I_probe), max(I_probe)]
print, 'the offset is of the order:', ionic_offset, ' Is small enough (y/n)? '
; print, 'Is small enough (y/n)? '
answer=get_kbrd(1)
; i correct the offset only if the user says that's not enough small
if answer eq 'n' then begin
; for correcting the value vertically i have to perform l=m*d*0.4
; the 0.4 is to avoid divergence
offset_correction=linear_fit(1)*ionic_offset*0.4
; I introduce the correction
I_probe_smoo=I_probe_smoo-offset_correction
endif
endwhile
if answer eq 'r' then begin
GOTO, AGAIN2
endif
; plot the correct linear fit
oplot, V_probe, I_linear
wait, 1
; Subtract from current the ionic offset
I_new=I_probe_smoo-I_linear
I_new_p=I_probe_smoo_p-I_linear
I_new_m=I_probe_smoo_m-I_linear
; Print everything again with new current values
plot, V_probe, I_new, $
    xtitle='Probe voltage [V]', $
    ytitle='Probe Current [mA]'
oplot, [V_float, V_float], [min(I_new), max(I_new)]
oplot, [V_plasma, V_plasma], [min(I_new), max(I_new)]
oplot, V_local, I_linear
wait, 1

; Now we should repeat the procedure for electronic current using logarithmic plot
I_log=log(abs(I_new))
I_log_p=log(abs(I_new_p))
I_log_m=log(abs(I_new_m))
e_temp=indgen(10, /DOUBLE)
e_temp_p=indgen(10, /DOUBLE)
e_temp_m=indgen(10, /DOUBLE)
answer='y'
while ((answer eq 'y') OR (answer eq 'Y')) do begin
    plot, V_probe, I_log, title='Logarithmic plot', $
        xtitle='Probe voltage [V]', $
        ytitle='Probe Current [mA]', TICKLEN = 0.2
    oplot, [V_float, V_float], [min(I_log), max(I_log)]
    oplot, [V_plasma, V_plasma], [min(I_log), max(I_log)]

for rep=0,9 do begin
; Ask the user to define the x-coordinates which correspond to the ion current contribution
print, 'Use the mouse to mark left point of electron current'
cursor, x3, y3, /data, /down
print, 'Use the mouse to mark right point of electron current'
cursor, x4, y4, /data, /down
; inform the user how many data must be yet taken
; print, 9-rep
; Take potential value smaller then x3
tmp1=where(V_probe lt x3, indx)

```



```

; Choose the biggest one
point1=tmp1(indx-1)
; Take potential value bigger then x4
tmp2=where(V_probe gt x4)
; Choose the smallest one
point2=tmp2(0)
; Evaluate local potential in log
V_local_log=V_probe[point1:point2]
; Evaluate local current in log
I_local_log=I_log[point1:point2]
I_local_log_p=I_log_p[point1:point2]
I_local_log_m=I_log_m[point1:point2]
; Perform linear fitting
linear_fit_log=linfit(V_local_log,I_local_log,yfit=I_coeff)
linear_fit_log_p=linfit(V_local_log,I_local_log_p,yfit=I_coeff)
linear_fit_log_m=linfit(V_local_log,I_local_log_m,yfit=I_coeff)
; oplot,V_local_log,I_coeff
; Evaluate electronic temperature
e_temp(rep)=1./linear_fit_log(1)
e_temp_p(rep)=1./linear_fit_log_p(1)
e_temp_m(rep)=1./linear_fit_log_m(1)
; print,e_temp(rep)
; print,e_temp_p(rep)
; print,e_temp_m(rep)
endfor

err_temp=sqrt(total((e_temp-(total(e_temp))/10)^2))/3
err_temp_p=sqrt(total((e_temp_p-(total(e_temp_p))/10)^2))/3
err_temp_m=sqrt(total((e_temp_m-(total(e_temp_m))/10)^2))/3

e_temp=(total(e_temp)/10+total(e_temp_p)/10+total(e_temp_m)/10)/3
e_temp_err=(err_temp+err_temp_p+err_temp_m)/3
print,e_temp
print,e_temp_err
; Print results and ask if it's correct
print,'Electronic temperature= ',e_temp
print,'Do you want to repeat the line fitting? y/n '
answer=get_kbrd(1)
endwhile
; Evaluation of electron density, we use -I since on the beginning we invert the current sing ;
Ie=-I_probe_smoo(V_plasma_index)
;Ie_err=1/(sigma(V_plasma_index))
Ie_err=sigma(V_plasma_index)
; Prove area
Ap=2*pi*length*radius
Ap_err=2*pi*sqrt((0.1e-3/length)^2+(0.01e-3/radius)^2)*Ap
; density

n_electron=Ie(0)/(q_electron*Ap*((q_electron*e_temp)/(2*pi*m_electron))^(0.5))

n_electron_err=(1/q_electron)*sqrt((Ie_err(0)/Ie(0))^2+(Ap_err/Ap)^2+
+(0.5*e_temp_err/e_temp)^2)*(Ie(0)/(Ap*((q_electron*e_temp)/(2*pi*m_electron))^(0.5)))

print,Ap_err/Ap
print,Ie_err/Ie
print,e_temp_err/e_temp

print,n_electron
print,n_electron_err
ciao

print,'Batteries used?(##)'
batteries1=get_kbrd(1)

```

```

batteries2=get_kbrd(1)
batteries=batteries1*10+batteries2
print, batteries
V_plasma=V_plasma+9*batteries
V_float=V_float+9*batteries

batteries_sigma=0.133764
V_plasma_err=1.08
V_plasma_err=sqrt(batteries*(batteries_sigma)^2+V_plasma_err^2)
if V_plasma_err gt V_float_err then V_float_err=V_plasma_err

print, exp_name, chamber_pos, V_plasma,V_plasma_err, V_float,V_float_err, e_temp,e_temp_err,n_electron,n_electron_err
print, 'Do you want to repeat the entire analysis?(y/n)'
answer=get_kbrd(1)
if((answer eq 'y')OR(answer eq 'Y'))then begin
GOTO, AGAIN
endif

printf,out_file, exp_name, chamber_pos, V_plasma,V_plasma_err, V_float,
V_float_err,e_temp,e_temp_err,n_electron,n_electron_err,format='(A,7F8.2,2E12.3)'

endif
endwhile
print, 'End of data'
; in multifile scan i should not close all, otherwise close the output file
; but it should close the input file so that on the second run it can be opened againg
; with the new file
close,1
close,out_file
end

;#####_END OF ERROR_ANALYSIS_CORE_#####

```

# Bibliography

- [1] M.G.Kivelson and C.T.Russell *Introduction to space physics*, Cambridge University Press, Cambridge, 1995.
- [2] M. Kallenrode *Space Physics: an introduction to plasmas and particles in the heliosphere and magnetosphere, 2<sup>o</sup> edition*, Springer, Verlag Berlin Heidelberg, 2001.
- [3] M.C.Kelley *The Earth's Ionosphere*, International Geophysics Series, Academic Press, 1989.
- [4] J.M.Cornwall: *Magnetospheric ion acceleration process*, Wellesley, MA, June 3-7, 1985 (A87-37326 16-46). Washington, DC, AGU, 1986.
- [5] R.W.Schritt Wieser *Nonlinear potential structures in plasmas*, Specialised Course, Institute for Ion Physics, University of Innsbruck, Austria, May 2002.
- [6] R.J.Goldstone and P.H.Rutherford *Introduction to plasma physics*, IOP, Bristol, 1995.
- [7] T.H.Stix *Waves in plasma*, American Institute of Physics IOP, New York, 1992.
- [8] M.A.Raadu *The physics of double layers and their role in astrophysics* Physics Reports, 178:2597, 1989.
- [9] I.B.Bernstein, J.M.Greene and M.D.Kruskal. *Exact Nonlinear Plasma Oscillations* Physical Review, 108:546550, Nov. 1957.
- [10] F.F.Chen *Introduction to plasma physics and controlled fusion, 2ed.*, Plenum, New York, 1984.
- [11] F.F.Chen, J.P.Chang *Lecture notes on principle of plasma processing*, Plenum/Kluwer, Los Angeles, 2002.

- [12] M.A.Lieberman, A.J.Lichtenberg *Principles of plasma discharges and material processing*, J. Wiley, New York, 1994.
- [13] U.Flender et. al. *RF Harmonic suppression in Langmuir probe measurements in RF discharges*, Plasma sources sci. Technol. 5, 1996.
- [14] G.Neumann et. al. *Plasma-density measurements by microwave interferometry and Langmuir probes in anrf discharge*, Rev science instrum., Vol. 64/1,1993
- [15] I.D.Sudit and F.F.Chen *RF compensated probes for high-density discharges*, Plasma Sources Sci. Technol., 3:162, 1993.
- [16] R.W.Boswell *A Study of Waves in Gaseous Plasma*, PhD thesis, The Flinders University of South Australia, 1970.
- [17] R.W.Boswell *Plasma Production using a Standing Helicon Wave*, Phys. Lett., 33A(7):457, 1970.